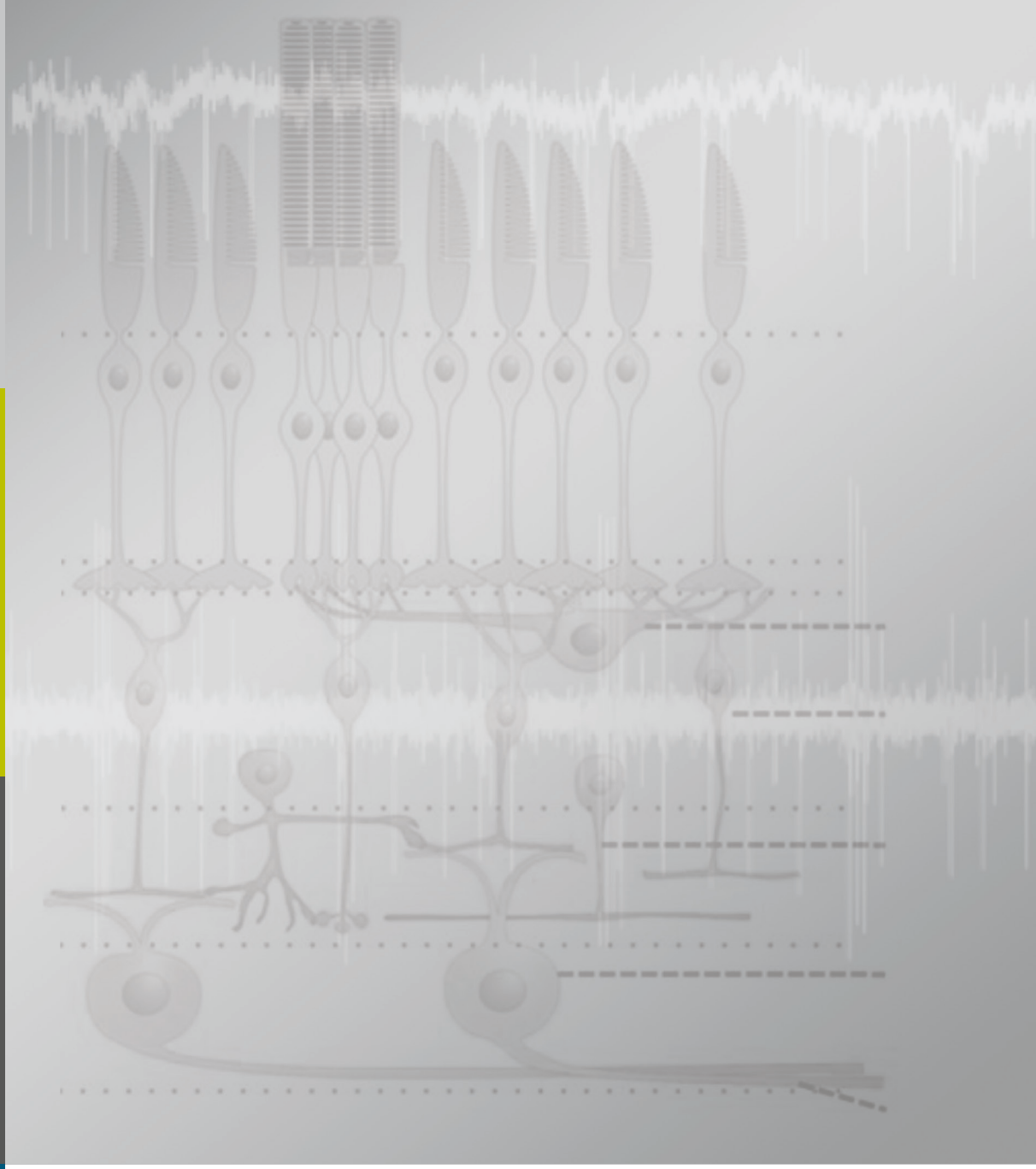

Immunohistochemical and electrophysiological characterization of the mouse model for Retinitis Pigmentosa, *rd10*

Sonia Biswas

JÜLICH
FORSCHUNGSZENTRUM

Member of the Helmholtz Association

Schriften des Forschungszentrums Jülich
Reihe Schlüsseltechnologien / Key Technologies Band / Volume 96

Forschungszentrum Jülich GmbH
Institute of Complex Systems
Zelluläre Biophysik (ICS-4)

Immunohistochemical and electrophysiological characterization of the mouse model for Retinitis Pigmentosa, *rd10*

Sonia Biswas

Schriften des Forschungszentrums Jülich
Reihe Schlüsseltechnologien / Key Technologies Band / Volume 96

ISSN 1866-1807 ISBN 978-3-95806-011-1

Bibliographic information published by the Deutsche Nationalbibliothek.
The Deutsche Nationalbibliothek lists this publication in the Deutsche Nationalbibliografie; detailed bibliographic data are available in the Internet at http://dnb.d-nb.de.

Publisher and Distributor: Forschungszentrum Jülich GmbH
Zentralbibliothek
52425 Jülich
Tel: +49 2461 61-5368
Fax: +49 2461 61-6103
Email: zb-publikation@fz-juelich.de
www.fz-juelich.de/zb

Cover Design: Grafische Medien, Forschungszentrum Jülich GmbH

Printer: Grafische Medien, Forschungszentrum Jülich GmbH

Schriften des Forschungszentrums Jülich
Reihe Schlüsseltechnologien / Key Technologies, Band / Volume 96

D 82 (Diss. RWTH Aachen University, 2014)

ISSN 1866-1807
ISBN 978-3-95806-011-1

The complete volume is freely available on the Internet on the Jülicher Open Access Server (JuSER) at www.fz-juelich.de/zb/openaccess.

Abstract

In the human disease retinitis pigmentosa (RP) the photoreceptors degenerate over time but the retinal network, in particular the retinal output neurons, the ganglion cells (RGCs) persist, providing a target for electrical stimulation by retinal prostheses. However, remodelling of the retinal network might interfere with this therapeutic approach. In the widely used mouse model of retinal degeneration, *rd1,* the loss of photoreceptors leads to rhythmic electrical activity of 10 to 16 Hz in the remaining retinal network. This kind of activity is not observed in wild type retina. Recent studies suggest that these oscillations are formed within the electrically coupled network of AII amacrine cells and ON-bipolar cells. Another mouse model, *rd10*, displays a delayed onset and slower progression of degeneration, making this mouse strain a better model for human RP.

In this thesis, the *rd10* retina was characterized immunohistochemically and electrophysiologically. It was observed that photoreceptors degenerate over time. Inner retinal cells did not degenerate, but horizontal cells and bipolar cells displayed loss of dendrites. Some somata were slightly misplaced. In horizontal cells sprouting of ectopic processes was also observed. Electrophysiological recordings *in vitro* using multi electrode arrays (MEA) revealed rhythmic electrical activity in *rd10* retina. Regular patterns of local field potentials (LFP) occurred with frequencies between 3 and 5 Hz. Oscillations in LFPs were often accompanied by rhythmic bursts of RGC spikes phase-locked to LFPs. The difference in the oscillation frequency between *rd1* and *rd10* raised the question whether oscillations have different origins in the two models. A pharmacological analysis suggests that both excitatory as well as inhibitory mechanisms are involved in the generation of spontaneous rhythmic activity in *rd10* retina. Oscillations were abolished by blockers of ionotropic glutamate receptors and gap junction blockers. Frequency and amplitude of oscillations were modulated strongly by blockers of inhibitory receptors and to a lesser extent by blockers of HCN channels.

In summary, although there are certain differences in the pharmacological modulation of rhythmic activity between *rd1* and *rd10* the overall pattern looks similar. This suggests that rhythmic activity may be generated by similar mechanisms in *rd1* and *rd10* retina. Future work must focus on the question, whether this rhythmic activity compromises the efficacy of electrical stimulation by retinal prostheses.

Zusammenfassung

Im Verlauf der Krankheit Retinitis Pigmentosa (RP) degenerieren zwar die Photorezeptoren in der Netzhaut des menschlichen Auges, das nachgeschaltete retinale Netzwerk mit den in das Gehirn projizierenden Ganglienzellen bleibt jedoch erhalten und bildet somit die Basis für eine elektrische Stimulation durch eine retinale Prothese. Krankhafte Veränderungen innerhalb des retinalen Netzwerkes könnten den Erfolg eines solchen therapeutischen Ansatzes allerdings beeinträchtigen. Im häufig als Modell für retinale Degeneration verwendeten Mausstamm *rd1* führt der Verlust der Photorezeptoren im verbleibenden retinalen Netzwerk zu rhythmischer elektrischer Aktivität, die mit 10 – 16 Hz auftritt. In der Wildtypretina kann eine solche elektrische Aktivität nicht beobachtet werden. Frühere Studien lassen vermuten, dass diese Oszillationen von elektrisch miteinander gekoppelten AII-Amakrinzellen und ON-Bipolarzellen hervorgerufen werden. In einem zweiten Mausmodell, *rd10*, degenerieren die Photorezeptoren erst später und zudem langsamer, was diesen Mausstamm zu einem potentiell besseren Modell für menschliche RP macht.

In der vorliegenden Arbeit wurde die *rd10* Retina sowohl immunhistochemisch als auch elektrophysiologisch charakterisiert. Während die Photorezeptoren im Laufe der Zeit degenerierten, blieben die Neurone der inneren Retina zwar erhalten, die Dendriten von Horizontal- und Bipolarzellen bildeten sich allerdings zurück. Zudem verlagerten sich die Somata bestimmter Zelltypen. Die Horizontalzellen bildeten außerdem ektopische Ausläufer in die innere Retina aus. Elektrophysiologische Messungen an *rd10* Retinae *in vitro* mit Multielektrodenarrays (MEA) zeigten elektrische Oszillationen in den lokalen Feldpotentialen (LFPs) zwischen 3 und 5 Hz. Diese Oszillationen wurden von rhythmischen, phasengekoppelten Aktionspotentialsalven retinaler Ganglienzellen begleitet. Die Unterschiede in der Oszillationsfrequenz zwischen *rd1* und *rd10* Retina könnten bedeuten, dass die Oszillationen durch unterschiedliche Mechanismen hervorgerufen werden. Eine pharmakologische Analyse in der *rd10* Retina zeigte, dass sowohl exzitatorische als auch inhibitorische Mechanismen an der Entstehung der Oszillationen beteiligt sind. Die Oszillationen verschwanden, wenn ionotrope Glutamatrezeptoren oder gap junctions blockiert wurden. Frequenz und Amplitude der Oszillationen wurden durch Blockade inhibitorischer Rezeptoren stark verändert, zu einem geringeren Teil auch nach Blockade von HCN Kanälen.

Zusammenfassend ist festzustellen, dass zwar gewisse Unterschiede in der pharmakologischen Modulation der rhythmischen Aktivität zwischen *rd1* und *rd10* Retina gezeigt werden können, es aber grundsätzlich zahlreiche physiologische Übereinstimmungen gibt. Vermutlich liegen somit den Oszillationen in der *rd1* und der *rd10* Retina die gleichen physiologischen Mechanismen zugrunde. Künftige Untersuchungen werden zeigen müssen, ob diese rhythmische Aktivität die elektrische Stimulation durch retinale Prothesen erschwert oder gar verhindert.

Table of Contents

Contents

II Abbreviations

%	Percent
µl	10^{-6} litre
3D MEA	3 Dimensional Multi Electrode Array(s)
AC	Amacrine Cell(s)
AMD	Aged Related Macular Degeneration
BC	Bipolar Cell(s)
BiMEA	Bi-directional Multi Electrode Array
C57BL/6	C57 black 6 mouse strain
C57BL/6J-Pde6b^{rd10}/J	*rd10* mouse
CaBP	Calcium Binding Protein
cGMP	cyclic guanosine 3'-5' monophosphate
CGP 54626	[*S*-(*R**, *R**)]-[3-[[1-(3,4-Dichlorophenyl)ethyl]amino]-2-hydroxypropyl] (cyclohexylmethyl) phosphinic acid
CNQX	6-cyano-2,3-dihydroxy-7-nitro-quinoxaline-2,3-dione disodium
CNTF	Ciliary Neurotrophic Factor
cpfl	cone photoreceptor function loss
Cs^+	Cesium
CsCl	Cesium Chloride
Cy2, Cy3, Cy5	Carbocyanine derivatives
DDW	Double Distilled Water
DL-AP5	DL-2-amino-5-phosphonopentanoic acid
DMSO	Dimethyl sulfoxide
e.g.	*exempli gratia*, for example
ERG	Electroretinogram
et al.	*et alii*, and others
FFT	Fast Fourier Transformation

GABA	γ-aminobutyric acid
GC	Ganglion Cell(s)
GCL	Ganglion Cell Layer
GFAP	Glial Fibrillary Acidic Protein
Go_{α}	a type of GTP-binding protein subunit belonging to the Gi_{α} family
GS	Glutamine Synthase
$G_{\beta\gamma}$	a type of GTP-binding protein subunit belonging to the $Gi_{\beta\gamma}$ family
h	Hour
HBSS	Hank's Balanced Salt Solution
HC	Horizontal Cell(s)
HCN	Hyperpolarization-activated Cyclic Nucleotide-gated
Hz	Hertz
I	Current
IAA	Iodoacetic Acid
IgG	Immunoglobulin
iGluR	Ionotropic Glutamate Receptors
INL	Inner Nuclear Layer
IPL	Inner Plexiform Layer
IS	Inner Segments
ISI	Inter spike Interval
kHz	10^3 Hertz
kΩ	10^3 Ohm
L-APB/L-AP4	L-(+)-2-Amino-4-phosphonobutyric acid
LCA	Leber Congenital Amaurosis
LFP	Local Field Potential(s)
M6	6 month
MC	Müller Cell(s)

mcd	10^{-3} candela
MCS	Multi Channel Systems
MEA	Multi Electrode Array(s)
MFA	Meclofenamic Acid
mg	10^{-3} gram
mGluR6	Metabotropic Glutamate Receptor 6
min	Minute
mm	10^{-3} meter
mM	10^{-3} Molar
mnd	Motor Neuron Degeneration
MNU	N-methyl-N nitrosourea
ms	10^{-3} second
NA	Numerical Aperture
nclf	Neuronal Ceroid Lipo Fuscinosis
NFL	Nerve Fibre Layer
nm	10^{-9} meter
nr	Nervous
Ø	Diameter
OFF- cell	cell that shows hyperpolarizing light response
ON-cell	cell that shows depolarizing light response
ONL	Outer Nuclear Layer
OPL	Outer Plexiform Layer

OS	Outer Segments
PA	Paraformaldehyde
PB	Phosphate Buffer
pcd	Purkinje Cell Degeneration
pH	Negative logarithm of the effective hydrogen-ion concentration
PKCα	Protein Kinase C α
PNA	Peanut Agglutinin
Px	Postnatal Day x
r mouse	rodless retina mouse, now *Pde6b*^{rd1}
R	Resistance
R-CPP	3-((*R*)-2-Carboxypiperazin-4-yl)-propyl-1-phosphonic acid
RD	Retinal Degeneration(s)
rd3 to rd10	Retinal Degeneration 3 – 10
rds	Retinal Degeneration Slow, now *Prph*^{rd2}
RP	Retinitis Pigmentosa
RPE	Retinal Pigment Epithelium
RT	Room Temperature
s	Second
SD	Standard Deviation
TiN	Titanium Nitride
TPMPA	(1,2,5,6-Tetrahydropyridin-4-yl)methylphosphinic acid

TRPM1 or MLSN1	Transient Receptor Potential cation channel subfamily M member 1 or Melastatin 1
USH2A	Usher Syndrome 2A
V	Potential
vit	Vitiligo, now *Mitf*$^{mi\text{-}vit}$
vs	Versus
WT	Wild type
ZD7288	4- Ethylphenylamino-1,2-dimethyl-6-methylaminopyrimidinium chloride
λ_{max}	Lambda max
µm	10^{-6} meter
µV	10^{-6} Volt

1. Introduction

In humans, vision is the most important sense. Our eyes provide us with roughly 70% of the information that we receive about our environment.

1.1 Anatomy of the eye

The primary function of the eye is to capture light and convert visual information into neuronal signals that can be processed by the brain. The eye is a small sphere with a diameter of 25 millimeters in a normal person. The sphere is covered with a tough, white tissue called the sclera that protects and physically supports the eye (Figure 1.1). The transparent cornea refracts light as it enters the eye. The cornea covers the iris, lens, and pupil. The colored part of the eye is called iris. The iris contains muscles that control the level of light entering the eye by contracting or dilating the pupil, the opening in the center of the iris. The biconvex, transparent lens lies behind the iris and helps in focusing light on the retina. The retina covers the back of the interior of the sphere. The space between the lens and the retina is filled with a clear, gel-like substance called the vitreous.

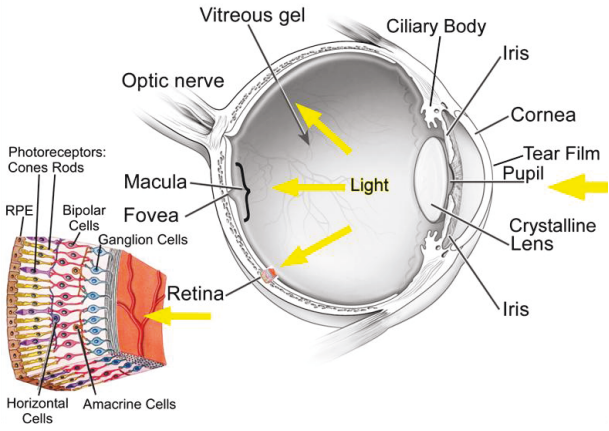

Figure 1.1 Human eye and retina (http://www.intechopen.com/books/topics-in-adaptive-optics/the-need-for-adaptive-optics-in-the-human-eye). The figure shows the different parts of the eye: cornea, iris, pupil, lens, vitreous gel, retina, and optic nerve. Light is projected by the optical apparatus onto the retina. The retina comprises different cell types: photoreceptors (rods and cones), bipolar cells, horizontal cells, amacrine cells, and ganglion cells.

1.2 The retina

Ramón y Cajal worked in the late 19th century using Golgi's silver nitrate staining of neurons (Ramón y Cajal, 1889). Cajal was the first scientist who identified the major retinal cell types and the information flow through the retinal network. The retina functions as both an image detector and a processing unit. It converts the optical information into electrical and chemical signals and relays them to the brain through the optic nerve, which is composed of ganglion cell axons (approximately 1.1 million in number). The typical mammalian retina is approximately 200 μm thick and is made up of different retinal cells: photoreceptors (rods and cones), horizontal cells, bipolar cells, amacrine cells, and ganglion cells (Figure 1.2, (Wässle, 2004; Sung & Chuang, 2010). These highly organized retinal cells are located in the 3 cell layers of retina. The outer nuclear layer (ONL) harbors the rod and cone photoreceptor cell bodies. The inner nuclear layer (INL) comprises somata of bipolar cells, horizontal cells, and amacrine cells. The third layer is the ganglion cell layer (GCL), consisting of ganglion cells and their axons as well as displaced amacrine cells. Signal processing begins at the first synaptic level in the outer plexiform layer (OPL) where the photoreceptors make contacts to bipolar cells and horizontal cells. Ganglion cells are the output neurons of the retina which relay information to the higher centre of the central nervous system for image processing and visual perception (Wässle, 2004).

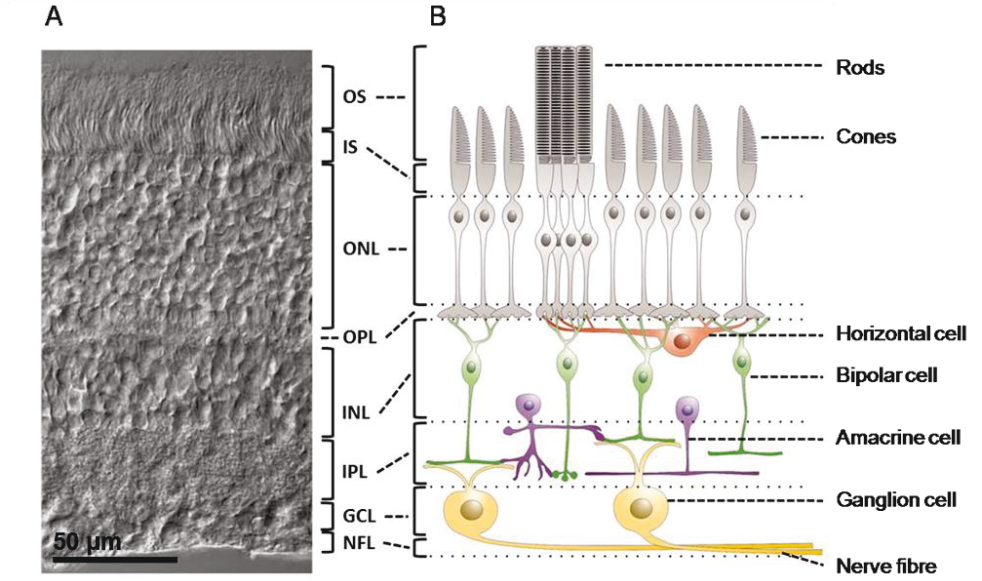

Figure 1.2 The retina and its different cell types. A) Differential Interference Contrast (DIC) image of a vertical section through the mouse retina. Scale bar 50 µm. B) Schematic drawing (taken and modified from Dr. Anja Mataruga doctoral thesis, 2006) of a vertical section through a retina. Different cells are marked: rods and cones, horizontal cell, bipolar cell, amacrine cell, ganglion cell. The retina is composed of different layers: OS, outer segments; IS, inner segments; ONL, outer nuclear layer; OPL, outer plexiform layer; INL, inner nuclear layer; IPL, inner plexiform layer; GCL, ganglion cell layer; NFL, nerve fibre layer. Light enters the retina from ganglion cell side.

1.2.1 Photoreceptors

Photoreceptors are small, light capturing cells whose somata form the outer nuclear layer (ONL) of the retina. The two types of photoreceptors are rods (120 millions, in a human eye) and cones (6-7 millions, per human eye). Rods are responsible for vision at a low light level and cones are responsible for vision at bright light levels and colour vision (Wässle, 2004). Rods and cones both can be divided into 2 parts: the inner part includes the inner segment, the cell body, axon and synaptic ending. The outer segment (OS) is the portion of the photoreceptor cells in which phototransduction takes place (Yau & Hardie, 2009; Sung & Chuang, 2010). The other neurons of the neurosensory retina modulate the signal from the photoreceptor cells. Retinal pigment epithelium (RPE) cells are located behind the retina. Their processes are in contact with the OS of the photoreceptors. RPE cells are pigmented and

function as photon sink which absorb all the photons that have not been absorbed by the photoreceptors (Sung & Chuang, 2010). RPE cells also play an important role in recovering bleached photopigments (Strauss, 2005). The RPE forms the blood brain barrier between the retina and the choroid. The choroid is a vascular network that supplies nutrients to the retina.

1.2.1.1 Rods

Rods are more sensitive to light than cone cells and are responsible for night vision and vision in dim light. In humans, the ratio of rods to cones is approximately 20:1. Rods are distributed throughout the retina except the fovea (which is the area of central vision). In the dark, rod OS have a high concentration of cyclic guanosine 3'-5' monophosphate (cGMP), which opens ion channels leading to the influx of sodium and calcium which finally changes the membrane potential and causes depolarization. Thus, rods are depolarized in dark and release the neurotransmitter glutamate from their synapse, the rod spherule.

In the mammalian retina, rod signals are processed in a specialized circuitry in which all rods contact a single type of bipolar cell called the rod bipolar cells (Masland, 2001). These rod bipolar cells pass the visual information to ganglion cells via another interneuron, the AII amacrine cell.

1.2.1.2 Cones

Cone photoreceptors function in bright light conditions and mediate colour vision. Human and primate cones contain one of three types of cone photopigments each with different wavelength sensitivity: L-cones (red or long wavelength, λ_{max} = 560 nm), M-cones (green or middle wavelength, λ_{max} = 530 nm), and S-cones (blue or short wavelength, λ_{max} = 425 nm). In darkness, the membrane potential of cones is depolarized and glutamate release from the cone's complex synaptic terminal, called the cone pedicle (Wässle, 2004) is high. Light hyperpolarizes the cones, thereby reducing the glutamate release. Glutamate released by cones is sensed by bipolar cells and horizontal cells.

1.2.2 Horizontal cells

Horizontal cells (HCs) are laterally connecting interneurons that receive excitatory (glutamatergic) signals from photoreceptors and feed inhibitory signals to bipolar cells and/or photoreceptors (Schwartz, 2002). HCs are very important for the generation of concentric antagonistic receptive fields in the retina that enhance contrast detection and reduce

redundancy of signals transmitted to the ganglion cells (Masland, 2001). Most mammals have two types of horizontal cells (A- and B-type, in primate H1 and H2), which can be distinguished morphologically and functionally but some species, like mice and rats, possess only one type of horizontal cell (Suzuki & Pinto, 1986; Peichl & Gonzalez-Soriano, 1994). Three per cent of all cells in the inner nuclear layer are horizontal cells (Jeon *et al.*, 1998). Horizontal cells are connected to each other by an extensive network of gap junctions (Nelson *et al.*, 1975).

1.2.3 Bipolar cells

Bipolar cells (BCs) collect input from photoreceptors and relay it to ganglion cells. The mammalian retina contains approximately 12 types of BCs (Ghosh *et al.*, 2004). One type of bipolar cell is the rod bipolar cell, while the rest are cone bipolar cells. BCs are physiologically classified into two main functional groups (ON and OFF) based on their response to illumination. Illumination results in depolarization of ON-bipolar cells and hyperpolarization of the OFF-bipolar cells. ON-bipolar cells have processes that ramify distally from their soma in sublamina b of the inner plexiform layer (IPL) close to the ganglion cell layer where they contact ON-ganglion cells. OFF-bipolar cells axons stratify close to their soma in sublamina a of the IPL where they contact OFF-ganglion cells. Both ON and OFF pathways are morphologically separated and remain so, until they reach the visual cortex (Werblin & Dowling, 1969; Suzuki & Kaneko, 1990).

1.2.4 Amacrine cells

Amacrine cells (ACs) are inhibitory interneurons that form lateral processes ramifying in the second synaptic layer, the inner plexiform layer (IPL). The majority of AC bodies are present in the INL and some AC (called displaced AC) bodies are displaced into the GCL. Amacrine cells play a vital role in controlling the synaptic output from bipolar cells onto ganglion cells via inhibitory feedback mechanisms (Masland, 2001). Amacrine cells also provide feed forward inhibition to other amacrine cells and ganglion cells. Glycine and γ-aminobutyric acid (GABA) are the major inhibitory transmitters of the mammalian retina (Pourcho, 1996). Approximately 40% of cells in the inner retina of mouse are amacrine cells (Jeon *et al.*, 1998). Approximately 30 different types of the amacrine cells are found (Masland, 2001) that have different neurotransmitters like GABA, glycine, dopamine, acetylcholine, and others. Therefore, amacrine cells are the most diverse class of inhibitory interneurons within the

retina. So far, only a few amacrine cell types are functionally well understood. The most intensely studied amacrine cell types include the AII (Bloomfield & Dacheux, 2001), A17 (Schubert & Euler, 2010), polyaxonal (Famiglietti, 1992; Volgyi *et al.*, 2001; Olveczky *et al.*, 2003), and starburst amacrine cells (Masland, 2001; Zhou & Lee, 2008). AII and A17 cells play important roles in the classical rod pathway while starburst cells are involved in the generation of directional selectivity (Briggman *et al.*, 2011; Vaney *et al.*, 2012).

1.2.5 Ganglion cells

Ganglion cells (GCs) are the output neurons of the retina. They collect visual information (primary excitatory information from BCs and inhibitory information from ACs) and transmit it as electrical signals to different parts of the brain (Wässle & Boycott, 1991). GCs are located in the ganglion cell layer (GCL) and have large cell bodies and prominent dendritic arbors. There have been multiple attempts to morphologically classify GCs in different species (Brown & Major, 1966; Honrubia & Elliott, 1970; West & Dowling, 1972; Boycott & Wässle, 1974; Cleland *et al.*, 1975; Grun, 1975; Naka & Garraway, 1975; Wyatt & Day, 1976). Based on their light evoked responses, GCs can be divided into three main classes: ON ganglion cells fire action potentials upon illumination, OFF-ganglion cells fire action potentials at the offset of illumination, and ON/OFF ganglion cells increase firing in response to illumination changes both at the beginning and at the end of the light stimulus (Schiller, 2010). Therefore, ON ganglion cells receive excitatory input from ON-bipolar cells, OFF-ganglion cells from OFF-bipolar cells, and ON-OFF ganglion cells from both types of bipolar cells. These classes have been further subdivided based on their morphology and function, which can also vary between different animal species.

1.2.6 Müller cells

Müller cells (MCs) are one of the distinct types of glial cells and the most predominant (90%) form of retinal glia. The somata of MCs make up 16% of the cells in the inner nuclear layer of mouse retina (Jeon *et al.*, 1998). The function of MCs is to provide structural support to the neuronal retina and to serve as housekeeper cells helping to remove excess neurotransmitter from the extracellular space (Dowling, 1987). MC bodies are located in the INL but their processes span the entire retina from the inner border of the GCL to the distal border of the ONL. MCs vary in population density and morphology depending on the region of the retina in which they are located. For e.g., in the central retina MCs density is higher and MCs have

long, fine trunks and a narrow end foot. Müller cells become activated by pathogenic stimuli (Bringmann *et al.*, 2009).

1.3 Vision and diseases

285 million people are estimated to be visually impaired worldwide: 39 million are blind and 246 million have low vision (http://www.who.int/mediacentre/factsheets/fs282/en/). 82% of people living with blindness are aged 50 and above. Retinal degenerative diseases are among the leading causes of blindness in older people (Gaillard & Sauve, 2007).

1.3.1 Retinal degenerative diseases

Retinal degenerations (RDs) are a vast and heterogeneous group of inherited degenerative diseases (dystrophies) of the retina that lead to progressive visual loss. It is estimated that more than 15 million people worldwide suffer from visual loss due to an inherited RD. Most of the retinal degenerative diseases are characterized by the progressive loss of photoreceptor cells, with the exception of glaucoma and some forms of vitreoretinal degeneration. In humans, more than 160 retinal genes have already been indentified that can lead to vision loss due to the death of rod and cone photoreceptors (Rivolta *et al.*, 2002). The two most prevalent disorders among them are: age-related macular degeneration (AMD) and retinitis pigmentosa (RP).

1.3.1.1 Aged Related Macular Degeneration (AMD)

Age-related macular degeneration (Friedman *et al.*, 2004) is characterized by degeneration of photoreceptors in the central retina and is the leading cause of worldwide blindness among the ageing population. The cause of macular degeneration is unknown. The extent of vision loss depends upon whether the patient has the wet or dry form of AMD. The wet form only occurs in ~ 10% of all AMD cases, and is commonly associated with more severe vision loss. It progresses at a rapid rate and is characterized by the leakage of red blood cells which can lead to permanent damage of the light-sensitive retinal cells, causing blind spots and central vision loss (Gehrs *et al.*, 2006; Huang *et al.*, 2011). More common is the dry form occurring in 70-90% of all cases. In contrast to the wet form of AMD, the dry form progresses at a much slower rate and is often characterized by the thinning of the macula overtime.

1.3.1.2 Retinitis pigmentosa (RP)

Retinitis pigmentosa (RP) is a heterogeneous family of genetically inherited neurodegenerative diseases affecting approximately 1 in 4000 people worldwide (Bunker *et al.*, 1984; Berson, 1993). RP results primarily in the loss of the rods and secondarily cone photoreceptors. This is followed by the degeneration of the RPE (Huang *et al.*, 2011). There exists a wide variety of genes that cause RP but mutations in the rhodopsin gene (RHO) comprise a large proportion of ~25% of the cases (RP dominant) followed by the Usher syndrome 2A (USH2A gene, ~20% recessive disease). The heterogenecity of the disease leads to large variability in the pattern of symptoms, age of onset and severity of the disorder. This variability in turn makes it difficult to predict the time course of photoreceptor degeneration. In adolescence patients experience problems in dark adaptation as well as night blindness. Young adult patients often have a loss of peripheral vision leading to tunnel vision. In the final stage of disease, patients experience a narrowing of the tunnel vision and eventually loss of central vision (Bunker *et al.*, 1984; Hartong *et al.*, 2006).

1.4 Animal models for retinal degeneration

Several animal models have been investigated in order to better understand the various forms of retinal degenerative diseases. They are basically categorized into two groups depending on whether photoreceptor degeneration is induced by a genetic modification or by physical or chemical treatment.

1.4.1 Genetic animal models

The first documented hereditary models for retinal degeneration was a mouse strain (*r* mouse) that lacked rod photoreceptors (Keeler, 1924) followed by an identical mouse strain (*rd* mouse) discovered (extinct *r* mice are believed to have been rediscovered as *rd* mice) almost 30 years later (Bruckner, 1951). Parallel to the identification of novel retinal disease genes numerous genetically engineered mouse models carrying those genetic defects were generated.

The Jackson Laboratory has developed a large collection of mouse mutants of RD. To date, fifteen naturally occurring mouse mutants that exhibit photoreceptor degeneration have been identified. A brief summary of retinal degeneration in various mouse models, their loci of genetic defect, together with their corresponding chromosome homolog in human and onset of disease, is given in Table 1.1.

	Gene	Mouse Chromosome	Human Chromosome	Retinal ONL Disappears by Month
Retinal degeneration 1	***Pde6b^{rd1}***	5	4p16	1
Motor neuron degeneration	***mnd***	8	8p or 13q	6
Nervous	***nr***	8	8p or 13q	10
Purkinje cell degeneration	***pcd***	13	5q	13
Retinal degeneration 2	**rds/*Prph2^{rd2}***	17	6p	12
Retinal degeneration 3	***rd3^{rd3}***	1	1q32	4
Retinal degeneration 4	***rd4***	4	1p36	2
Retinal degeneration 5	***rd5***	7	11p15	8
Retinal degeneration 6	***rd6***	9	11q23	24
Retinal degeneration 7	***rd7***	9	15q23	30
Retinal degeneration 9	***rd9***	X	X21.1	30
Retinal degeneration 10	***Pde6b^{rd10}***	5	4p16	2
Vitiligo	***Mitf$^{mi\text{-}vit}$***	6	3p14	10
Cone photoreceptor function loss	***cpfl1***	19	10q25	30
Neuronal ceroid lipofuscinosis	***nclf***	9	15q21	13

Table 1.1 Mouse models of retinal degeneration. 15 naturally occurring mouse mutants for photoreceptor degeneration with the preservation of other retinal cell types. Different mutants: retinal degeneration (earlier *rd*, identical with rodless retina, *r*, now *Pde6b^{rd1}*); Motor neuron degeneration (*mnd*); nervous (*nr*); Purkinje cell degeneration (*pcd*); retinal degeneration slow (*rds*, now *Prph^{Rd2}*); retinal degeneration 3 – 10 (*rd3 to rd10*); vitiligo (*vit*, now *Mitf$^{mi\text{-}vit}$*); cone photoreceptor function loss (*cpfl1*) and neuronal ceroid lipo fuscinosis (*nclf*). Taken and modified from: http://eyemutant.jax.org/retinal_degen.html

1.4.2 Inducible, acute animal models of retinal degeneration

Several studies described various physical and chemical methods for inducing photoreceptor stress/damage in the vertebrate retina. These methods proved to be rapid and cost-effective in comparison to available genetic models of RP (Wang *et al.*, 2011). There are several methods for inducible photoreceptor degeneration. Damage produced by exposure of strong light on albino rats causes retinal degeneration (Noell *et al.*, 1966; Rapp & Williams, 1980; Taylor *et al.*, 2012). Intraperitoneal or intraocular injections of pharmaceuticals such as iodoacetic acid (IAA) (Liang *et al.*, 2008; Scott *et al.*, 2011; Nan *et al.*, 2013; Rösch *et al.*, 2014b) or N-methyl-N nitrosourea (MNU) (Nagar *et al.*, 2009; Jeong *et al.*, 2011; Yamauchi *et al.*, 2011; Chen *et al.*, 2014; Rösch *et al.*, 2014a) induce photoreceptor loss.

In the retina, IAA and MNU lead to selective photoreceptor degeneration. MNU is an alkyline agent and belongs to the group of the nitrosoureas (Tsubura *et al.*, 2010). Like the other chemical agents of this group, it is toxic, carcinogenic, teratogenic, embryotoxic and mutagenic (Sigma Aldrich, 2013). The systemic application of MNU induces selective and progressive photoreceptor degeneration in the retina of rat (Nakajima *et al.*, 1996; Yoshizawa *et al.*, 2000), mouse (Nambu *et al.*, 1997; Nagar *et al.*, 2009; Rösch *et al.*, 2014a), hamsters (Herrold, 1967; Taomoto *et al.*, 1998), rabbits (Ogino *et al.*, 1993), and non-human primates (Tsubura *et al.*, 2010). Nagar *et al*. (Nagar *et al.*, 2009) showed that the long term effects of MNU-triggered photoreceptor degeneration in the mouse retina are strikingly similar to the chronic morphological consequences that have been identified in humans with photoreceptor degeneration diseases.

1.5 Potential treatments

Currently, there is no cure for retinal degenerative diseases. However, there are treatments, drugs, and therapies that can be used to slow the progression of degeneration. Wet AMD is treatable but it is expensive and it needs repeated intraocular injections by either bevacizumab (Avastin) or ranibizumab (Lucentis).

RP treatments are divided into different categories. Firstly, the gene therapy which deals with the replacement of the defective gene by a normal gene. Gene therapy treatment has been successful in animal models of RP. Clinical trials for gene replacement in patients with Leber Congenital Amaurosis (LCA) have begun (Smith *et al.*, 2009). However, a gene therapy approach is limited to a particular gene defect and the numbers of RP mutations are huge (Rivolta *et al.*, 2002) meaning that for each mutation a specific approach has to be found.

Secondly, pharmaceutical therapy using agents that prolong the life and function of photoreceptor cells. Bok (Bok, 2005) showed that ciliary neurotrophic factor (CNTF) could delay photoreceptor cell degeneration in an animal model. Thirdly, the photoreceptor cell replacement by transplantation e.g. of stem cells. Canola et al. (Canola *et al.*, 2007) observed positive results upon stem cell transplantation in animal models of RP. Finally, in recent years, the electrical retinal prosthesis has proven to be a promising approach for RP and AMD treatments and several groups worldwide have conducted clinical trials.

At present, there are fourteen clinical trials worldwide with different designs (http://en.wikipedia.org/wiki/Retinal_prosthesis). The prosthesis is designed to send electrical signals to bypass defective or dead photoreceptors and stimulate the remaining intact cells of the retina. Image data from a camera are processed by a video signal-processing unit that converts the image data into stimulation data. These data and power are then transmitted wirelessly through a telemetry circuitry and decoded. Patterns of stimuli generated from the chip are then transmitted through a microelectrode array to the retina to trigger firing of the retinal output neurons, the ganglion cells.

1.5.1 Prosthetic approach

There are three types of retinal implants currently in clinical trials: epiretinal implants (on the retina), subretinal implants (behind the retina), and suprachoroidal implants (above the vascular choroid). Retinal implants provide the user with low resolution images by electrically stimulating surviving retinal cells. Such images may be sufficient for restoring specific visual abilities, such as light perception and object recognition.

1.5.1.1 Epiretinal implants

Epiretinal implants consist of a silicon platinum electrode array mounted onto the inner surface of the retina, directly stimulating ganglion cells and bypassing all other retinal layers (Figure 1.4). The array is stabilized using micro tacks, along with the slight mechanical pressure provided by the vitreous humour. The epiretinal implant requires an external video camera to acquire images (Chader *et al.*, 2009). The external camera and image processing chip are generally mounted onto eyeglasses for the patient (Weiland *et al.*, 2005). The image processing involves reducing the resolution of the image and converting the image into a spatial and temporal pattern of stimulation to activate the appropriate retinal cells (Zrenner, 2002; Chader *et al.*, 2009). Epiretinal implants are advantageous as they bypass a large

portion of the retina, relying on the function of ganglion cells in the innermost layer of the retina. Therefore, epiretinal implants could provide visual perception to individuals with retinal diseases extending beyond the photoreceptor layer. Additionally, the location of epiretinal implants allows the vitreous humor to serve as a heat sink for the implant (Piyathaisere *et al.*, 2003). However, the main disadvantage of epiretinal implants is the need for an external apparatus, which can be cumbersome to wear.

The first epiretinal implant, the ARGUS device, included a silicon platinum array with 16 electrodes (Chader *et al.*, 2009). The ARGUS II device received marketing approval in February 2013 and in Europe in Feb 2011, becoming the first approved implant. This discovery paved path to the development of several implants by various institutions.

1.5.1.2 Subretinal implants

Subretinal implants are logged on the outer surface of the retina, between the photoreceptor layer and the retinal pigment epithelium (Figure 1.4), directly stimulating retinal cells and relying on the normal processing of the inner and middle retinal layers (Weiland *et al.*, 2005). A subretinal implant consists of a silicon wafer containing light sensitive microphotodiodes. The incident light passes through the retina and generates currents within the microphotodiode. The resultant current is relayed to the retinal cells via an array of microelectrodes. This mechanism leads to a visual perception of the original incident image. In contrast to epiretinal implants subretinal implants do not require video camera and encoder Subretinal placement is also simpler, as it places the stimulating array directly adjacent to the damaged photoreceptors (Weiland *et al.*, 2005; Chader *et al.*, 2009). The main disadvantage of subretinal implants is the lack of sufficient incident light to enable the microphotodiodes to generate adequate currents. The compact nature of the subretinal space imposes significant size constraints on the implant. The close proximity between the implant and the retina also increases the possibility of thermal damage to the retina from heat generated by the implant (Zrenner, 2002). Chow's group at Optobionics (IL, USA) manufactured the artificial silicone retina (ASR) microchip as a device for a clinical test in patients (Chow *et al.*, 2004; Chow *et al.*, 2010).

1.6 The aim of the current study

Currently, there is no treatment for RP. However, the persistent inner retina provides a target for different therapies. One possibility is to electrically stimulate the remaining retina by neural prostheses or optical stimulation. In addition to the classical epiretinal and subretinal prostheses, a new approach was designed, the BiMEA (Bi-directional multi electrode array) based on penetrating electrodes (Figure 1.4). It enables to penetrate the retina with electrode shafts from the ganglion cell side and stimulate at different depths in the retina. The penetrating shafts comprise both stimulating and recording electrodes. Hence, the device could in principle determine its stimulation efficiency by recording the retinal output upon stimulation.

The BiMEA project is a collaboration between different groups. The penetrating electrodes are designed and fabricated in the Institute für Werkstoffe der Elektrotechnik, RWTH, Aachen in Prof. Dr. rer. nat. Wilfried Mokwa's laboratory. The initial testing of these electrodes is done in the Institute of Complex Systems-8, Forschungszentrum Jülich in Prof. Dr. rer. nat. Andreas Offenhäuser's laboratory. The stimulation unit and amplifiers are designed at the Fraunhofer IMS Duisburg headed by Prof. Dr. Anton Grabmaier. The experiments on higher animal models and clinical aspects are performed at RWTH Aachen University, Dep. of Ophtalmologie / IZKF Aachen under Prof. Dr. med. Peter Walter's supervision. The characterization of retinal degeneration models is performed in the Institute of Complex Systems-4, Forschungszentrum Jülich in Prof. Dr. rer. nat. Frank Müller's laboratory (part of this study).

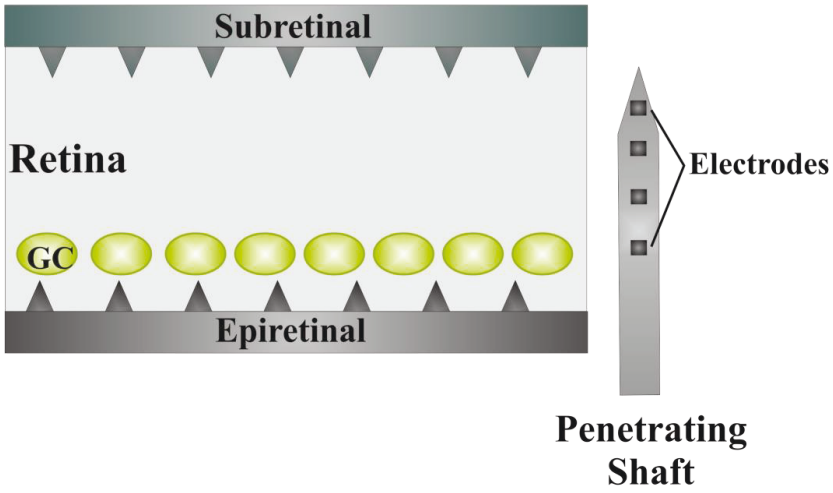

Figure 1.4 Different approaches for retinal prostheses. Scheme represents the two main variants of retinal prosthesis: epiretinal (on the retina) and subretinal (behind the retina). The third approach using penetrating shafts has stimulating and recording electrodes in the same shaft. GC, ganglion cells.

1.7 Motivation and approach of the study

To explore the mechanisms of retinal degeneration in human RP and to establish experimental therapies mouse models of retinal degeneration are essential tools to work with. The most commonly used mouse model for RP is the *rd1* mouse that carries a mutation in the gene for rod phosphodiesterase (Bowes *et al.*, 1990; Strettoi & Pignatelli, 2000; Chang *et al.*, 2002). In retinae of *rd1* mice, distinct degeneration of photoreceptors begins around postnatal day 8 (P8) and by P21 all rods have degenerated. Cones also degenerate but with slower pace. The fast degeneration in *rd1* mice is a major drawback of the model. Rod degeneration starts while the retina is still in the process of differentiation. An alternative mouse model to *rd1* is the *rd10* mouse. These animals have a mutation in the same gene as for *rd1*; however, the onset of photoreceptor degeneration is delayed. In *rd10* mice, rods start to degenerate after P16. By this time, all retinal layers and cell types as well as synaptic connections have been established and the major phase of retinal differentiation is over. Maximal photoreceptor degeneration occurs between P21 and P25. By P60, only cones have survived. Hence, *rd10* mice mimic the disease process in human RP more closely than *rd1* mice (Gargini *et al.*, 2007; Phillips *et al.*, 2010). In every attempt to restore vision, success crucially depends on

the functional integrity of the remaining retinal ganglion cells and their ability to reliably transmit visual signals to the brain. Thus, the present study aims at characterizing the genetic model *rd10* in two ways: morphologically using immunohistochemistry to investigate the morphological changes in the remaining retina and functionally via multi electrode arrays (MEA).

1.7.1 Morphological characterization of the *rd10* mouse model

In 1974, Kolb and Gouras first noted indications of altered retinal circuitry following retinal degeneration (Kolb & Gouras, 1974). Still, for nearly twenty years, the idea of retinal remodelling was not recognized. However, recent research shows that photoreceptor degenerative diseases are characterized by consequent morphological changes of the remaining retinal tissue, called "remodelling" (Strettoi & Pignatelli, 2000; Marc *et al.*, 2003; Strettoi *et al.*, 2003; Jones & Marc, 2005). The "retinal remodelling" theory presented by Marc and Jones (2003) (Marc & Jones, 2003) very clearly enumerated the processed in the retina that go well beyond the loss of photoreceptors. As the functional and structural consequences of photoreceptor degeneration could affect vision rescue attempts, further studies on both genetic and non-genetic animal models of retinal degeneration like the *rd10* mouse must be done.

1.7.2 Functional characterization of the degenerated retina by electrophysiology

Recent studies on *rd1* mice have shown that the neurophysiological properties of photoreceptor degenerated retina differ significantly from those of a normal retina (O'Hearn *et al.*, 2006; Ye & Goo, 2007b; a; Jensen & Rizzo, 2008; Margolis *et al.*, 2008; Stasheff, 2008). The most significant alteration noticed is the spontaneous rhythmic electrical activity occurring at frequencies of 10 Hz or above (Ye & Goo, 2007b; Stasheff, 2008). This spontaneous rhythmic electrical activity is also called "intrinsic neuronal oscillations". In *rd1,* frequencies of these oscillations are in the range of 10 – 16 Hz whereas in *rd10* frequencies are between 3-7 Hz (Ye & Goo, 2007b; Margolis *et al.*, 2008; Borowska *et al.*, 2011; Goo *et al.*, 2011a; Menzler & Zeck, 2011). The source of the rhythmic activity has been attributed to dystrophic bipolar cells (Menzler & Zeck, 2011) or, in contrast to a circuit of dystrophic AII amacrine and cone bipolar cells (Borowska *et al.*, 2011). Pharmacological analysis has shown that both amacrine cells and bipolar cells are necessary and sufficient to drive aberrant activity in *rd1* (Trenholm *et al.*, 2012).

As the degeneration process differs between *rd1* and *rd10*, rhythmic activity might have different origins in both retinal models. In the present study, the properties of rhythmic activity in *rd10* retinae were investigated using a pharmacological approach.

2. Materials and Methods

Parts of the following materials and methods were described in Biswas *et al.* (Biswas *et al.*, 2014).

2.1 Materials

2.1.1 Animals

Adult wild type mice (C57BL/6; Elevange Janvier, France) were used for control experiments. C57BL/6J-Pde6b^{rd10}/J mutants (from here on, *rd10* mice) were obtained from the Jackson Laboratory, USA. In this line, the *rd10* mutation was backcrossed onto the C57BL/6J background for 5 generations before intercrossing to homozygosity. Animals were kept in a local facility in a 12-hour light/dark cycle with water and food *ad libitum*. All experiments were performed in accordance with the German Law for the Protection of Animals and after approval were obtained by the regulatory authorities, the Forschungszentrum Jülich and the Landesamt für Natur, Umwelt und Verbraucherschutz of the land North-Rhine Westfalia.

Mice treated with N-Methyl-N-Nitrosourea (MNU) were used for a comparative electrophysiological study and were obtained from the Augenklinik, Klinikum Aachen, Germany. Adult C57/BL/6J mice were intra-peritoneally injected with 60 mg/kg body weight of MNU (Sigma Aldrich, Germany) in the Augenklinik by Sarah Rösch. Seven to ten days after the injection, retinae of injected mice were studied electrophysiologically in collaboration with Sarah Rösch, Christine Haselier, and Prof. Peter Walter from the Augenklinik. The procedure of injections as well as the effects of MNU on the retina are described in detail in Rösch et al. (Rösch *et al.*, 2014a).

2.1.2 Instruments used

Cryostat: Cryo-Star HM 560 Cryostat (Microm, Germany)

Confocal Laser Scanning Microscope: TCS SP5 II (Leica Microsystems, Heidelberg, Germany).
Laser: one Argon laser (458, 488 nm) and three Helium-Neon lasers (543, 594, 633 nm)
Objective: Oil immersion 63x with NA 1.4

Multi electrode array system:	USB-MEA60-Up-System (Multi Channel Systems MCS GmbH, Reutlingen, Germany) Standard MEAs (Multi Channel Systems MCS GmbH, Reutlingen, Germany) 3D MEAs (Qwane Biosciences, Lausanne, Switzerland)

2.1.3 Solutions and buffers

Phosphate Buffer (PB)	81 mM Na_2HPO_4 19 mM NaH_2PO_4 pH 7.4
Hank's Balanced Salt Solution (HBSS)	0.137 M NaCl 5.4 mM KCl 0.25 mM Na_2HPO_4 5 mM Glucose 0.44 mM KH_2PO_4 1.3 mM $CaCl_2$ 1.0 mM $MgSO_4$ 4.2 mM $NaHCO_3$ pH 7.4

Fixative

4% Paraformaldehyde (PA) in PB

Solutions for immunohistochemistry

10% Sucrose in PB (with 0.05% NaN_3)	
30% Sucrose in PB (with 0.05% NaN_3)	
Incubation solution I (CTA) in PB	5% Chemiblocker (Chemicon International, Temecula, USA) 0.5% Triton X-100 (Sigma, Germany) 0.05% NaN_3
Incubation solution II (CT) in PB	5% Chemiblocker (Chemicon International, Temecula, USA) 0.5% Triton X-100 (Sigma, Germany)
Richardson Blue	0.5% Azure II 0.05% Methylene blue (in 0.05% $Na_2B_4O_7$)
1mM TO-PRO®-3 Iodide in DMSO (Stock)	

Solution for multi electrode array recordings

AMES buffer	8.8 grams AMES salt (Sigma Aldrich, Germany) for 1 litre solution 32 mM $NaHCO_3$ Equilibrated with 5% CO_2/95% O_2 pH 7.4
Pharmacological solutions	All pharmacological agents (blockers, agonists & antagonists) were diluted in AMES buffer from their stock solutions to the desired concentration.

2.2 Methods

2.2.1 Immunohistochemistry

2.2.1.1 Retinal tissue preparation

Wild type mice (C57BL/6; postnatal weeks 6-8) and *rd10* mice (postnatal days 6, 14, 25, 32, 45, 60, and 180) were deeply anesthetized with isoflurane (Piramal Healthcare Ltd., UK) and decapitated. The eye balls were enucleated with a small curved blades scissors and transferred into a small petri dish with Hanks balanced salt solution (HBSS) under a binocular microscope. The eyes were enucleated and opened by an encircling cut at the limbus. The retina in the eye cup was immersion fixed in 4% paraformaldehyde (PA) in phosphate buffer (PB) for 30 min at room temperature and washed several times with PB. Tissue was incubated in 10% sucrose in PB for 1 h, followed by 30% sucrose in PB overnight at 4°C.

2.2.1.2 Sectioning

The retinae were flat embedded and frozen in optimal cutting temperature (OCT) compound (NEG-50, Richard Allan Scientific, Thermo Fisher Scientific, Germany). Vertical sections (i.e. perpendicular to the retinal layers, 20 µm thick) were cut on a cryostat at -20°C (HM 560 CryoStar; MICROM; Walldorf; Germany). Three retinal sections were collected per Superfrost Plus slide (Menzel, Braunschweig, Germany) and slides were stored at -20°C for immunohistochemistry.

2.2.1.3 Immunohistochemistry procedure

In this work, the indirect immunohistochemical method was used to detect different specific retinal proteins. This method involves an unlabeled primary antibody that binds to the target antigen in the tissue and a fluorescently labelled secondary antibody that binds to the primary antibody. The secondary antibody was raised against the immunoglobulin (IgG) of the animal species in which the primary antibody was raised (Figure 2.1).

For immunohistochemistry, slides with the sections were thawed and dried at room temperature. Subsequently, tissue sections were encircled with a grease pen (Fettstift, Liquid Blocker, SCI Science Services, Munich, Germany) that allows to work with very small incubation volumes (100 µl per slide). The following incubation steps were carried out at

room temperature (RT). The incubation process was performed in a humid chamber (lined with damp tissues inside the box).

Sections were pre-treated with blocking solution 5% Chemiblocker (Chemicon, Hofheim, Germany), 0.5% Triton-X100, 0.05% NaN3 in PB for 1 hour, followed by incubation with primary antibodies overnight, diluted in the same solution. Sections were washed in PB for 10 minutes and incubated in secondary antibodies diluted in 5% Chemiblocker, 0.5% Triton-X100 in PB for 1 h, washed in PB for 10 minutes and coverslipped with Aqua Polymount (Polysciences, Eppelheim, Germany). When required, TO-PRO®-3 (Invitrogen, Germany) was added to the secondary antibody solution. TO-PRO®-3 intercalates into the DNA and thus stains the nuclei of all cells. Sections were examined with a confocal laser scanning microscope (Leica TCS SP5, Leica Microsystems, Heidelberg, Germany). Images were processed and printed with ImageJ and Adobe Photoshop.

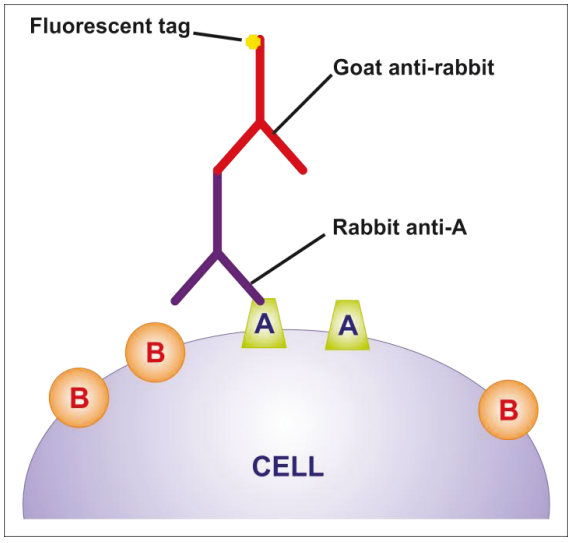

Figure 2.1 The indirect method of immunohistochemical staining, uses a primary antibody (rabbit anti-A, e.g.) against the antigen being targeted (A) and a secondary antibody raised against the immunoglobulin (IgG) of the animal species in which the primary antibody has been raised (goat anti-rabbit). The secondary antibody is fluorescently labelled. Modified from Wikipedia, http://en.wikipedia.org/wiki/Immunohistochemistry.

2.2.1.3.1 Primary antibodies

Primary antibodies used in this study are listed in Table 2.1.

Table 2.1. List of primary antibodies.

Antibody	Antigen	Species	Dilution	Source
AB5405	Opsin red/green	rb	1:800	Chemicon International, Hofheim, Germany
AB5585	Recoverin	rb	1:2000	Chemicon International, Hofheim, Germany
Blue	Opsin blue	gt	1:200	Santa Cruz Biotechnology
CabP	Calbindin	ms	1:1000	Sigma, Deisenhof, Germany
GFAP	Glial fibrillary acidic protein	ms	1:400	Sigma Immuno Chemicals, USA
GS	Glutamine synthase	ms	1:2000	BD Biosciences, Heidelberg, Germany
mGluR6	Metabotropic receptor 6	rb	1:1000	Sigma, Deisenhof, Germany
PG2-1A4.1.1	HCN4	rt	1/1 (0.75-1.0%Trition)	E.Kremmer, Helmholtz Zentrum München A. Mataruga, ICS-4, FZJ
PKCα	protein kinase C α	ms	1:50	Transduction laboratories
TRPM1	Transient receptor potential cation channel subfamily M member 1	rb	1:100	Sigma, Deisenhof, Germany

2.2.1.3.2 Secondary antibodies

Secondary antibodies used in this study are listed in Table 2.2.

Table 2.2. List of secondary antibodies and nuclear stain.

Antibody	Host species	Dilution	Source
Anti-goat Cy2	donkey	1:400	Dianova, Hamburg, Germany
Anti-mouse Cy3	donkey	1:100	Dianova, Hamburg, Germany
Anti-rabbit Cy2	donkey	1:400	Dianova, Hamburg, Germany
Anti-rabbit Cy3	donkey	1:500	Dianova, Hamburg, Germany
Anti-rabbit Alexa488	goat	1:500	Molecular Probes, Darmstadt, Germany
Anti-rat Alexa488	goat	1:500	Molecular Probes, Darmstadt, Germany
TO-PRO®-3	-	1:1000	Invitrogen, Germany

2.2.1.3.3 Confocal Laser Scanning Microscopy

Confocal laser scanning microscopy is a technique for obtaining high-resolution optical images with depth selectivity. The key feature of confocal microscopy is its ability to acquire in-focus images at different depths, a process known as optical sectioning. Optical sections were made on a Leica confocal laser scanning microscope (System TCS SP5 II, Leica Microsystems, Heidelberg, Germany) using a 63x oil-immersion objective (NA 1.4). The intensity of laser and filter settings were carefully controlled by the Leica TSC Power Scan software. Pictures were taken at 1024x1024 pixels. The gain and the signal offset were adjusted for each channel so that within the 8-bit images no structural information was lost. In most of the cases, z-stacks were created to show the structure of whole cells with all their processes within one image. Here, the settings were made such that the distance between two consecutive optical sections was less than 1 micron. For double or triple staining, the different

fluorophores were scanned sequentially to rule out crosstalk between the fluorescence detection channels. The following band pass filter settings were used: green fluorescence (Cy2) at 500-540 nm, red fluorescence (Cy3) at 580-650 nm and infrared fluorescence (Cy5) at 680-750 nm.

2.2.1.3.4 Image acquisition and processing

For preliminary image processing, the software LAS AF (Leica Microsystems, Heidelberg, Germany) and ImageJ were used. Afterwards, contrast and brightness of the images were optimized and the layout was processed in Adobe Photoshop.

2.2.2 Multi electrode array (MEA)

2.2.2.1 Background of extracellular recordings

Multi electrode arrays can be used to record extracellular signals from neurons.

The cell membrane is a semi permeable lipid bilayer that separates different ion concentrations (charges) on the inner and outer side of the membrane. Therefore, the cell membrane has the electrical properties of a plate capacitor. The electrochemical gradient results in a membrane potential that can be measured directly with an intracellular electrode. When ion channels are opened due to chemical or electrical stimulation the resistance of the membrane decreases. Ions are moving through the open channels along their electrochemical gradient which results in an inward or outward flow of ions, measured as a transmembrane current.

The extracellular space is conductive as the resistance is very low, if it is not zero, according to Ohm's law, V = R x I (V=potential, R=resistance & I=current).

The extracellular currents that occur upon neuronal activity result in small voltage changes that can be recorded with extracellular electrodes. Extracellular signals are smaller than transmembrane potentials, with the amplitude decreasing with the distance of the signal source to the electrode. Therefore, a close connection between electrode and cell membrane is very important for a high signal-to-noise ratio.

A microelectrode array (MEA) is an arrangement of several electrodes (in this study, 60) allowing recording at once from several sites of a tissue like the retina.

The following components are important for an extracellular recording system:

- Signal source (here retinal tissue);
- Multi electrode array (MEA);
- Filter, amplifier (here MEA1060);
- Recording hardware (USB-MEA devices) and software (MC_Rack).

2.2.2.2 *Invitro* retinal preparation

Retinae from mice of the C57BL/6J strain were used for control experiments. Mice of the mutant strain C57BL/6J-Pde6b^{rd10}/J (*rd10* mouse) and mice treated by intraperitoneal injection of N-methyl-N-nitrosourea (MNU; injections performed by Sarah Rösch, Augenklinik, Aachen, Germany) were used as retinal degeneration models. The preparation scheme for retinal recordings is shown in Figure 3.2. Animals were deeply anesthetized with isoflurane and decapitated. The eye balls were enucleated and transferred to AMES medium (Sigma Chemicals, Germany). AMES medium was buffered with sodium bicarbonate (according to manufacturer's instructions) and equilibrated with a gas mixture of 95% oxygen and 5% carbon dioxide, bringing the pH of the solution to 7.38 - 7.40. The interval between death and transfer of the eye to AMES medium was 1 to 2 minutes. The eye was hemisected parallel to the ora serrata. Carefully the front part of the eye with cornea, lens, and vitreous body was removed without damaging the retina. The retina was cut into halves while still in the eye cup, then the retina was detached from the eye cup. One full retina with eye cup and half retina from second eye were stored in oxygenized AMES buffer for next experiments. A second half retinal piece was transferred with the ganglion cell side up onto a nitrocellulose filter (pore size 0.8 µm, MF-Millipore™ Membrane Filters, Millipore, Germany). The size of the Millipore filter was 5 mm x 5 mm with a central hole of 2 mm diameter. The filter/retina sandwich was transferred onto an inverted petri dish and the excess amount of buffer was aspirated with filter paper. The filter/retina sandwich was placed onto the MEA with the ganglion cells facing the electrodes. The retina was left dry for 30 seconds to 1 minute to improve the attachment of the tissue to the electrodes. Then the MEA chamber was filled with AMES medium and transferred to the amplifier for the recordings. The MEA was fitted with a perfusion inlet working on the phenomenon of gravity and the flow rate of 3-4 ml/min was maintained throughout the experiment with the help of clamps in tubing for the continuous inflow of oxygenized AMES buffer and pharmacological agents. For the outflow of buffers, MEA chamber was fitted with perfusion outlet working with the help of peristaltic pump. Physiological responses were studied under these conditions for approximately a period of one hour per piece of retina after the animal had been sacrificed.

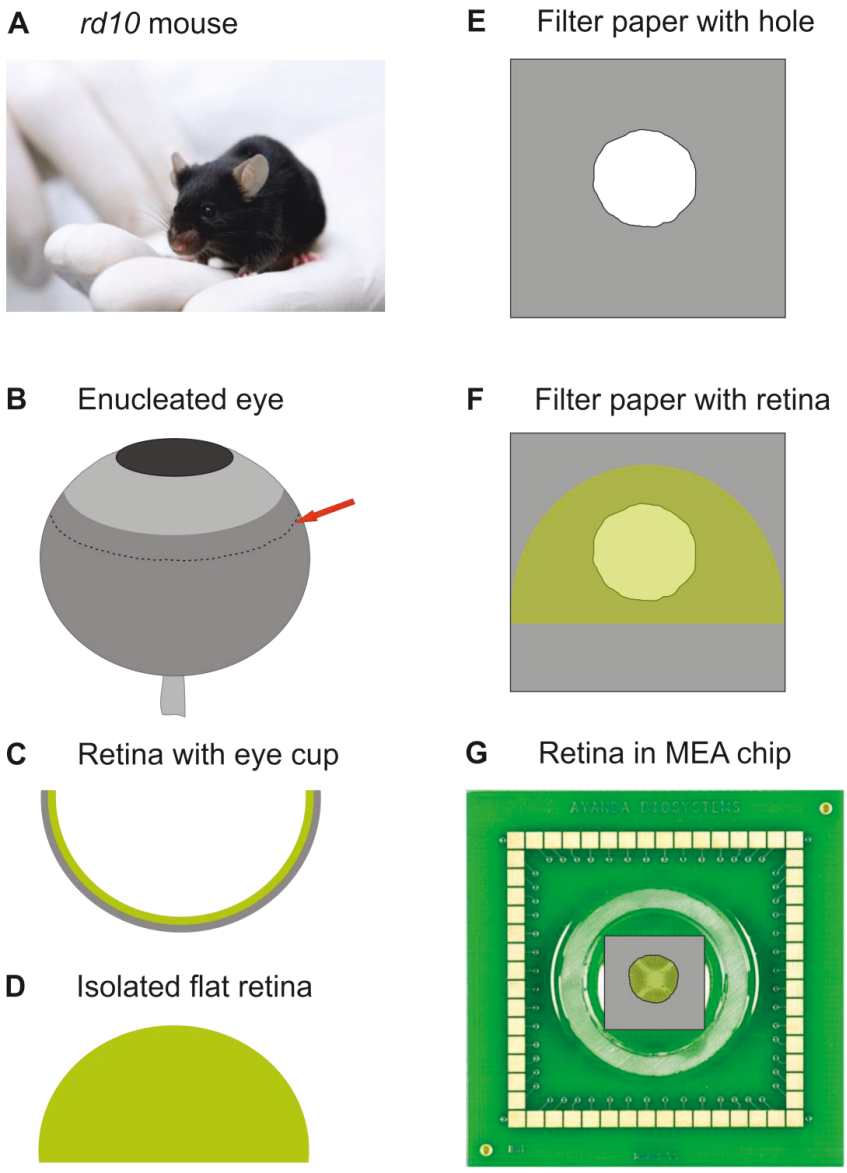

Figure 2.2 Schematic presentation of the preparation steps for retinal MEA recordings. A) The eye of *rd10* mouse indicated by orange dashed square. B) The enucleated eye is opened close to the equator with scissors indicated by a red arrow. C) The retina with eyecup. D) One flattened half of the isolated retina. E) Filter (size 5 mm x 5 mm) with a hole of 2 mm. F) Retina placed on top of the filter with ganglion cells up. G) 3D MEA with retina sandwiched in-between electrodes and filter with ganglion cells facing electrodes.

2.2.2.3 Setup for retinal recordings

2.2.2.3.1 MEA system

The multi electrode array (MEA) system that includes the basic measurement equipment needed for *in vitro* retinal recordings was manufactured by Multi Channel Systems (MCS GmbH, Reutlingen, Germany). It comprized MEAs, a preamplifier stage with a heating system, perfusion cannula (PH01), temperature controller (TCX-Control), computer and software for data recording. In Figure 2.3, the parts of the MEA setup are presented. The system has been developed for performing electrophysiological extracellular recordings with multiple channels from an isolated retina.

Figure 2.3 The components of the MEA work station used in this study. Preamplifier with heating system, perfusion cannula (PH01), temperature controller (TCX-Control), computer and software for recording the data.

The MEA system amplifier (as shown in Figure 2.4) used in the measurements (MEA60-Up-System) had a gain of 1200 and a recording bandwidth from 1 Hz to 8 kHz. It was designed for the use with upright microscopes and had an integrated heating element and temperature sensor. The device had an integrated analog-digital converter (ADC) board. The digitally

converted electrode signals were transmitted to a data acquisition computer via USB 2.0 (High Speed). The ADC of the MEA system was done with an MC_Card with a data resolution of 14 bits and a conversion rate of 12.8 MB/s. The maximum sampling frequency for each channel was 50 kHz. The card had 64 analog and 16 digital input channels, and 16 digital output channels.

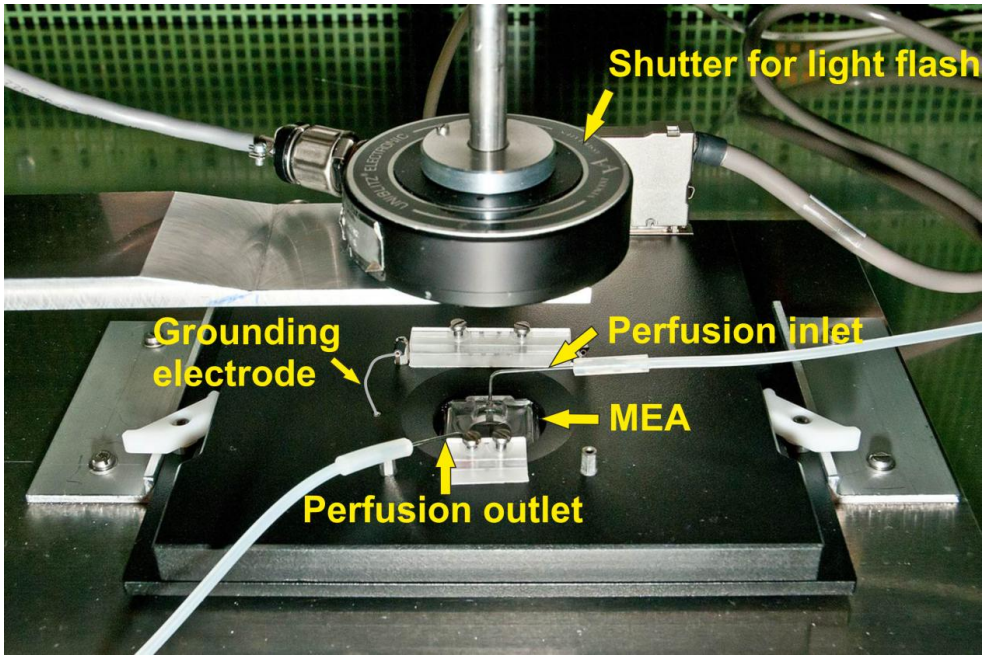

Figure 2.4 The components of the experimental setup showing the preamplifier fixed on a table for stability. The MEA with the retina was placed in the centre of the preamplifier for recording, connected with perfusion inlet and perfusion outlet for the continuous perfusion flow. The system was grounded with a reference electrode as indicated. For light stimulation experiments, a white LED (17,000 mcd) with a shutter was used.

2.2.2.3.2 Multi electrode arrays (MEAs)

Two types of MEAs from two different companies were used. The standard MEA (Multi Channel Systems MCS GmbH, Reutlingen, Germany) had 60 active electrodes in an 8 x 8 matrix layout (4 electrodes on corners for analogue signal) with electrode diameters (ø) of 10 µm or 30 µm and inter electrode distances of 100 µm or 200 µm. Electrodes were coated with porous titanium nitride (TiN) to minimize the electrical impedance. The impedance level for MEA electrodes was 50 kΩ at 1 kHz.

The 3D MEA (Qwane Biosciences SA, Lausanne, Switzerland) had 60 platinum electrodes in an 8 x 8 matrix with an electrode diameter (ø) of 30 µm, electrode height of 25-35 µm, and an inter electrode distance of 100 µm or 200 µm. The impedance level for 3D MEA electrodes was 600-900 kΩ at 1 kHz. Retinal activity was recorded with a bandwidth ranging from 10 to 3000 Hz with a gain of 1200.

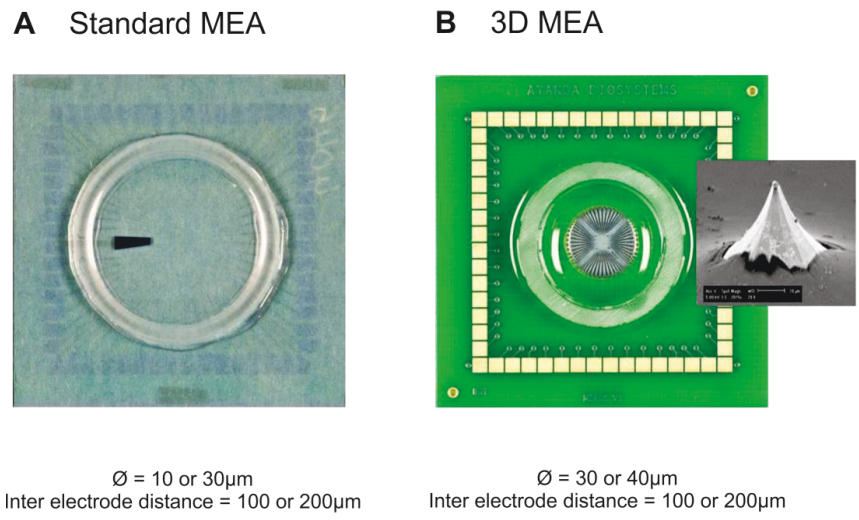

Figure 2.5 MEAs used in the study. A) The standard MEA with 60 electrodes arranged in 8x8 matrix layout embedded in the glass substrate. The electrodes have diameters (ø) of 10 µm or 30 µm and inter electrode distances of 100 µm or 200 µm. The reference electrode is integrated in the MEA at position of the 15th electrode. B) The 3 dimensional (3D) MEAs with 60 electrodes arranged in 8x8 matrix embedded in glass substrate. The shape of the electrodes is conical. The electrodes have diameters (ø) of 30 µm, height of 25-35 µm and inter electrode distance of 100 µm or 200 µm.

2.2.2.3.3 Coating of the MEAs

MEAs were pretreated in two steps on the day of the experiment. First, MEAs were treated in a plasma cleaner (Diener Electronics, Germany) in the coating mode for 2-3 minutes at 55% power in O_2 gas. Second, MEAs were coated for minimum 2 hours with 0.5 mg/ml of Poly-D-Lysine (Sigma, Germany) before explanting the retina onto the electrodes. Both pretreatments were found to strongly improve the recording quality by improving the electrode-tissue contact. Poor electrode-tissue contact was found to be a significant source of noise and a major factor of worsening the quality of the recording.

2.2.2.4 Pharmacological stimulation

Different pharmacological agents were used to target different channels and receptors. Stocks of drugs were prepared in double distilled water or Dimethyl sulfoxide (DMSO) depending on the solubility of the compounds and are stored in -20^0C. Before the experiment, stock solution was diluted in AMES to the desired concentration of the pharmacological agent.

The following pharmacological agents were used: L-(+)-2-Amino-4-phosphonobutyric acid (L-APB), 100 µM, agonist at mGluR6; 6-cyano-2,3-dihydroxy-7-nitro-quinoxaline-2,3-dione disodium (CNQX), 20 µM, AMPA/kainate receptor antagonist; DL-2-amino-5-phosphonopentanoic acid (DL-AP5), 50 µM, NMDA receptor antagonist; 3-((*R*)-2-Carboxypiperazin-4-yl)-propyl-1-phosphonic acid (R-CPP), 40 µM, NMDA receptor antagonist; strychnine, 10 µM, glycine receptor antagonist; bicuculline, 30 µM, $GABA_A$ receptor antagonist; [*S*-(*R**,*R**)]-[3-[[1-(3,4-Dichlorophenyl)ethyl]amino]-2-hydroxypropyl] (cyclohexylmethyl) phosphinic acid (CGP 54626), 2 µM, $GABA_B$ receptor antagonist; (1,2,5,6-Tetrahydropyridin-4-yl)methylphosphinic acid (TPMPA), 100 µM, $GABA_C$ receptor antagonist; meclofenamic acid (MFA), 100 µM, gap junction blocker; cesium chloride (CsCl), 3 mM, HCN channel blocker and 4-Ethylphenylamino-1,2-dimethyl-6-methylaminopyrimidinium chloride (ZD7288), 100 µM, HCN channel blocker.

2.2.2.5 Data Acquisition

2.2.2.5.1 Spontaneous activity

All 60 electrodes could be monitored simultaneously during an experiment. Each channel measured the voltage at a single electrode relative to a ground electrode in the bathing medium. With the grounded electrodes and the retina patch mounted on the array, baseline values were around ± 10 - 12 µV.

Spontaneous activity or spikes (Figure 3.6 A) and spike bursts were recorded from both wild type and *rd10* mouse by using MC_Rack (Data acquisition tool, MCS, Reutlingen, Germany). Digitized data were recorded onto the computer's hard drive (MC_Rack) and further analysed offline. After transfer of the retina to the recording chamber and start of perfusion, recordings were allowed to stabilize for 2 - 5 min as indicated by stable amplitudes of action potentials.

The extracellular electrodes pick up all the signals produced in the nearby area from neurons. In the recordings, two components can be distinguished; action potentials and local field potentials (LFPs). Retinal ganglion cells generate action potentials that are also referred to as 'spikes'. In extracellular recordings from the retina, action potentials appear as sharp spikes, which can be readily distinguished from the baseline (Figure 3.6 A). LFPs reflect changes in neuronal activity like depolarization below spike threshold or changes in the synaptic currents in groups of neurons. LFPs have a slower time course than action potentials. Thus, both components can be easily separated by using different filter settings: high pass (200 - 300 Hz) filtering for spikes and low pass (50 Hz) filtering for LFPs.

2.2.2.5.2 Spike waveform analysis

Spike sorting is an analytical technique used in the analysis of electrophysiological data. Spike sorting algorithms use differences in the shape of spikes collected from an electrode in the tissue to distinguish the activity of one or more neurons from each other and to assign spikes to different neurons. The spiking neurons in the retina are the ganglion cells, the output neurons. The exact time course of a spike event recorded by the electrode depends on the size and shape of the ganglion cell and the distance of the recording electrode from the ganglion cell etc. Each electrode can record the spikes generated by several ganglion cells in its vicinity. Spike shapes are unique and quite reproducible for each individual ganglion cell, which can be used to distinguish spikes produced from different neurons. The techniques often use tools such as principal components or wavelet analysis.

Action potential or spike waveforms taken for further analysis were ≥ 50 µV in amplitude. To distinguish responses from different cells that might appear on the same electrode, a component of the data acquisition software (MC_Rack, MCS, Germany) as well as commercially available software was used for automated sorting of spikes. Each spike originated from single ganglion cell was sorted, and the spike train was time-stamped offline by a spike extraction program (Offline spike sorter, Plexon, Dallas, TX). Further, subsequent analysis was performed to determine whether spikes were generated by the same or different ganglion cells.

Further, the cross-correlation function and the inter spike interval (ISI) analysis can be done. The cross-correlation function between two spike trains determines the time differences between a spike from one cell and a spike from the other cell.

2.2.2.5.3 Fast Fourier Transforms (FFTs)

Evoked neural spikes from retinal ganglion cells convey visual information from the eye to the brain. Each ganglion cell generates different spike train of different form, shape and size, which was sorted and analysed by using spike sorter. Apart from the individual spiking activity from retinal ganglion cell, the whole network of retina generates local field potential (LFP) which can be diagnosed as bigger fluctuations in the baseline. To quantify and analyse these LFPs, some computational algorithm such as Fast Fourier Transform (FFT) was needed. Fourier analysis converts time (or space) to frequency of the LFP and vice versa. FFT gathered the huge information from the recording in the form of simple digits which enables to understand the model system in a better way. The frequency spectra of the LFPs were derived through FFT on the basis of maximum dominating frequency in the baseline recording. The FFT waveforms were constructed with the help of series of processes. First, the raw data got converted into ASCII file with the help of MC_DataTool. Then, FFT was plotted with the custom made script in MATLAB by using low pass filter settings to quantitatively analyse the LFPs under normal and pharmacological application. All MEA recordings were analysed using FFT.

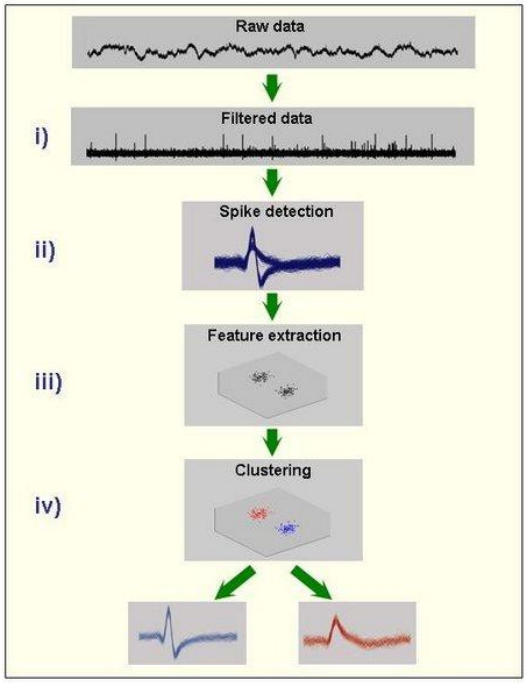

Figure 2.6 Basic steps for the spike sorting. i) The continuous raw data is band-pass filtered with 300 Hz. ii) Spikes are detected, usually using an amplitude threshold. iii) Relevant features of the spike shapes are extracted. iv) These features are the input of a clustering algorithm that performs the classification and different waveforms from a recording can be distinguished.
Taken from http://www.scholarpedia.org/article/Spike_sorting.

2.3 Software Used

Table 2.3 lists the used software.

Table 2.3. Software.

Software	Purpose	Company
WCIF ImageJ 1.37c	Data processing	Wayne Rasband, USA
Photoshop	Image processing	Adobe system, USA
MC_RACK	Data recording and processing	MCS, Reutlingen, Germany
MC_Data Tool	Data processing	MCS, Reutlingen, Germany
Neuroexplorer	Data processing	Plexon, Dallas, USA
Offline Sorter	Data processing	Plexon, Dallas, USA
MATLAB	Data processing and analysis	Mathwork, USA
OriginLab 8	Graphic drawing	OriginLab Corporation, USA
CorelDRAW	Figure drawing	Corel corporation, USA

3. Results

3.1 Immunohistochemical characterization of the *rd10* retina

The aim of this study was to morphologically and functionally characterize the retina of the *rd10* mouse model of retinitis pigmentosa (RP). Several immunohistochemical studies of the *rd10* mouse retina have already been published (Gargini *et al.*, 2007; Phillips *et al.*, 2010). The authors have shown that degeneration occurs in the outer retina, that retinal thickness is reduced considerably over time and that retinal remodelling takes place in the remaining neuronal layers. However, not all issues have been addressed in these studies. In the first part of my study I will provide a comprehensive overview on the degeneration of different retinal cell types. Defined postnatal stages [P6 (postnatal stage 6), P14, P20, P25, P32, P45, P60, and M6 (6 months)] were chosen to monitor the morphology of the developing and degenerating retina. Sections of these postnatal stages were characterized by cell type-specific immunohistochemical markers to reveal pathological changes in identified cell types over time. For comparison, sections of adult wild type mice (C57BL/6) were stained with the same antibodies to show the normal staining pattern in a healthy retina.

3.1.1 Development of *rd10* retina over time (P6 to M6)

Earlier studies of developing *rd10* retina showed that the number of photoreceptor cell rows in the ONL decreases over time (Gargini *et al.*, 2007; Phillips *et al.*, 2010). To investigate the degeneration in the ONL and to get an overview about the fundamental thickness of all retinal layers in the developing *rd10* retina, TO-PRO®-3 was used. TO-PRO®-3 is a fluorescent dye that stains cell nuclei. Figure 3.1.1 shows the TO-PRO®-3 staining in wild type (A) and *rd10* (B-H) retinae at different postnatal stages. Pictures were taken from the central part of the retina near the optic nerve.

The retina can be divided into two parts (compare Figure 3.1.1A). The outer part harbours the photoreceptors with their somata located in the outer nuclear layer (ONL), the inner segments in the inner segment layer (IS) and the outer segments in the outer segment layer (OS). Within the outer plexiform layer (OPL) the photoreceptors synaptically contact neurons of the inner retinal part, horizontal cells and bipolar cells. The cell bodies of horizontal, bipolar and amacrine cells are located in the inner nuclear layer (INL). Bipolar and amacrine cells are synaptically connected to ganglion cells in the inner plexiform layer (IPL). Within the

ganglion cell layer (GCL) somata of ganglion cells and also of displaced amacrine cells are located. The axons of the ganglion cells cluster in the nerve fibre layer (NFL) and relay the visual signals to the brain via the optic nerve. TO-PRO®-3 only stains nuclei and, therefore, the nuclear layers. The IS, OS, OPL, IPL, and NFL are not labelled.

Figure 3.1.1A shows a TO-PRO®-3 staining in adult wild type retina. The ONL was composed of 12 rows of photoreceptor somata. The inner retinal part from the outer border of the INL to NFL revealed a thickness of 80 to 100 µm. The number of cell rows in the ONL as well as the thickness of the inner retina is typical for a healthy retina (Gargini *et al.*, 2007). It should be noted that the retina develops postnatally and reaches maturity only around P35. In particular in the first two weeks (represented by the staining at P6 and P14) the nuclear layers are thicker than in the adult retina as cell division is still going on. The sections shown here from P6 (Fig. 3.1.2B) and P14 (Fig. 3.1.2C) *rd10* retina do not differ from those of wild type retina at the same developmental stage (not shown). The major differences between *rd10* and wild type retina can be observed from P14 on and affect mostly the outer retina, while the inner retina remains less affected. The number of cell rows in the ONL declined to 8 around P25 in the central retina (D). At P32 (E), only 2-3 rows of photoreceptors were residual, at P45 (F) around 1 or 2 rows remained and at P60 (G) it was difficult to identify a clear OPL and thus to distinguish between the outer and the inner retina. In the central retina of 6 month old animals (H) all somata in the ONL were degenerated. However, photoreceptors in *rd10* degenerate within an obvious centre-to-periphery gradient. The number of rows in the ONL decreases in the central retina first, whereas degeneration in the periphery is delayed by 2–3 days (Gargini *et al.*, 2007). As a consequence, photoreceptors of the central retina are completely degenerated after 6 months, but still persist in the more peripheral areas as a discontinous row. In the extreme retinal periphery up to two rows remained (data not shown). These data are in accordance with published results (Gargini *et al.*, 2007).

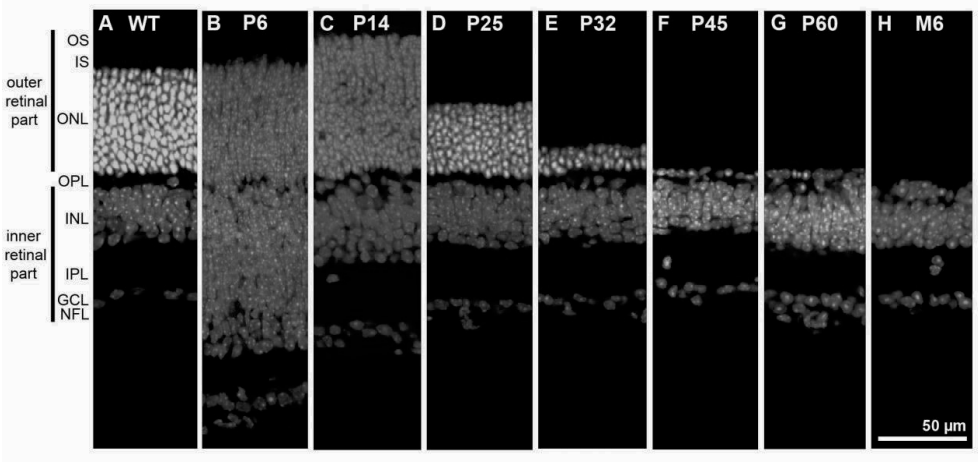

Figure 3.1.1 Comparison of confocal images of TO-PRO®-3 stained retinal sections of wild type mice (A, WT) and *rd10* mice at different postnatal stages (B-H). A) In the adult wild type retina, the ONL exhibits 12 rows of photoreceptor somata. The number of photoreceptors clearly declines at P25 (D). After 2 months photoreceptors are completely degenerated in the central retina. OS, outer segments; IS, inner segments; ONL, outer nuclear layer; OPL, outer plexiform layer; INL, inner nuclear layer; IPL, inner plexiform layer; GCL, ganglion cell layer; NFL, nerve fibre layer. Scale bar: 50 µm.

3.1.2 Photoreceptors and type 2 cone bipolar cells in *rd10* retina

By means of TO-PRO®-3 staining I could show that the ONL degenerates over time in *rd10* retina and that only the inner retina persists after 2 months. In this chapter I first verified the loss of photoreceptors with a specific marker and investigated whether cones degenerate later than rods, as claimed in earlier publications (Carter-Dawson *et al.*, 1978; Garcia-Fernandez *et al.*, 1995; Jimenez *et al.*, 1996; LaVail *et al.*, 1997; Lin *et al.*, 2009).

3.1.2.1 Both types of photoreceptors and type 2 cone bipolar cells

To confirm the degeneration of photoreceptors in *rd10* over time I used antibodies against recoverin, a specific marker for both types of photoreceptors and also for type 2 cone bipolar cells in the mouse retina. Thus, this staining not only enabled me to analyse the degeneration of the outer retina but also to check if cone bipolar cells survive in *rd10* retina.

Figure 3.1.2 represents the staining against recoverin of wild type mouse (A) and *rd10* retinae at the different postnatal stages P6 (B), P14 (C), P20 (D), P32 (E), and after 6 months (F). In the wild type retina (A), the photoreceptors were completely recoverin-positive: the outer segments, the inner segments, the somata in the ONL and the terminal systems in the OPL were strongly marked. Much more weakly, somata (arrowhead), axons (arrow 1) and terminal systems in the IPL (arrow 2) of type 2 cone bipolar cells were stained. In the *rd10* retina at postnatal stage 6 (B), many developing photoreceptors with their somata (arrowhead), axons (arrow 1), terminal systems (arrow 2), and maturing inner segments were already strongly immunoreactive for recoverin. At P14 (C), the ONL displayed 12 – 14 rows of photoreceptors and inner as well as outer segments had clearly developed. Additionally, in the INL first immunoreactivity was visible in the somata (arrowhead) and terminal systems (arrow) of developing type 2 cone bipolar cells. At P20 (D), the ONL was reduced to 7 – 8 rows of somata. Despite this clear degeneration, the inner (arrow 1) and outer segments (arrow 2) of the remaining photoreceptors were still distinguishable but shorter than normal. Furthermore, type 2 cone bipolar cells appeared normal (arrow 3). At postnatal stage 32 (E), 2-3 rows of photoreceptors remained and only residuals of degenerated inner segments were visible (arrowhead). Type 2 bipolar cells were still immunoreactive (arrow 1). In the 6 months old retina (E), some still strongly recoverin-positive photoreceptors were recognizable, but they formed a discontinous row (arrowhead) rather than a clear layer. Thus, neither an ONL nor OPL could be clearly distinguished. Note that this picture was taken in a rather peripheral piece of retina, where photoreceptors survive longer than in central retina (Gargini *et al.*, 2007). Hence, surviving photoreceptors are not in disagreement with the picture shown in Fig. 3.1.1 (TO-PRO®-3 staining) that was taken in the central retina. At 6 months of age, still some somata (arrow) of recoverin-positive type 2 bipolar cells were labelled in the INL, but once more much weaker than at P20.

In summary, after 6 months of degeneration, nearly all photoreceptor somata in the ONL were vanished. The still strongly marked remaining photoreceptor somata in the peripheral retina exhibited no more than residuals of inner segments (data not shown).Type 2 bipolar cells still could be found, but although their general morphology seemed unaltered, the expression level of recoverin had clearly decreased in this cell type.

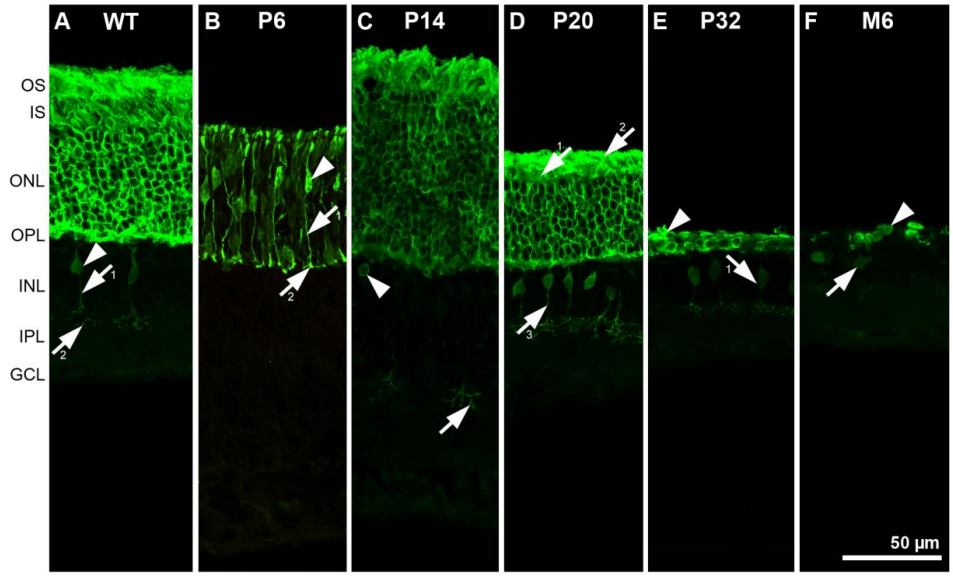

Figure 3.1.2 Comparison of retinal sections of wild type mice (WT, A) and *rd10* mice at different postnatal stages (B-F) stained against recoverin. A) In the wild type retina, the complete outer retina is stained as well as type 2 bipolar cells. B) In *rd10* retina at P6 developing photoreceptors already are recoverin-positive. C) At P14 ONL displays 12–14 cell rows. First developing type 2 bipolar cell somata (arrowhead) and their terminal systems (arrow) are visible in the INL. At P20 (D), the ONL is reduced to 7 – 8 rows of somata. Type 2 cone bipolar cells are marked (arrow 3). E), 2-3 rows of photoreceptors remain with residuals of degenerated inner segments (arrowhead). E) In the 6 months old retina some still strong recoverin-positive photoreceptor somata remain as a discontinuous row (arrowhead). Somata (arrow) of type 2 bipolar cells are marked very weakly. For details see text. Scale bar: 50 µm.

3.1.2.2 The remaining photoreceptors in *rd10* retina are cones

As shown in the previous figure, some photoreceptor somata can be found in *rd10* retina even at the age of 6 months. Since the antibody against recoverin labels rods as well as cones, the staining does not distinguish between both cell types. Thus, in my next approach I used two specific markers for cone opsins, which stained the cones quantitatively: one antibody against red/green opsin and a second antibody against blue opsin. Red/green opsin is sensitive to light of middle to long wavelength while blue opsin is sensitive to light of short wavelength, in the mouse even to ultraviolet light. Cones located in the dorsal part of the mouse retina express red/green opsin, whereas cones in the ventral part can either express blue opsin alone or in conjunction with red/green opsin (Haverkamp *et al.*, 2005). Thus, for this figure I carefully

chose comparable areas on the analysed sections which were taken along the dorso-ventral axis of the retina.

Figure 3.1.3 shows a double staining with antibodies against red/green opsin (green) and against blue opsin (red) on vertical sections of wild type retina (A) and *rd10* retinae (B-F) at the different postnatal stages P6, 14, 25, 60, and after 6 months. In the adult wild type retina cone outer segments were immunoreactive for red/green opsin (green) as well as for blue opsin (red). Double positive outer segments appear yellowish green. The green staining in the inner retina is unspecific background staining. At postnatal stage 6 all cones express blue opsin (Szel *et al.*, 1994) as shown for *rd10* (B): cones were completely marked (developing outer segment: arrowhead, inner segment: arrow 1, soma: arrow 2, axon: arrow 3, synaptic terminal: arrow 4). At P14 (C) red/green (arrow 1) and blue opsin (arrow 2) positive cone outer segments were present as well as double positive outer segments (arrow 3). Within the next two shown postnatal stages P25 (D) and P60 (E), the cone outer segments degenerated considerably and lost their typical morphology (compare to A). After 6 months (F) only within periperal retinal areas immunoreactive cell bodies remained (blue opsin positives in the ventral part, red/green positives in the dorsal retinal part, data not shown), whereas the central retina only displayed some residual blue opsin positive structures within the INL (arrowhead).

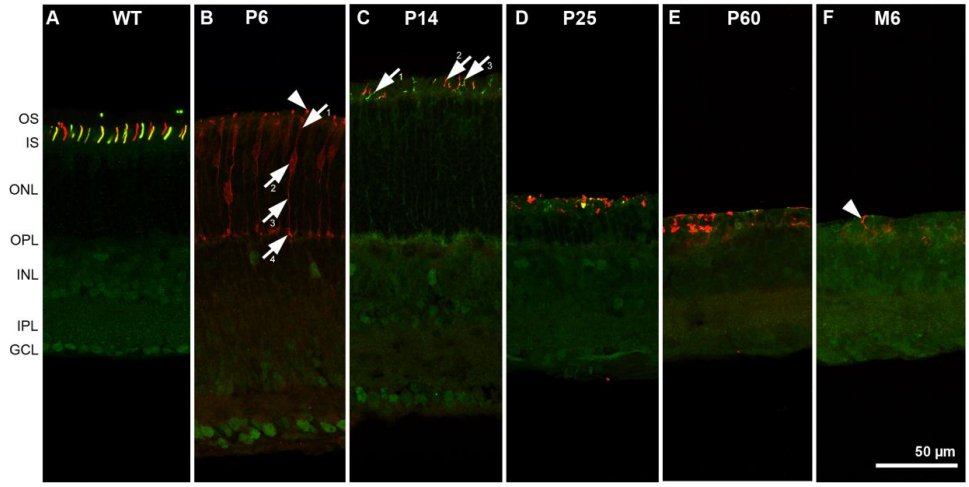

Figure 3.1.3 Immunohistochemical staining against red/green opsin (green) and blue opsin (red) of wild type (A) and *rd10* retinae of different postnatal stages (B-F). A) In the adult wild type retina, cone outer segments are immunoreactive for blue opsin (red) or double positive for blue and red/green opsin (yellowish green). The staining in the inner retina represents unspecific background. B) In *rd10* retina at P6, all cones express blue opsin. C) At P14, red/green (arrow 1) and blue opsin positive (arrow 2) outer segments are present as well as double positive outer segments (arrow 3). D, E) At P25 and P60, cone outer segments are degenerated and have lost their typical morphology. F) After 6 months the central retina only reveals some residual blue opsin positive structures within the INL (arrowhead). Scale bar: 50 µm.

3.1.3 Bipolar cells in *rd10* retina

The mouse retina harbors around 12 known types of bipolar cells: 11 types of cone bipolar cells and one type of rod bipolar cell (Boycott & Wässle, 1991; Wässle *et al.*, 1994; Euler & Wässle, 1995; Ghosh *et al.*, 2004). Bipolar cells transfer the light signals from the photoreceptors to the ganglion cells and thus provide for the vertical pathway in the retina. I presented already results concerning type 2 bipolar cells in chapter 3.1.2.1. In the following I used two more antibodies as bipolar cell type specific markers, anti HCN4 (antibody termed 1A4) and anti PKCα, to check which influence the degeneration of the outer retina has on these types of neurons.

3.1.3.1 Type 3a bipolar cells in *rd10* retina

The antibody 1A4 against HCN4 (hyperpolarization-activated and cyclic nucleotide-gated channel 4) is not only a reliable marker for type 3a bipolar cells but also stains a small population of amacrine cells (Mataruga *et al.*, 2007).

Figure 3.1.4 shows the immunohistochemical staining against HCN4 of adult wild type retina (A) and *rd10* retinae (B-F) at the different postnatal stages 6, 14, 25, 60 and after 6 months. In the adult wild type retina HCN4-positive type 3a cone bipolar cells were completely labelled. The somata (arrowhead) and axons (arrow 1) were more weakly immunoreactive, whereas their dendrites in the OPL (arrow 2) and especially the terminal systems in the IPL (arrow 3) displayed a much stronger immunoreactivity. Additionally, some amacrine cell bodies were weakly HCN4-positive (arrow 4). In *rd10* retina at postnatal stage 6 (B) only few somata showed a weak immunoreactivity in the developing INL (arrowhead). At P14 (C), HCN4 staining became stronger in bipolar cell somata (arrowhead) and their primary dendrites (arrow 1) stratifying in the OPL (arrow 2). The bipolar cells terminal systems in the IPL showed the strongest label (arrow 3). Moreover, some weakly stained amacrine cell bodies could be detected (arrow 4). At P25 (D), the staining pattern resembled the adult wild type retina (compare to A). HCN4-positive bipolar cells (soma: arrowhead) and amacrine cells (soma: arrow 1) were clearly stained and the IPL revealed the typical immunoreactive band which is formed by the intensely positive type 3a axon terminals (arrow 2). At P60 (E), morphological changes in the OPL were clearly visible: irregular ectopic HCN4-positive dendrites of bipolar cells were found in the degenerating OPL (arrowheads). Immunoreactive bipolar cells (arrow 1) with their terminal systems (arrow 2) as well as HCN4-positive amacrine cells (arrow 3) were still clearly stained. After 6 months (F), the central retina displayed only some faintly stained cell bodies (arrowheads) and it was hard to distinguish between bipolar cells and amacrine cells. Nevertheless, some positive bipolar cell dendrites were visible in the OPL (arrow 1). However, the stronger immunoreactive terminal systems of the bipolar cells were still well detectable (arrow 2).

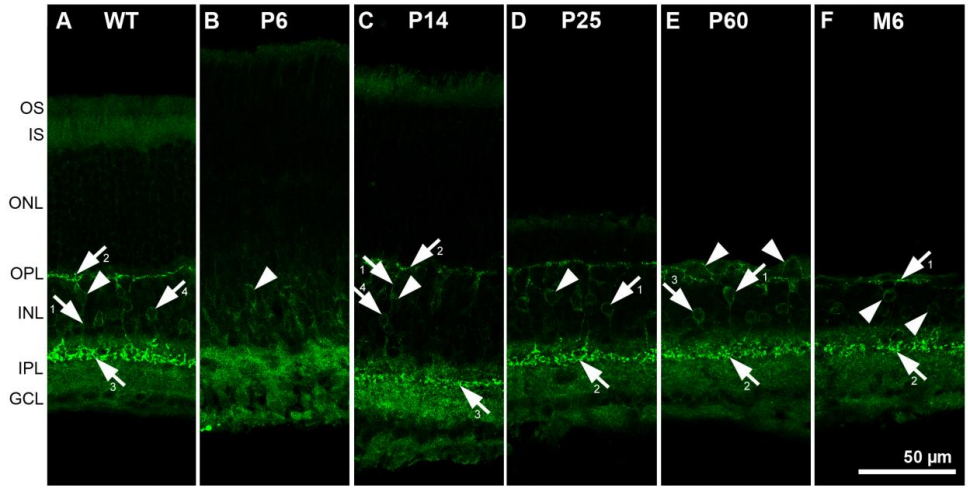

Figure 3.1.4 Immunohistochemical stainings against HCN4 in wild type (A) and *rd10* retinae (B-F) of different postnatal stages. A) In adult WT retina HCN4-positive bipolar cells are completely marked. B) At P6, only some few HCN4-positive somata are visible in the developing INL (arrowhead). C) At P14, HCN4-positive bipolar cells (arrows 1 – 3) as well as some immunoreactive amacrine cells (arrow 4) are observed. D) At P25, the staining pattern resembles the adult wild type retina (compare A). E) HCN4-positive dendrites of the bipolar cells traverse the degenerating OPL (arrowheads). Immunoreactive bipolar cells as well as HCN4-positive amacrine cells are still clearly stained. F) After 6 months, only few faintly stained cell bodies (arrowheads) are detectable in the central retina (arrowheads). Some positive bipolar cell dendrites are visible in the OPL (arrow 1) while axon terminal systems of type 3a bipolar cells in the IPL are still strongly immunoreactive. For details see text. Scale bar: 50 µm.

3.1.3.2 Rod bipolar cells persist even after months of degeneration in *rd10* retina

In mouse, rod bipolar cells account for the most numerous subtype of bipolar cell. These cells have elliptically shaped somata of about 6 µm in diameter, a bushy chandelier-like dendritic arborization and long axons that stratify in the innermost stratum of IPL (Figure 3.1.5). Rod bipolar cells can be stained with antibodies against the α-isoform of protein kinase C (PKCα, (Haverkamp & Wässle, 2000). PKCα-positive amacrine cells and some cells in the GCL are also marked. I checked the influence of the degenerating outer retina on rod bipolar cells by using the antibody against PKCα.

Figure 3.1.5 shows the immunohistochemical staining against the PKCα on vertical sections of wild type retina (A) and *rd10* retinae (B-E) at the different postnatal stages 6, 14, 32, and M6. In the adult wild type retina (A), rod bipolar cells were completely and intensely stained.

The bushy dendrites in the OPL (arrowhead, see also insert), the cell body (arrow 1), and the long axon (arrow 2) with its strongly immunoreactive thickened terminal systems in the IPL (arrow 3) were marked. Additionally, some amacrine cell bodies in the INL were PKCα-positive (arrow 4) as well as some somata of ganglion cells or displaced amacrine cells in the GCL (not visible in figure A, but compare figure D, arrow 4). In the *rd10* retina at postnatal stage 6 (B), only some weakly stained maturing cell bodies in the developing INL (arrowhead) and in the GCL (arrow) were visible. At P14 (C), rod bipolar cells were as immunoreactive as in adult wild type retina (dendrites: arrowhead, soma: arrow 1, axon: arrow 2, terminal systems: arrow 3). Nevertheless, the dendrites were much shorter and rarer than in wild type (compare inserts of figures A and B). Some weakly stained amacrine cell bodies in the INL (arrow 4) and some cells in the GCL (not visible here) were also PKCα-positive. At postnatal stage 32 (D), some of the rod bipolar cell somata had migrated into the OPL (arrowhead). Furthermore, immunoreactive dendrites had vanished completely (compare insert). The axons (arrow 1) and terminal systems (arrow 2) of the rod bipolar cells displayed a much weaker immunoreactivity than before or in adult wild type. Still, some faintly stained PKCα-positive amacrine cells (arrow 3) and cell bodies in the GCL (arrow 4) were observed. After 6 months (E), many rod bipolar cell somata were displaced from the INL, protruding in the remaining ONL (arrowhead). It is not as easy as before to distinguish between bipolar and amacrine cell somata. Some putative rod bipolar cell somata (arrow 1), their axons (arrow 2) and terminal systems (arrow 3) displayed weaker immunoreactivity than in earlier postnatal stages or in wild type retina. Nevertheless, still, some faintly PKCα-positive amacrine cell bodies in the INL (arrow 4) and cell bodies in the GCL (arrow 5) were visible.

In summary it seems, that the loss of photoreceptors leads to the reduction of PKCα expression in rod bipolar cells and amacrine cells. Furthermore, the rod bipolar cells become disorganized.

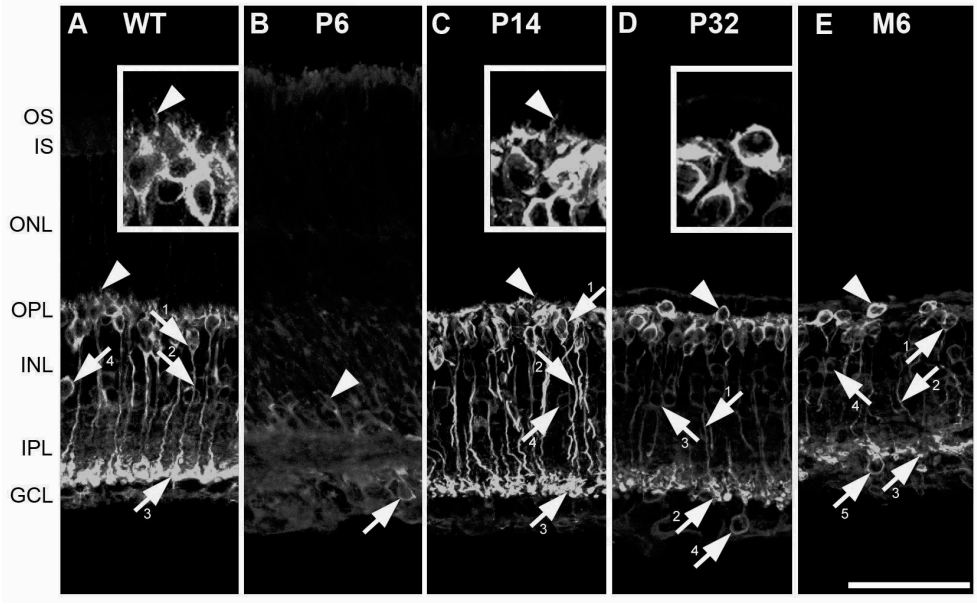

Figure 3.1.5 Immunohistochemical staining against PKCα in wild type (A) and *rd10* retinae (B-E) of different postnatal stages. A) In adult WT retina, rod bipolar cells are completely stained. Additionally, some amacrine cell bodies (arrow 4) and some cell bodies in the GCL are PKCα positive (not visible in figure A, compare figure D, arrow 4). B) At P6, some weakly stained cell bodies in the developing INL (arrowhead) and GCL (arrow) are visible. C) At P14, rod bipolar cells are stained as strongly as in wild type retina, but the dendrites are much shorter and rarer than in wild type (compare inserts of figures A and B). Arrow 4: weakly stained amacrine cell body. D) Some rod bipolar cell somata have migrated into the OPL (arrowhead) at P32. Dendrites are completely lacking (compare insert). Axons (arrow 1) and terminal systems (arrow 2) are more weakly immunoreactive than before. Arrow 3: PKCα-positive amacrine cell; arrow 4: ganglion cell body. E) Lots of displaced immunoreactive rod bipolar cell somata after 6 months (arrowhead). Somata (arrow 1), axons (arrow 2) and terminal systems (arrow 3) display weaker immunoreactivity than in wild type. Arrow 4: faintly PKCα-positive amacrine cell body; arrow 5: PKCα-positive cell body in the GCL. For details see text. Scale bar: 50 µm (overview), 20 µm (insert).

3.1.4 Horizontal cells in *rd10* retina

In the inner nuclear layer of the mouse retina 3% of all cells are horizontal cells and 39% are amacrine cells (Jeon *et al.*, 1998). While bipolar cells form vertical excitatory pathways, horizontal cells together with amacrine cells provide for lateral pathways in the retina and are important for the processing and enhancement of contrasts.

In the following I used an antibody against calbindin D (CaBP), which stains horizontal cells as well as some subtypes of amacrine cells (Peichl & Gonzalez-Soriano, 1994; Haverkamp & Wässle, 2000) to investigate the impact degeneration of the outer retina has on these two important classes of retinal interneurons. While Gargini and co-workers (Gargini *et al.*, 2007) reported only slight changes in horizontal cells in *rd10*, more pronounced changes were described by Phillips and co-workers (Phillips *et al.*, 2010). Therefore, in the following changes in horizontal cells were studied in detail.

Figure 3.1.6 shows the immunohistochemical stainings against CaBP in vertical sections of wild type retina (A) and *rd10* retina (B-E) of the different postnatal stages 6, 14, 32, and after 6 months. In the adult wild type retina (A), horizontal cells were strongly immunoreactive.The large cell bodies near the OPL (arrow 1) were marked as well as the dendritic and extensive axonal arborization (arrow 2) in the OPL. Horizontal cells contact cones with their dendritic processes and rods with their strongly arborized axon terminal system by sending two processes into the invagination at the rod spherule base. As rod spherules are also found in the inner two rows of ONL, horizontal cell processes form typical pairwise dot-like postsynaptic endings in the OPL and the innermost ONL (arrowhead, see insert). In the inner retina, three weaker bands were marked in the IPL (1-3). Band 1 and 3 are formed by the ON- (1) and OFF-cholinergic amacrine cells (3), respectively, band 2 in the middle of the IPL is formed by NO synthase-positive amacrine cells (Haverkamp *et al.*, 2000). Some weakly immunoreactive amacrine cell bodies were detectable in the INL (arrow 3) and as displaced amacrine cells in the GCL (arrow 4). Furthermore, some large CaBP-positive ganglion cell somata (Haverkamp & Wässle, 2000) could be found (arrow 5). The 6 days old *rd10* retina (B) revealed large immunoreactive somata of horizontal cells near the OPL (arrow 1). Additionally, the arborization of the maturing horizontal cell processes was stained (arrow 2). Within the IPL, two broad bands were CaBP-positive (1 and 2) and labeled somata were visible in the INL (arrow 3) as well as in the GCL (arrow 4). At P14 (C), the first signs of degeneration could be observed in the central retina. Some horizontal cell bodies (arrow 1) were displaced towards the inner part of the INL. The fine end-terminal processes in the OPL wee stained, but clear punctuate staining of the dendritic and axonal synaptic endings as in wild type retina could not be observed (arrowhead, compare insert C with insert A). The IPL revealed 2 immunoreactive bands (1 and 2) and CaBP-positive amacrine cell somata in the INL (arrow 2) and in the GCL (arrow 3). Sometimes larger putative ganglion cell somata

could be found (not visible here). At P32 (D), some of the horizontal cell processes grew through the INL (arrow 1). Although the retina was fully developed, the fine postsynaptic processes in the OPL were not as clearly detectable as in wild type (arrowhead, compare also insert A with insert D). The IPL revealed the same three CaBP-positive bands as in wild type (1-3). Within the INL and GCL the typical immunoreactive amacrine cell somata were visible (arrow 2 and 3) and in the GCL some putative large ganglion cell somata could be found (arrow 4). After 6 months in the central retina (E) horizontal cells had totally lost their fine end-terminal processes emerging from higher order branches in the OPL (arrowhead, compare insert). Lots of somata were shifted into the middle or inner part of the INL (arrow 1). Horizontal cell processes spread through the INL (arrow 2). Weakly immunoreactive amacrine cell somata were still visible in the INL (arrow 3) and GCL (arrow 4) as well as the three distinct bands of amacrine cells in the IPL (1-3). Some CaBP-positive large putative ganglion cell somata were also detectable (here not visible).

In summary, after months of degeneration of the outer retina, horizontal cells and amacrine cells are still present. The CaBP-positive amacrine cells and their stratification within the IPL seem to be little affected. However, horizontal cells seem to undergo a substantial remodelling process as also observed by (Barhoum *et al.*, 2008; Phillips *et al.*, 2010).

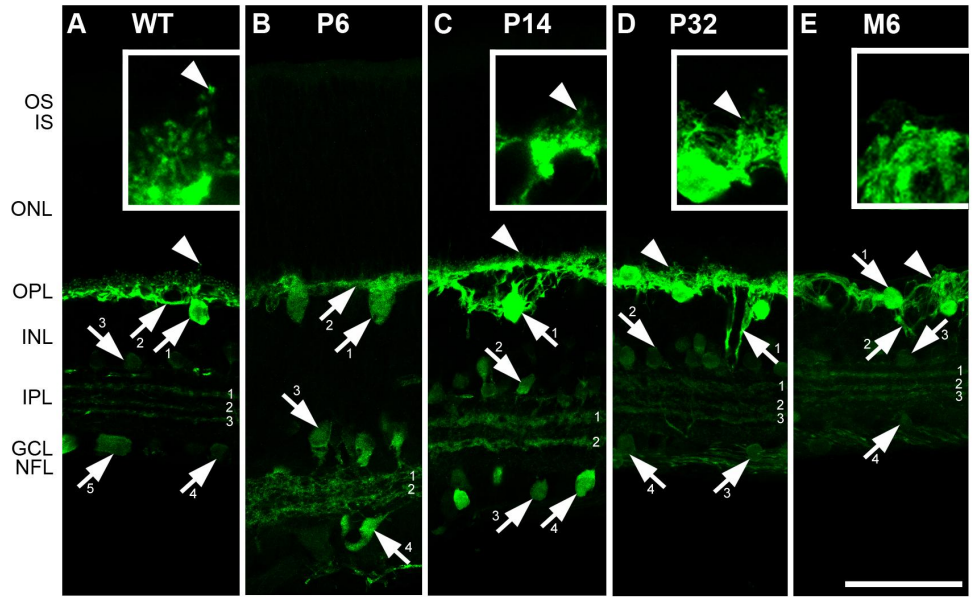

Figure 3.1.6 Immunohistochemical staining against CaBP in wild type (A) and *rd10* retinae (B-E) of different postnatal stages. A) In adult WT retina, horizontal cells are strongly immunoreactive for CaBP. Some types of amacrine cells are more weakly immunoreactive (1, 2, 3: three positive bands formed by amacrine cell processes). Faintly immunoreactive amacrine cell bodies in the INL (arrow 3) and in the GCL (arrow 4). Arrow 5: large CaBP positive ganglion cell soma. B) At P6, large immunoreactive somata near the OPL (arrow 1) and dendritic and axonal arborization of the maturing horizontal cells are stained (arrow 2). 1 and 2: two broad CaBP positive bands in the IPL. Immunoreactive somata in the INL (arrow 3) as well as in the GCL (arrow 4). C) At P14, some horizontal cell bodies started to migrate to the inner part of the INL (arrow 1). The postsynaptic endings in the OPL are faintly stained (arrowhead, insert). Two immunoreactive bands (1 and 2) in the IPL are marked, furthermore amacrine cell somata in the INL (arrow 2) and GCL (arrow 3) and also ganglion cells (arrow 5). D) At P32, some processes of CaBP positive horizontal cells grow through the INL (arrow 1). The fine postsynaptic processes in the OPL are not as clear detectable as in wild type retina (arrowhead, compare also insert D with insert A). Three CaBP positive bands in the IPL (1-3) and immunoreactive amacrine cell somata are visible in the INL (arrow 2) and GCL (arrow 3), additionally some putative large ganglion cell somata (arrow 4) in the GCL. E) After 6 months (E), the horizontal cells totally lost their fine, end-terminal processes in the OPL of the central retina (arrowhead, insert). Lots of somata are shifted towards the inner INL (arrow 1). Immunoreactive amacrine cell somata are visible in the INL (arrow 2) and GCL (arrow 3) as well as the three distinct bands in the IPL (1-3). Scale bar: 50 µm (overview), 20 µm (insert).

3.1.5 mGluR6 receptors in the ON pathway in *rd10* retina

In wild type retina, synaptic transmission between rods and rod bipolar cells as well as cones and cone ON-bipolar cells occurs through glutamate and a specific type of metabotropic glutamate receptor, mGluR6 by generating a hyperpolarizing postsynaptic potential in these bipolar cells in the presence of light (Nomura *et al.*, 1994; Masu *et al.*, 1995; Mataruga *et al.*, 2007; Koike *et al.*, 2010a). Thus, mGluR6 mediates the vertical ON pathways in the mammalian retina.

Figure 3.1.6 shows the staining against mGluR6 in wild type mouse (A) and *rd10* retinae at the postnatal stage P60 (B) and after 6 months (C). In the wild type retina (A) mGluR6 was found in two morphologically distinct structures. By double labelling with antibodies against PKCα (data not shown but see references) the cloud of fine puncta spreading from the OPL into the first row of somata in the ONL (punctuate staining in A, arrowheads) could be identified as dendritic tips of rod bipolar cells (Nomura *et al.*, 1994; Mataruga *et al.*, 2007). By double labelling with peanut agglutinin (PNA, data not shown) the mGluR6-positive dendritic tips of cone ON-bipolar cells invaginating the cone pedicles were identified (arrows in A). As the dendritic tips are densely packed, at this magnification puncta merge into a flat continuously stained structure (Nomura *et al.*, 1994; Mataruga *et al.*, 2007). As a consequence of the loss of photoreceptor input during retinal degeneration, the distribution of mGluR6 changed. In *rd10* retina at P60 (B), punctate mGluR6 staining could not be observed. In contrast, a much weaker, cloudy immunoreactivity for mGluR6 could be found within the INL, probably on bipolar cell somata (as indicated by arrowheads). In the 6 month old *rd10* retina (C), immunoreactivity for mGluR6 was even weaker and seemed to be restricted to small areas (arrowheads).

In summary it seems that during the degeneration of the *rd10* retina the expression level of mGluR6 was dramatically reduced, most probably correlated with the degeneration of ON-bipolar cell dendritic processes.

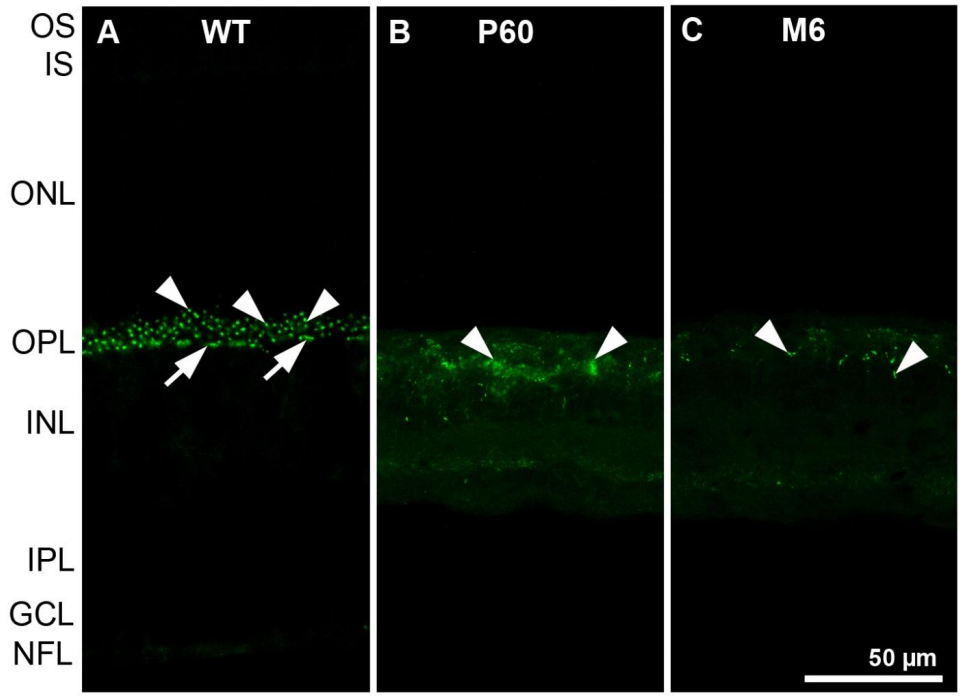

Figure 3.1.7 Immunohistochemical staining against mGluR6 in wild type (A) and *rd10* retinae (B-F) at P60 (C) and M6 (C). A) In adult WT retina mGluR6 is found on dendritic tips of rod bipolar cells (arrowheads) and cone ON-bipolar cells (arrows). In *rd10* retina at P60 (B), punctuate staining in the OPL has vanished, weak cloudy immunoreactivity is found within the INL (arrowheads). In M6 *rd10* retina (C), immunoreactivity for mGluR6 in the OPL has decreased furthermore and seems to be randomly distributed within the outer part of the INL (arrowheads). Scale bar: 50 µm.

3.1.6 TRPM1 in the ON pathway in *rd10* retina

TRPM1 (also known as melastatin 1, or MLSN1) is a non selective cation channel negatively regulated by glutamate (Koike *et al.*, 2010b) and was recently identified as the cation channel that mediates the depolarizing light response in ON-bipolar cells (Morgans *et al.*, 2009; Koike *et al.*, 2010b; Shen *et al.*, 2012).

Figure 3.1.7 shows a staining against TRPM1 of wild type mouse (A) and *rd10* retinae at P60 (B) and after 6 months (C). In the wild type retina (A) the antibody against TRPM1 stains the

somata (arrow 1) and processes of Müller cells with their endfeet (arrow 2). More weakly, somata and dendrites of ON-bipolar cells (arrowhead) are labelled.

Other studies showed that the corresponding presynaptic region could be marked with an antibody against CtBP2, a reliable marker for the presynaptic ribbon structure in the terminal systems of rod and cone photoreceptors (Schmitz *et al.*, 2000; Morgans *et al.*, 2005; tom Dieck *et al.*, 2005). The postsynaptic location of TRPM1 could further be confirmed by double labelling with peanut agglutinin (PNA), a reliable marker for cone end feet (Blanks & Johnson, 1984). Thus, TRPM1 was localized to the dendrites of both rod and cone ON-bipolar cells, where it is optimally positioned to respond rapidly to light induced changes in the synaptic glutamate levels (Krizaj *et al.*, 2010).
In *rd10* retinae at P60 (B) and M6 (C) Müller cell staining was similar to wild type but weaker (arrows 1 and 2). ON-bipolar cells were still weakly labelled by the TRPM1 antibody (arrowheads).

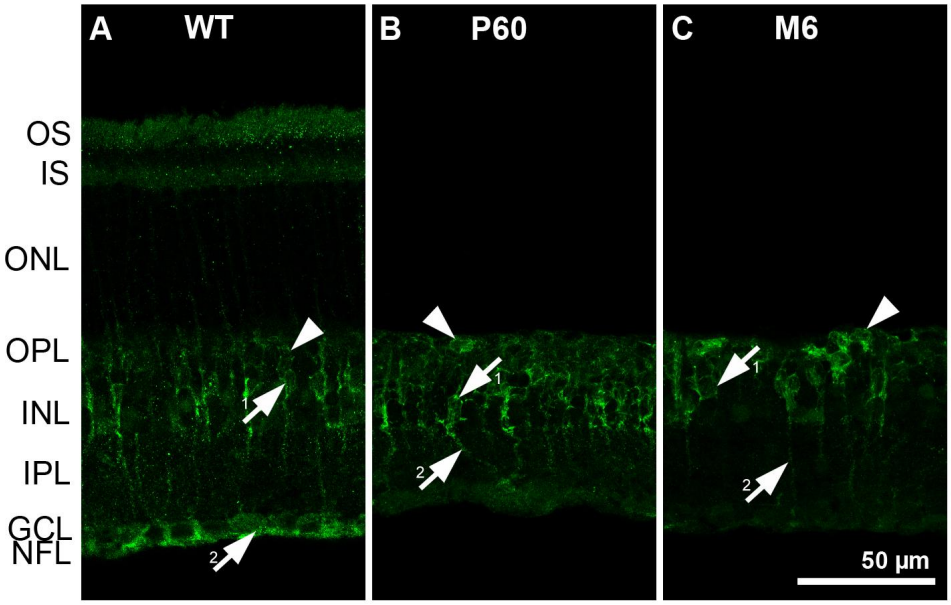

Figure 3.1.8 Immunohistochemical staining against TRPM1 in wild type (A) and *rd10* retinae at P60 (B) and M6 (C). A) In adult WT retina some somata (arrowhead) of ON-bipolar cells are faintly stained. Additionally, some putative Müller cell somata (arrow 1) with their processes and endfeet (arrow 2) could be observed. In *rd10* retinae at P60 (B) and M6 (C), staining was similar but weaker.

3.1.7 Gliosis in *rd10* retina

Müller cells are the major type of retinal non-neuronal cells and serve as support cells for the retinal neurons (Uga & Katsume, 1969; Miller & Dowling, 1970; Rasmussen, 1974). In the healthy wild type retina, Müller cells express glutamate synthetase (GS), whereas astrocytes express the glial fibrillary acidic protein [GFAP; (Eisenfeld *et al.*, 1984; Gargini *et al.*, 2007)]. However, upon injury of the retina or during photoreceptor degeneration, it has been reported that Müller cells become reactive and also start to express GFAP (Eisenfeld *et al.*, 1984; Marc *et al.*, 2003; Gargini *et al.*, 2007; Sarthy, 2007). In the following I checked if the photoreceptor degeneration of *rd10* might cause gliosis.

Figure 3.1.9 shows a double staining against GFAP (green) and GS (red) of wild type mouse (A) and *rd10* retinae at different postnatal stages (B-E). In the adult wild type retina (A),

processes of astrocytes were stained for GFAP in the NFL (arrow) and sometimes in the GCL (arrow 1). The GS-immunoreactive somata of Müller cells were localized in the middle of the INL (arrow 2). From here, their processes projected through all inner retinal layers as well as the ONL. There endfeet formed the outer (arrow 3) and inner (arrow 4) limiting membrane of the retina, respectively. In the *rd10* retina at postnatal stage 14, both staining resembled the staining patterns found in adult wild type retina. At P25 (C), GFAP-positive structures were detectable within the whole inner retinal layers (within the NFL: arrowhead; within the IPL: arrow 1; within the INL: arrow 2) as well as in the remaining outer nuclear layer (arrow 3). At postnatal stage 60 (D) and after 6 months (E), the staining against GFAP was restricted once more mostly to the NFL (arrowheads). Sometimes, some immunoreactive structures could be detected in the GCL (not shown) and IPL (not visible in D, but compare E, arrow 1). Within the last three shown postnatal stages, the expression of GS was as strong as in wild type retina or the P14 *rd10* retina, but only few clearly labelled Müller cell somata could be found (D, arrow 1; E arrow 2).

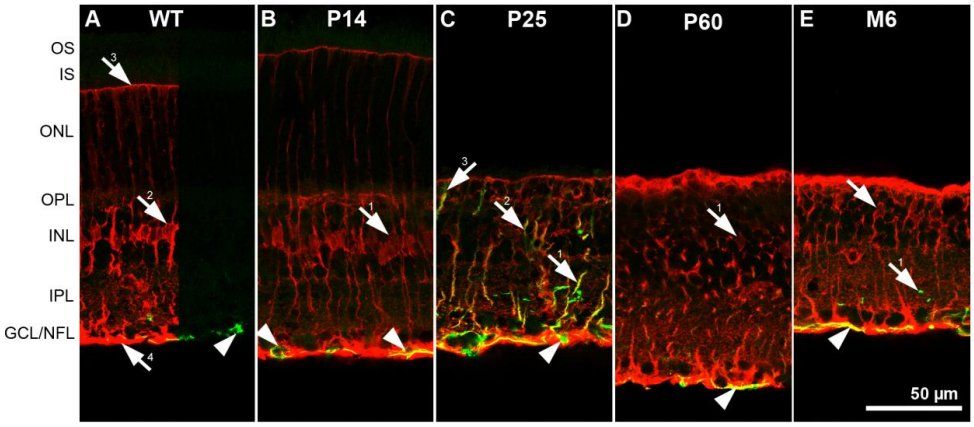

Figure 3.1.9 Immunohistochemical staining against GFAP (green) and GS (red) in wild type (A) and *rd10* retinae (B-E) of different postnatal stages. A) In adult WT retina, GFAP-positive structures are present in the NFL (arrowhead) and GCL (arrow 1). GS-positive Müller cell somata can be found in the middle of the INL (arrow 2). Their processes traverse the whole retina and form the outer (arrow 3) and inner limiting membrane (arrow 4). B) In *rd10* retinae at P14, GFAP-positive astrocytes are present in NFL (arrowheads). Müller cells span the whole retina from GCL to ONL/IS border. C) In *rd10* retinae at P25 (C), GFAP-positive structures are detectable within all inner retinal layers as well as in the remaining outer nuclear layer. At P60 (D) and after 6 months (E), the staining against GFAP is restricted again mostly to the NFL (arrowheads). Sometimes, some immunoreactive structures can be detected in the GCL (not shown) and IPL (E, arrow 1). Within the last three shown postnatal stages, the expression of GS is as strong as in wild type or P14 in *rd10* retina, only sometimes clearly labelled Müller cell somata can be found. Scale bar: 50 µm.

3.2 Functional electrophysiological characterization of the *rd10* retina

In the previous part, the mouse model for retinal degeneration, *rd10* was characterized using immunohistochemistry. During the first weeks postnatally, the photoreceptors degenerate and after few months only the inner retina persists. In this part of study, the physiological properties of the *rd10* retina were characterized using multi electrode arrays (MEAs).

3.2.1 MEA recording from wild type retina

Most experiments were performed using 3D MEAs with 60 electrodes arranged in an 8x8 matrix, as shown in Fig. 2.5 A & B. Retinae of both wild type and *rd10* mice were prepared as described in the methods section and a retinal piece was placed with the ganglion cell side down onto the electrodes of a 3D MEA. Figure 3.2.1 A shows a typical recording from a wild type retina. In the recording two components could be identified: a baseline and numerous short stochastically occurring voltage deflections. These fast voltage changes represent action potentials (spikes) from a ganglion cell. Recordings could be made for 1 to 1.5 hours from one piece of retina during continuous superfusion with oxygenized AMES solution. In the first experiments, the physiological condition of the retina was checked by recording the response of the retina to light flashes. Such an experiment is shown in Figure 3.2.1 B. Upon stimulation with a 100 ms long light flash (red arrow) a strong response could be observed in the recording: a negative going deflection was followed by a positive going deflection before the signal returned to the control baseline level. These large deflections are much slower than action potentials. They reflect the summed activity of many retinal cells and are also called local field potentials (LFPs). The response of a retina to light stimulation recorded on a MEA is in principle similar to the electroretinogram (ERG) recorded from the cornea of an intact eye and is, therefore, also called µERG. The spikes of retinal ganglion cells are superimposed on the µERG. In this recording, ganglion cell spikes were readily recorded before the light flash. During the first part of the negative deflection, no spikes could be observed but they returned during the second half of the response. This indicates that these spikes originated from an OFF-ganglion cell, whose activity was suppressed by the light flash. The origin of the different components in the µERG was not analysed as this was beyond the scope of this thesis. However, the fact that light responses can be recorded from the retinal pieces even after several hours *in vitro* indicates that the tissue was viable and healthy.

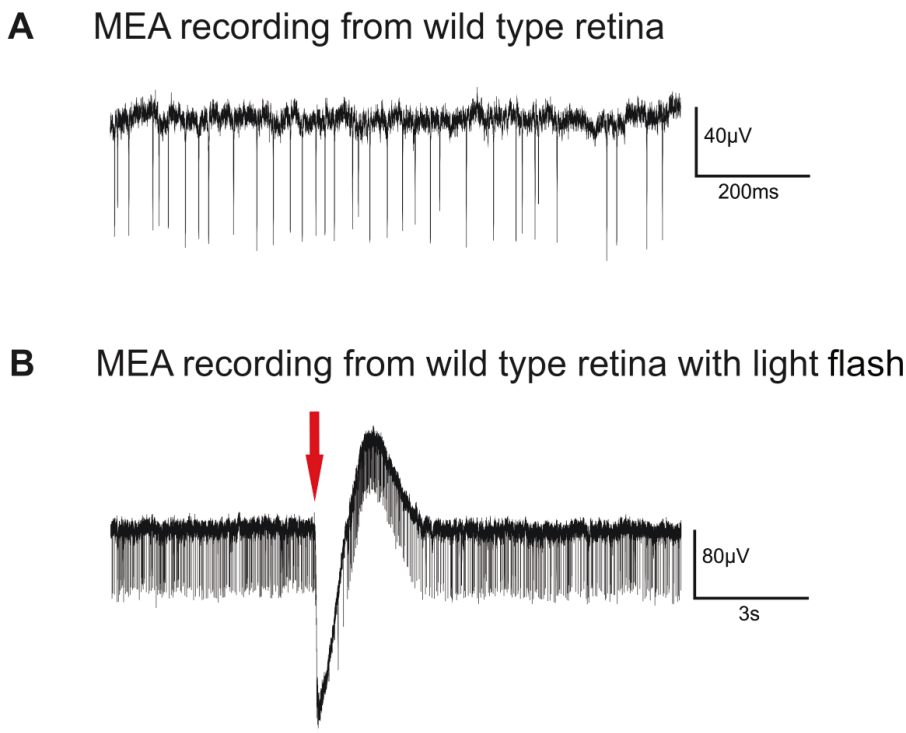

Figure 3.2.1 3D MEA recording from wild type retina. A) Extracellular recording from wild type retina, showing spontaneous action potentials from ganglion cells. B) Recording of a µERG from wild type retina. Red arrow: 100 ms light flash. The retina can still respond to light stimuli *in vitro*.

3.2.2 Functional characterization of *rd10* retina using multi electrode arrays (MEAs)

3.2.2.1 *rd10* retina shows spontaneous rhythmic activity

Figure 3.2.2 compares the recordings from the retinae of a wild type (left) and an *rd10* mouse (right). In both recordings the two components - action potentials and local field potentials (LFPs) - described in Figure 3.2.2 A & D could be isolated using appropriate filter settings. Figure 3.2.2 B & E show action potentials isolated using a high pass filter (300 Hz). The local field potentials are shown in Figure 3.2.2 C & F (low pass filter setting 50 Hz). In wild type retina, the baseline displayed only small fluctuations that can be interpreted as LFPs. In the *rd10* recording, large amplitude LFPs occured in a rhythmic fashion. These oscillations have

been described as "slow waves" by other groups (Ye & Goo, 2007b; Goo *et al.*, 2011a) in both *rd10* and *rd1* retina. Different studies have reported a frequency for these LFPs of 9 – 16 Hz in *rd1* and 4 – 5 Hz in *rd10* (Ye & Goo, 2007b; Borowska *et al.*, 2011; Goo *et al.*, 2011a; Menzler & Zeck, 2011; Trenholm *et al.*, 2012; Jae *et al.*, 2013; Toychiev *et al.*, 2013). In Figure 3.2.2 D-F, the peaks of the LFPs were separated by approximately 200 ms, corresponding to a frequency of around 5 Hz. Such oscillations in the LFPs were never observed in recordings of wild type retina as shown in Figure 3.2.2 A. In wild type retina, on most electrodes spontaneous spiking occurred in a stochastic manner (Figure 3.2.2 B). In *rd10* retina spiking occurred often in bursts. In Figure 3.2.2 E, two types of spikes were observed. Groups of 6 - 8 large amplitude spikes were fired in short bursts. These bursts were phase locked to the negative deflections in the LFPs. In addition, small amplitude spikes originating from another ganglion cell were fired randomly.

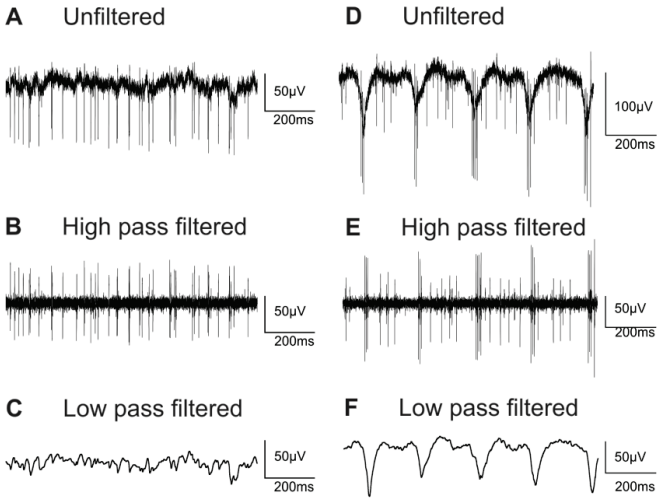

Figure 3.2.2 MEA recordings from wild type (A – C) and *rd10* (D - F) retina. A) Unfiltered recording from wild type retina, showing spontaneous activity from ganglion cells. B) Spontaneous activity obtained after high-pass filter settings with 300 Hz cut off frequency. C) Filtered baseline obtained by using low-pass filter settings with 50 Hz cut off frequency. D) Unfiltered recording from *rd10* mouse retina showing neural activity. E) Spontaneous spiking activity obtained after high-pass filtering. Large amplitude spikes occur in rhythmic bursts with inter-burst intervals of ~200 ms. Short amplitude spikes are fired more regularly. F) Local field potentials (LFPs) obtained after low-pass filtering.

3.2.2.2 Spikes from different ganglion cells can be sorted

Figure 3.2.3 represents an unfiltered recording of *rd10* retina. The frequency of the LFPs in the recording was around 5 Hz. Two types of spiking activity can be observed in Figure 3.2.3 A; first, the spikes with larger amplitude occurred in short bursts which were phase locked with the negative deflection in the LFPs. Second, the spikes with lower amplitude occurred in a stochastic manner. Spike sorting was performed by using spike sorter software (Figure 3.2.3 B, Spike2, Cambridge Electronic Design Limited, UK) to distinguish between spikes of different cells. Spike sorting grouped the spikes into clusters based on the characteristic features of spike amplitude and shape. The spike sorting confirmed that in Figure 3.2.3 A, the two different spiking patterns were from two different ganglion cells whose spikes differed in their waveforms (Figure 3.2.3 B, red and black waveform).

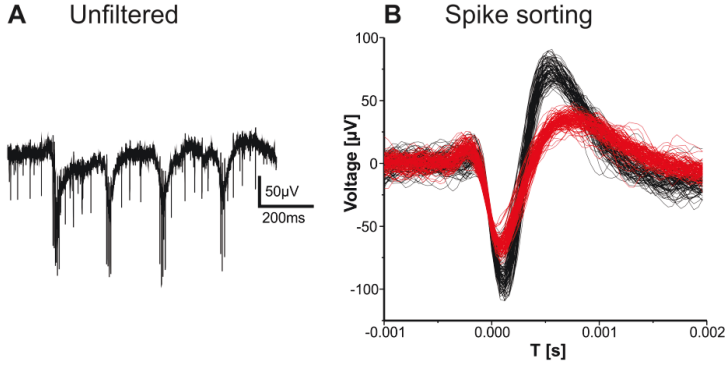

Figure 3.3.3 MEA recording from *rd10* retina. A) Unfiltered recording from *rd10* mouse retina. Local field potentials (LFPs) show large negative deflections. Spiking activities occur in two different patterns. First, large amplitude spikes occur in rhythmic bursts phase locked to the LFPs, and second, short amplitude spiking appear more regular and spontaneous. B) Spike sorting indicates that spiking activity was recorded from two different ganglion cells.

3.2.2.3 Spikes can be locked to different components of the LFP oscillations in *rd10*

In the recording shown in Figure 3.2.4 A (same recording as shown in Fig. 3.2.3 A), short bursts of large amplitude spikes were phase locked to the negative deflection in the LFPs. This was true for the activity of most ganglion cells. However, occasionally, spikes were also observed to coincide with other components of the LFPs. In the recording shown in Figure

3.2.4 D, groups of 3 – 4 large amplitude spikes were fired on the positive going or flat component of the LFP. Recordings were filtered with different filter settings for the spiking activities and for LFPs (Figure 3.2.4 B & C, E & F). As will be shown in chapter 3.2.1, the negative deflections in the LFPs originate from the activity of ON-bipolar cells. Spike bursts that coincide with negative deflections like in Figure 3.2.4 A, therefore, might originate from ON-ganglion cells, that were excited by ON-bipolar cell activity. In contrast, spikes shown in Figure 3.2.4 D and E might arise from an OFF-ganglion cell, whose activity was suppressed during the negative deflections but recovered in between.

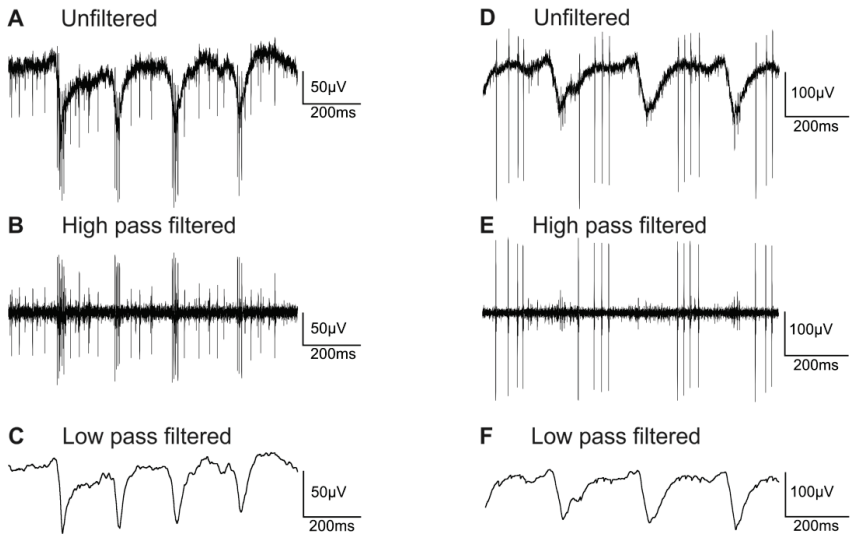

Figure 3.2.4 MEA recordings from *rd10* retinae. A) Unfiltered recording from *rd10* showing short spike bursts occurring during the negative deflection in LFPs. B) Unfiltered recording from another *rd10* showing groups of 3-4 spikes during the positive going deflections or flat components of LFPs.

3.2.2.4 Different frequencies in LFP oscillations can be observed in *rd10*

Spontaneous rhythmic electrical activity observed as LFP oscillations are a striking feature of *rd1* and *rd10* retina. In *rd1*, various studies (Ye & Goo, 2007; Borowska *et al.*, 2011; Goo *et al.*, 2011b; Menzler & Zeck, 2011; Trenholm *et al.*, 2012) reported a frequency of 10 – 16 Hz for these oscillations. In contrast, in *rd10* lower frequencies were observed. To quantify the

frequency in the LFPs, data were subjected to Fast Fourier analysis. In most cases, I determined frequencies of 3 – 4 Hz (Figure 3.2.5 A), in some cases LFP frequencies of 5 - 6 Hz were found (Figure 3.2.5 B). In general, these values are similar to those described in previous studies (Goo *et al.*, 2011b; Jae *et al.*, 2013). Usually, a clear main peak could be observed (e.g. at 3.17 Hz in Fig. 3.2.5 A). Often peaks at higher frequencies were also observed, mostly appearing as second and third harmonics (e.g. 6.13 Hz in Fig. 3.2.5 A).

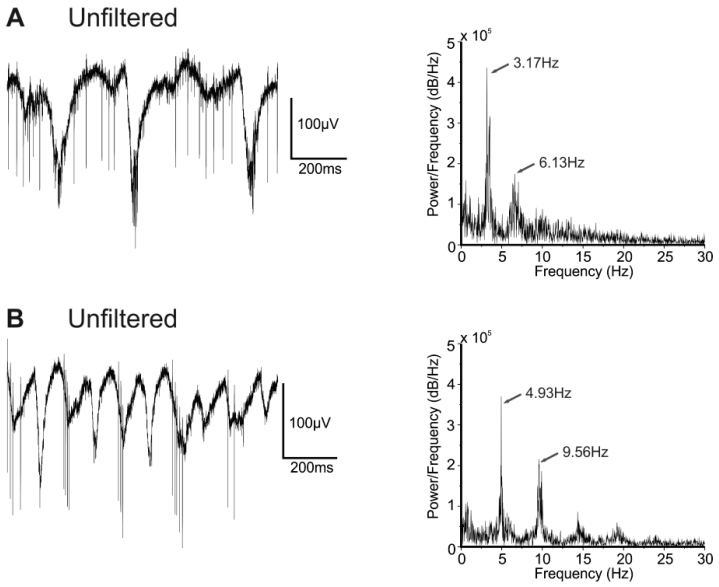

Figure 3.2.5 Different frequencies observed in LFP oscillations in *rd10*. A & B) Unfiltered recordings of different *rd10* retinae (left) with Fast Fourier Transformations (FFT; right). A) Main frequency at ~3 Hz with a second harmonic frequency at ~6 Hz. B) Frequencies at ~ 5 Hz and ~10 Hz.

3.2.2.5 Spontaneous rhythmic activity changes temporally in *rd10*

While oscillations were regularly observed, it is important to note that they were not always present. Oscillations could vary noticeably from retina to retina, from electrode to electrode and within the recording from one electrode over time.

Figure 3.2.6 A represents recordings from 60 electrodes in one *rd10* retina. The inter-electrode distance for this 3D MEA was 100 µm. In several electrodes no oscillations were

observed but spontaneous spike activity was noticed, e.g. at electrodes 12 and 21 indicated by the single asterisks. At most of the electrodes strong oscillations around 4 Hz were observed. The waveforms of oscillations were very similar between different electrodes. It was noticeable that the oscillations were minimally shifted between upper and lower electrodes. The corresponding negative deflections in the LFPs were marked from electrode 43 to 46 with a red line and from electrode 72 to 77 with a green line. Both lines show the same slope, which suggests that these oscillations were shifted with the same phase. The phase shift in the LFPs could indicate that these oscillations originated at one site of the retina and travelled as wave along the retina. The propagation velocity of these waves was calculated by dividing the electrode distance by the time delay between the negative deflections of LFPs at different electrodes.

Propagation velocity = electrode distance/time delay

$$= 100\ \mu m/30\ ms = 3.3\ mm/s$$

The measured propagation velocity was slower than the propagation velocity determined by Menzler and Zeck (Menzler & Zeck, 2011) in *rd1*. The difference in velocity could be due to differences between the two model systems.

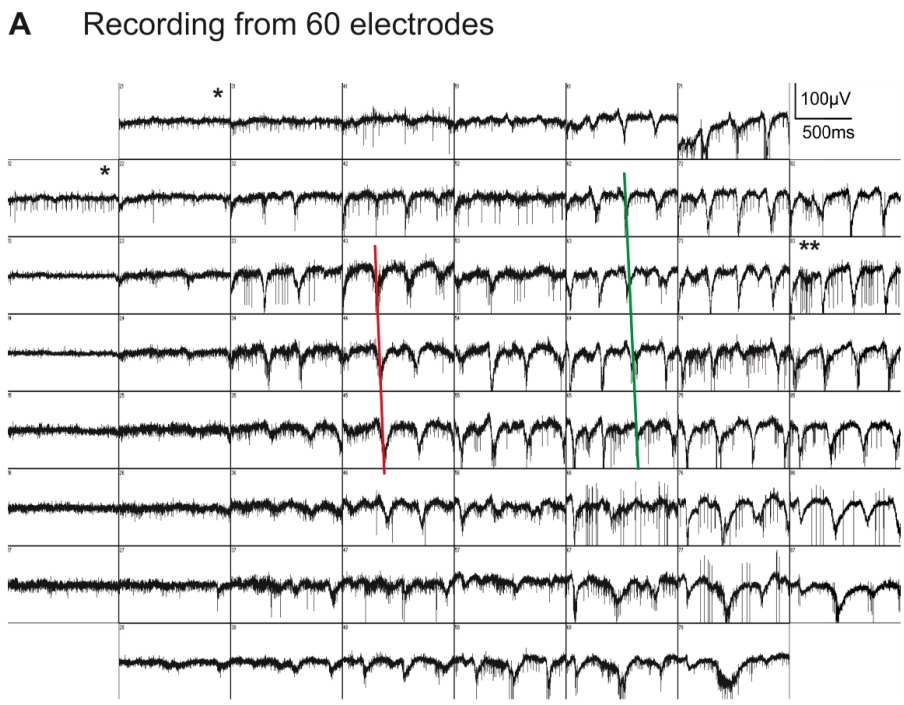

Figure 3.2.6 Spontaneous rhythmic electrical activity from *rd10* mouse retina can change. A) Activity recorded simultaneously from 60 electrodes with an 8x8 matrix with inter-electrode spacing of 100 µm in a 3D MEA. Oscillations were observed in the majority of channels along with spiking activity. Some channels showed no oscillations (e.g. indicated by single asterisks). The phase of the LFPs seemed to be shifted from upper rows to lower rows of electrodes as indicated by red and green lines.

Oscillations were varying within one electrode over time, too. Figure 3.2.7 shows the recording of one electrode over time (electrode 83, marked by two asterisks in Figure 3.2.6 A). Figure 3.2.7 A-C represents the recording of electrode 83 at 5, 30, and 60 minutes after the start of the experiment. Throughout the experiment, the retina was continuously superfused with oxygenized AMES buffer at a constant rate flow of 3 ml/min. The oscillations were present for the first 22 min (Figure 3.2.7 A), then vanished for about 30 min (Figure 3.2.7 B) and finally came back at 54 min with the similar shape and frequency as observed in the beginning of experiment (Figure 3.2.7 C). To quantify the frequency at different time points, FFTs were made at 5 min, 30 min, and 60 min (Figure 3.2.7 D-F). In the

beginning the frequency was around 4 Hz, followed by a time with no oscillations in the middle of experiment (no peak was observed in the FFT). At the end of the experiment oscillations with a frequency of 4.20 Hz appeared. Figure 3.2.7 G plots the change in frequency during the experiment over time. In the very beginning no oscillations were observed. After a few minutes, the retina suddenly displayed oscillations with a frequency of 4 Hz followed by a sudden drop to around 0 Hz at 24 min. No oscillations were observed for approximately 30 min. Finally, at the end of recording oscillations appeared again. At present it is unclear, why the retina "switches" from an oscillatory state to a non-oscillatory state. Spiking activity was present throughout the experiment indicating that a) loss of oscillations was not a result of loss of contact between the retina and the electrode, and b) that the retina was physiologically intact throughout the entire experiment. Hence, the "switching" most likely did not originate from an artefact but reflects an inherent property of the degenerated retinal tissue. In summary, these results suggest that the generation of oscillations may depend on some unknown parameters.

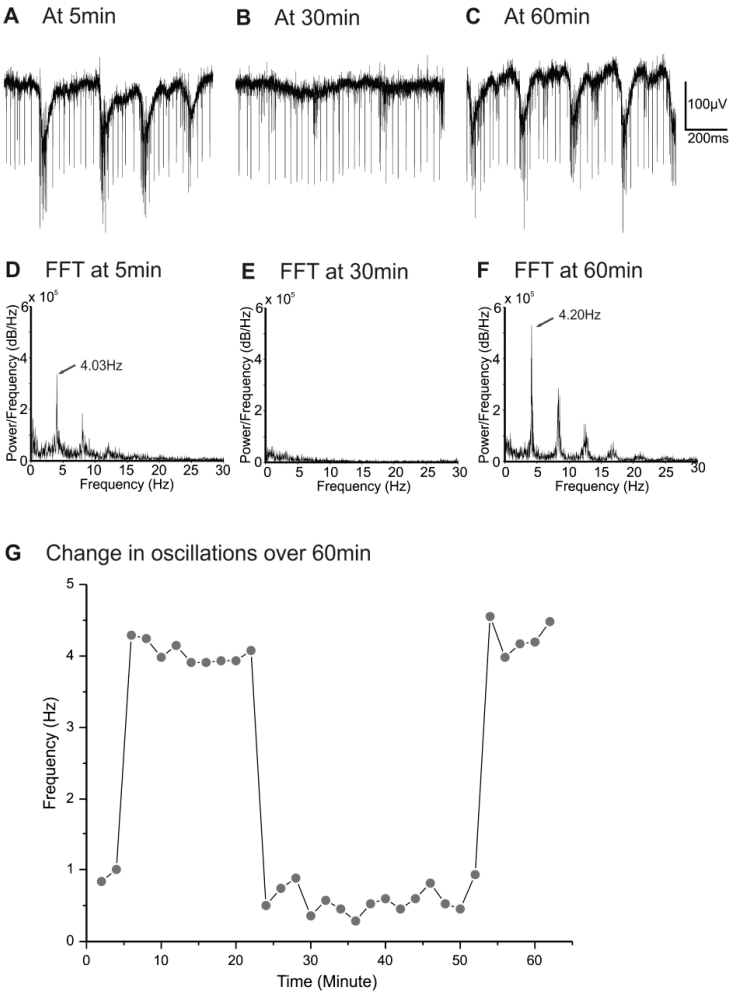

Figure 3.2.7 Spontaneous rhythmic activity in one *rd10* retina over time. A-C) Recording of electrode 83 (From Figure 3.2.6 A, E83, marked by two asterisks) obtained over time. Oscillations were visible during the first 22 min (A), vanished for the next 31 min, while spiking activity remained (B), and finally came back with similar frequency and shape (C). D-F) FFTs of one electrode at different time points. G) Plot showing the change in the oscillation frequency over time.

3.2.2.6 Effect of age on the frequency of oscillations in *rd10*

If the occurrence of oscillations in *rd10* retina results from a remodelling of the degenerating retina, it is important to monitor oscillations over the age of *rd10* animals. Animals between 1 month and 12 months of age were investigated. FFTs were evaluated and the values of the main frequencies were plotted versus the age of animals (Figure 3.2.8). At 1 month and 3 months, *rd10* retinae displayed frequencies of around 6 Hz which was lower than other studies reported by Jae *et al.* (Jae *et al.*, 2013); their frequency for *rd10* at this age was 9 Hz). From 4 to 12 months, frequencies were around 4 Hz. Table 1 summarizes the results of this developmental study. All the pharmacological experiments described in the following chapters were performed on animals older than 6 months.

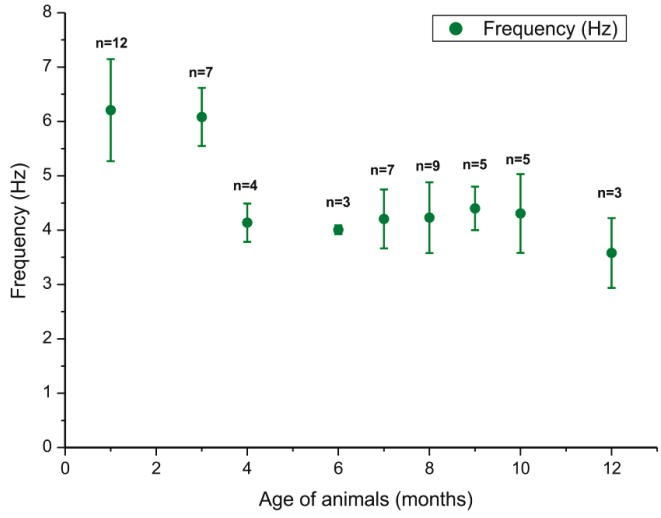

Figure 3.2.8 Plot of the frequency of LFPs vs age of animals. The frequency was lower in older animals.

Age of animals (Months)	Frequency (Hz) mean ± SD	Number of retinal pieces	Number of animals
1	6.21 ± 0.94	12	6
3	6.08 ± 0.53	7	3
4	4.14 ± 0.35	4	2
6	4.01 ± 0.08	3	2
7	4.21 ± 0.54	7	2
8	4.23 ± 0.65	9	5
9	4.40 ± 0.40	15	5
10	4.31 ± 0.73	5	3
11	4.03 ± 0.20	2	2
12	3.58 ± 0.64	3	3

Table 3.1 Experiments were performed on a total of 33 animals ranging from 1 – 12 months. The frequency of oscillations was slightly higher in animals between 1 and 3 months. Frequency is given as mean ± standard deviation (SD).

3.2.2.7 Rhythmic electrical activity depends on glutamatergic input

There is a clear difference in the frequencies of LFPs between *rd1* and *rd10* mouse models. In *rd1*, frequencies of 10 – 16 Hz were observed, in *rd10* frequencies were around 3 – 6 Hz. One explanation for this difference could be that the mechanism underlying the rhythmic electrical activity is a result of the degeneration process. As degeneration proceeds with different pace in the two models, the mechanisms that induce oscillation might differ between the two animal models. As *rd10* is progressively used as a model system for human RP, it is important to investigate the mechanisms underlying retinal oscillations in *rd10*. The origin of oscillations in *rd1* is still not clearly known but recent evidence suggests that cone ON-bipolar cells and AII amacrine cells are involved (Borowska *et al.*, 2011). Oscillations and rhythmic spiking activity of ganglion cells in *rd1* were inhibited by blockers of AMPA/kainate receptors and NMDA receptors (Ye & Goo, 2007b; Borowska *et al.*, 2011; Menzler & Zeck,

2011), indicating that glutamatergic excitation from cone bipolar cells is involved in the generation of oscillations.

Upon superfusion of *rd10* retinae with a mixture of AMPA/Kainate and NMDA receptors blockers (CNQX, 20 μM and DL-AP5, 50 μM) oscillations were abolished in a reversible way (Figure 3.2.9, n=9 retinal pieces from 3 animals aged 7 – 9 months). The recording in Figure 3.2.9 A shows the rhythmic electrical activity in LFPs and spiking activity from ganglion cells. Two types of spiking pattern were observed: firstly, spike bursts phase locked to the minima of LFPs and secondly, the spontaneous spiking activity most likely from another ganglion cell. The frequency of LFPs in this particular recording was around 4 Hz as shown by the FFT in the right panel. Upon application of CNQX and DL-AP5 (Figure 3.2.9 B), the oscillations were strongly diminished. Only a small peak was detected in the FFT. Interestingly, the spike bursts were also abolished while the randomly occurring spikes remained. The effect of the blockers was reversible upon washout, as LFPs re-appeared with a frequency of 3.5 Hz. The spike bursts also came back and were again phase locked to the minima in the LFPs (Figure 3.2.9 C). This experiment indicates that glutamatergic input was involved in the origin of oscillations.

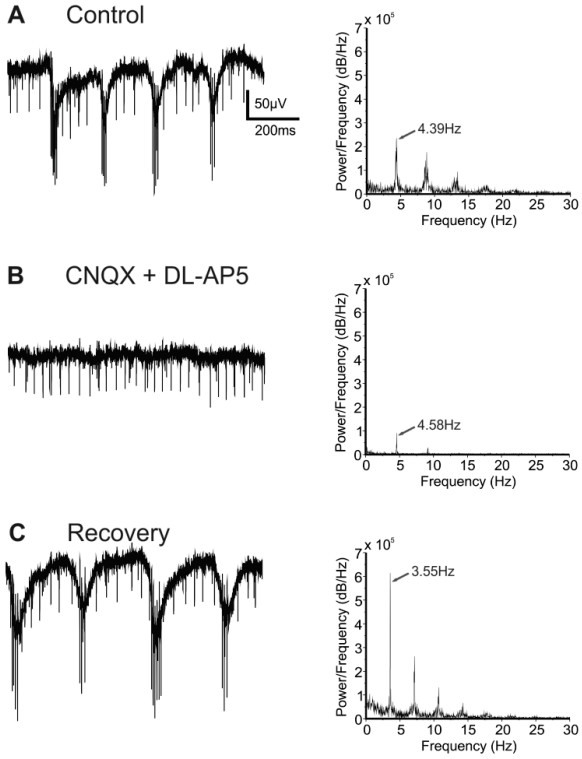

Figure 3.2.9 Glutamate receptor blockers CNQX & DL-AP5 abolish rhythmic electrical activity. A) Unfiltered recording displaying oscillations and spontaneous spiking activity. B) Application of CNQX & DL-AP5 completely blocked the oscillations and bursts of large amplitude spikes. Small amplitude spikes remained unaffected. C) The effect was reversible upon washout. Right panel shows the FFTs of the recordings during control, application and washout phase to depict the oscillation's frequency.

3.2.2.8 The contribution of the ON-pathway to rhythmic electrical activity is unclear

Different glutamate receptors are present on different types of bipolar cells. In principle, ON-bipolar cells (depolarized by light) and OFF-bipolar cells (hyperpolarized by light) were observed in the retina (Nelson, 1973; Kolb & Nelson, 1983; Bloomfield & Miller, 1986; Dacheux & Raviola, 1986; Müller *et al.*, 1988). OFF-bipolar cells have ionotropic glutamate receptors (iGluR) of the AMPA or kainate type. In contrast, ON-bipolar cells express the metabotropic receptor mGluR6 (Nakajima *et al.*, 1993; Nomura *et al.*, 1994). The

metabotropic glutamate agonist, 2-amino-4-phosphonobutric acid (APB or L-AP4, 100 µM) completely blocks the light responses of ON-bipolar cells (Slaughter & Miller, 1981).

As cone ON-bipolar cells seem to be involved in the generation of oscillations, I tested whether oscillations are modulated by stimulation of mGluR6. When the retina was superfused with the mGluR6 agonist L-AP4 the results were variable. In most of the experiments, there was no effect of L-AP4 on the frequency and amplitude of oscillations. In some cases, the LFPs diminished completely, in other experiments the frequency was reduced to around 1 Hz (Figure 3.2.10 B). The large variability might result from changes in the expression level of mGluR6 receptors in the dendritic tips and somata of bipolar cells during remodelling of the retina (Figure 3.1.7). A reduced expression of mGluR6 in bipolar cells changes the efficiency of the downstream signalling cascade in *rd10* retina (Puthussery *et al.*, 2009).

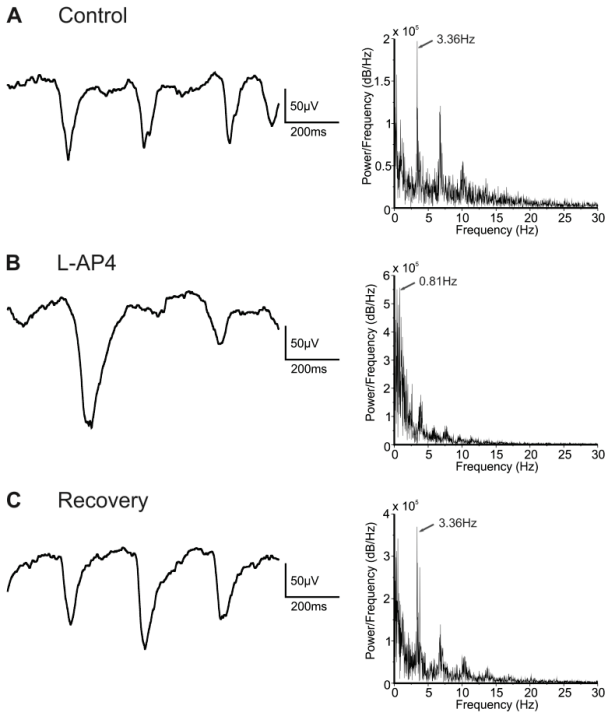

Figure 3.2.10 Effect of the mGluR6 agonist L-AP4 on LFPs. A) Unfiltered recording displaying rhythmic oscillations and spontaneous spiking activity. B) Application of L-AP4 partially blocked the rhythmic oscillations. C) The effect was reversible upon washout. Right panel shows the FFTs of the recordings during control, application and washout phase to depict the oscillation's frequency.

3.2.2.9 Rhythmic electrical activity is shaped by inhibitory input

Next, it was investigated whether inhibitory pathways are involved in the generation of oscillations. Inhibitory pathways in the retina are mainly represented by horizontal cells and amacrine cells. From different studies, it was evident that in *rd10* retina horizontal cells undergo remodelling by retracting dendrites (Phillips *et al.*, 2010) and by developing ectopic processes in the inner retina (Figure 3.1.6 D). Amacrine cells preserved their morphology for longer duration in *rd10* (Gargini *et al.*, 2007; Phillips *et al.*, 2010). Amacrine cells connect bipolar cells with ganglion cells and synaptically inhibit the downstream signalling pathway by release of GABA and glycine (Wässle, 2004). The mechanisms by which horizontal cells modulate the photoreceptor output are still discussed controversially.

Application of strychnine, a glycine receptor blocker and bicuculline, a $GABA_A$ receptor blocker had strong effects on the LFPs. The LFPs amplitude increased 2-4 folds upon co-application of the blockers. Sometimes the signal amplitude was so huge that it saturated the amplifier of the MEA system. The frequency under control condition (4 Hz, Figure 3.2.11 A) reduced to 1 Hz with application of blockers (Figure 3.2.11 B). The effect was reversible with the washout of blockers (4 Hz, Figure 3.2.11 C). A total of 15 retinal pieces from 10 animals aged from 6.5 – 10 months were analysed. To determine the frequency of the oscillations, FFTs were made and plotted in the right panel with respect the recordings shown on the left. When strychnine or bicuculline were applied alone, only minimal effects on the LFPs were observed (results not shown).

Apart from glycine and $GABA_A$ receptors, $GABA_B$ and $GABA_C$ receptors are also involved in inhibitory pathways in the retina (Müller *et al.*, 1992; Enz & Bormann, 1995; Varela *et al.*, 2003; Farajian *et al.*, 2011). Thus, for the next step all four inhibitory receptors were blocked by the mixture of glycine, bicuculline, CGP 54626, and TPMPA. With the application of this mixture, major changes in LFPs occurred. The amplitude of LFPs was increased by many fold and saturated the amplifier similar to the effect of the mixture of strychnine and bicuculline (Figure 3.2.12 B). The frequency under control conditions was around 5 Hz (Figure 3.2.12 A, B) but was reduced to values between 0.2 and 1 Hz with application of the inhibitory receptor blocker cocktail (Figure 3.2.12 B). The effect was reversible upon long washout (Figure 3.2.12 D). In wild type retina, this cocktail did not induce any kind of spontaneous rhythmic activity in the baseline as observed in *rd10* retinae (data not shown).

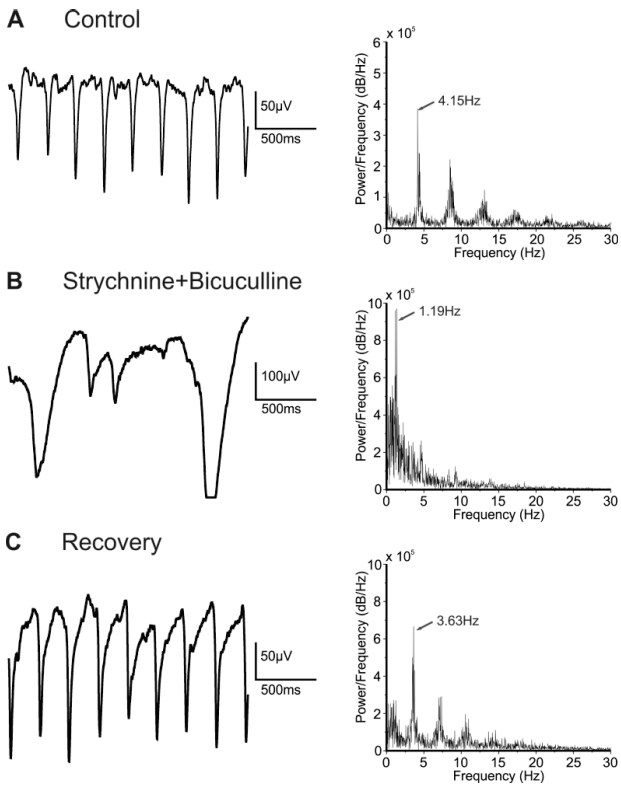

Figure 3.2.11 Effects of bicuculline and strychnine on rhythmic electrical activity. A) Control recording (low pass filtered) displaying LFPs with a main frequency of ~4 Hz (shown by FFT plot). B) Co-application of strychnine and bicuculline increased the LFP amplitude but reduced the frequency to ~1 Hz. C) The effect was fully reversible upon washout.

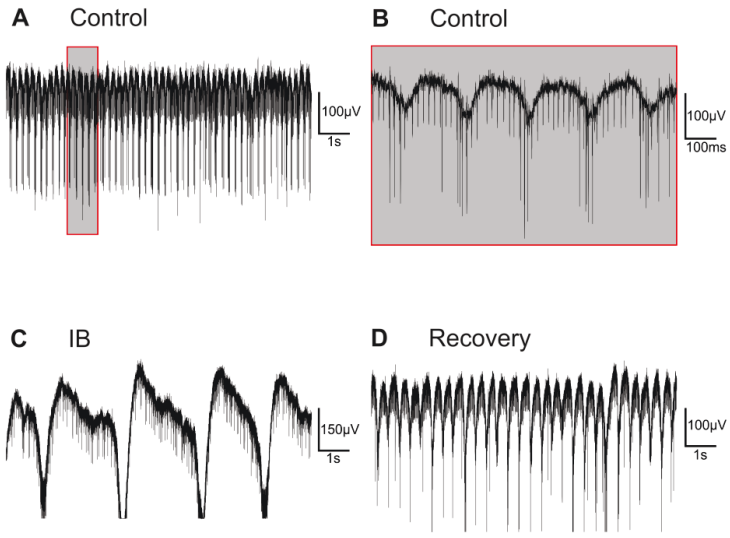

Figure 3.2.12 Effect of inhibition blockers on the LFPs. A) Unfiltered recording showing spontaneous spiking activity and oscillations. B) A part of the recording from A (indicated by the grey box) at higher time resolution. C) Co-application of strychnine, bicuculline, CGP 54626, & TPMPA (IB) reduced the frequency to around 0.4 Hz. The amplitude strongly increased, sometimes saturating the amplifier. D) The effect was reversible upon washout.

3.2.2.10 Blockage of glutamate receptors abolishes the effect of inhibition blockers

I found that blocking inhibition reduced the frequency of oscillations but increased the amplitude of LFPs many fold (Figure 3.2.12 C). It was also observed that blockers of glutamatergic transmission abolished the oscillations. In the following experiment I tested whether the pronounced effect of the inhibition blocker cocktail was abolished by glutamatergic blockers (CNQX and R-CPP). The large fluctuations as observed with the inhibition blocker cocktail totally disappeared upon application of glutamate receptor blockers (Figure 3.2.13 C; n=4 retinal pieces from 4 animals aged 9 – 12 months). The effect was reversible upon longer washout (Figure 3.2.13 D).

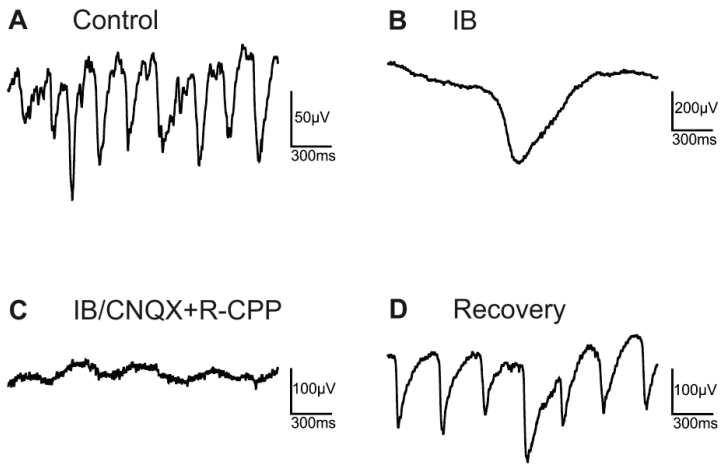

Figure 3.2.13 Glutamate receptor blockers abolish baseline fluctuations induced by inhibition blockers. (A) Control recording (low pass filtered), showing LFPs with a frequency ~4 Hz. (B) Upon application of inhibition blockers (strychnine, bicuculline, TPMPA, CGP 54626), the LFP frequency was reduced to below 1 Hz. Note the change in the amplitude scale. (C) Application of glutamate receptor blockers (CNQX & R-CPP) nearly abolished baseline fluctuations. (D) Upon washout of all agents typical oscillations of ~4 Hz were observed.

3.2.2.11 Rhythmic electrical activity in *rd10* depends on gap junctions

Many cell types in the retina are coupled via electrical synapses in form of gap junctions. In the outer retina prominent coupling is found between horizontal cells. In the inner retina, AII amacrine cells are electrically coupled to each other and also to cone ON-bipolar cells (Kolb & Famiglietti, 1974). Meclofenamic acid (MFA) was found to block gap junctions in the retina (Pan *et al.*, 2007; Veruki & Hartveit, 2009; Veruki *et al.*, 2010; Trenholm *et al.*, 2012). It was shown that application of MFA abolishes the rhythmic spontaneous activity and reduced the spiking activity in *rd1* retina (Borowska *et al.*, 2011; Menzler & Zeck, 2011; Trenholm *et al.*, 2012; Toychiev *et al.*, 2013). This fact was found to be true for *rd10* retinae also (Fig 3.2.14, n = 9 retinal pieces from 4 animals aged 9 – 10 months). With the application of 100 µM MFA, not only rhythmic electrical activity was inhibited but also the ganglion cell spiking activity was completely abolished (Fig. 3.2.14 B). The effect was reversible upon longer washout (20 min, Fig 3.2.14 C). These results suggest that the gap junctions are involved in the generation of rhythmic electrical activity in *rd10* retina.

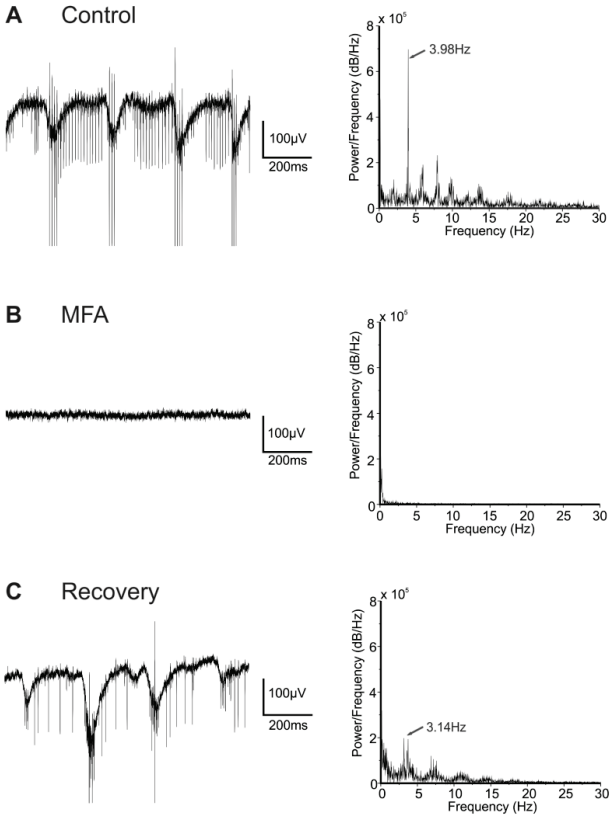

Figure 3.2.14 The gap junction blocker MFA abolishes rhythmic electrical activity. A) Unfiltered baseline, showing spontaneous activity and LFPs with a frequency of ~4 Hz. B) Application of the gap junction blocker (MFA) blocked all spontaneous activity. C) The effect was reversible upon washout. Right panel shows the FFTs of the recordings under control, application and washout phase for the depiction of oscillation's frequency.

3.2.2.12 Rhythmic electrical activity in *rd10* is modulated by HCN channels

In the retina, all four types of hyperpolarization-activated and cyclic nucleotide-gated (HCN) channels are present and are differentially expressed (Müller *et al.*, 2003; Ivanova & Müller, 2006; Fyk-Kolodziej & Pourcho, 2007; Knop *et al.*, 2008). In other systems, HCN channels

function as pacemaker channels (Brown *et al.*, 1979; Brown & Difrancesco, 1980; Maccaferri *et al.*, 1993; Kaupp & Seifert, 2001; Kanyshkova *et al.*, 2009). In the inner retina, HCN channels are found in particular in bipolar cells and amacrine cells (Müller *et al.*, 2003; Koizumi *et al.*, 2004; Knop *et al.*, 2008). HCN channels expressed in bipolar cells contribute to the generation of the rhythmic electrical activity in *rd1* retinae (Trenholm *et al.*, 2012). I tested whether this applies also to *rd10* retina. Different HCN channel blockers were used. With 3mM Cs^+ (Satoh & Yamada, 2000; Müller *et al.*, 2003; Koizumi *et al.*, 2004; Knop *et al.*, 2008; Van Hook & Berson, 2010), the frequency of the first peak in the FFT (4.4 Hz in the control recording, Fig 3.2.15 A) was slightly reduced to around 3 Hz (Fig 3.2.15 B). The frequency of the second peak (~10 Hz in the control recording) completely vanished with the application of Cs^+ solution. Moreover, the oscillations became less regular. This can be seen in the original recording (Figure 3.2.15 B; amplitudes of the negative deflections are quite different) and in the FFT (peak is broader). Upon washout the recording became similar to the control recording (Figure 3.2.15 C; n = 6 retinal pieces from 3 animals aged 9.5 – 10 months). Similar results were obtained with the HCN blocker ZD7288 (Satoh & Yamada, 2000; Koizumi *et al.*, 2004; Van Hook & Berson, 2010). The control recording showed a frequency of about 4.5 Hz (Figure 3.2.16 A). Upon superfusion with ZD7288 for about 10 min, the frequency reduced to 3 Hz (Figure 3.2.16 B). Even with prolonged washout, there was no full recovery (Figure 3.2.16 C; n = 4 retinal pieces from 1 animal aged 9 months) indicating that it was difficult to washout the blocker as has been described by previous studies (BoSmith *et al.*, 1993; Berger *et al.*, 1994; Harris & Constanti, 1995).

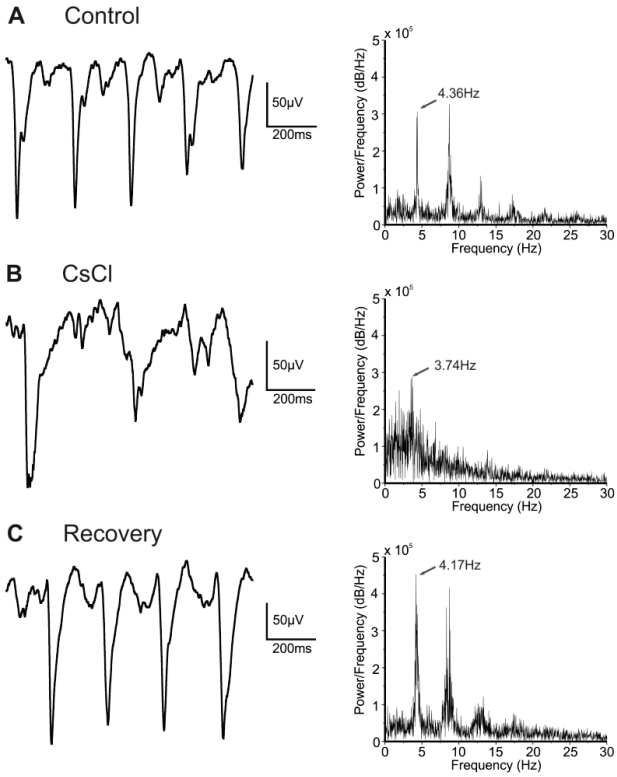

Figure 3.2.15 Blockage of HCN channels by 3 mM Cs^+ reduce the rhythmic electrical activity. A) Low pass filtered recording, frequency ~4 Hz. B) Blocking HCN channels with Cs^+ abolished the second harmonic peak and slightly reduced and broadened the first peak of the FFT. C) Recovery. Right panel shows the FFTs of the recordings under control, application and washout phase for the depiction of oscillation's frequency.

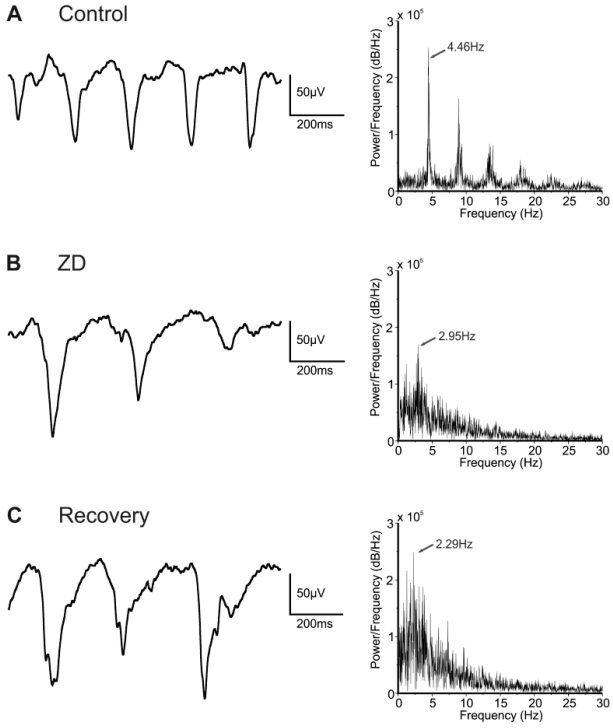

Figure 3.2.16 HCN channel blocker reduces the rhythmic electrical activity. A) Low pass filtered recording, frequency ~4 Hz. B) Blocking HCN channels with ZD7288 abolished the second harmonic peak and slightly reduced the first peak of the FFT. C) Recovery was not 100%. Right panel shows the FFTs of the recordings under control, application and washout phase for the depiction of oscillation's frequency.

3.2.3 Rhythmic electrical activity in MNU treated retinae

Spontaneous rhythmic electrical activity is typical for both genetic models of retinitis pigmentosa (RP) *rd1* and *rd10*. An interesting question was, whether other models of photoreceptor degeneration would generate similar activity. In collaboration with Sarah Rösch, Christine Haselier, and Peter Walter from the Augenklinik at the Uniklinikum Aachen, Germany, MEA recordings were performed on retinae of mice that had been treated with N-methyl-N-nitrosourea (MNU). MNU induces photoreceptor degeneration that is complete within less than two weeks (Nambu *et al.*, 1997; Nagar *et al.*, 2009; Tsubura *et al.*, 2010; Rösch *et al.*, 2014a). Injections were performed in Aachen. For these experiments, mice were

intraperitoneally injected with 60 mg MNU per kg body weight. The recordings were performed 7 – 10 days after the injections. Only a small number of animals were available, therefore, the pharmacological analysis could not be as elaborate as for *rd10* animals and results have to be considered as preliminary.

3.2.3.1 Rhythmic electrical activity in MNU injected retina may depend on the ON-pathway

Retinae of MNU treated mice showed oscillations with frequencies between 4 and 6 Hz. The waveform of the oscillations was very similar to that found in the genetic models of retinal degeneration (Figure 3.2.17 A). During application of L-AP4, an agonist at mGluR6 receptors on ON-bipolar cells, oscillations were almost completely blocked (Figure 3.2.17 B). The effect was reversible and the oscillations came back with a frequency of 6 Hz upon washout (Figure 3.2.17 C; n = 4 retinal pieces from 2 animals aged 2 weeks).

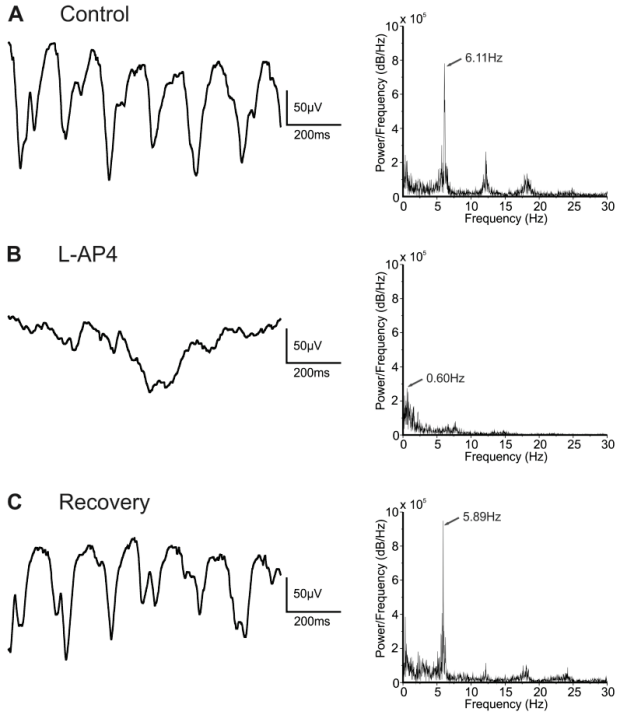

Figure 3.2.17 Metabotropic glutamate receptor agonist L-AP4 reduced the rhythmic electrical activity in retinae of MNU treated mice. A) Low-pass filtered recording with a frequency around 6 Hz. B) Application of L-AP4 almost abolished the oscillations frequency to ~ 0.60 Hz. C) The effect was reversible upon washout. Right panel shows the FFTs of the recordings under control, application and washout phase for the depiction of oscillation's frequency.

3.2.3.2 Rhythmic electrical activity in MNU treated retina depends on inhibitory pathways

I also investigated the impact of inhibitory pathways on the oscillations in MNU treated retinae. With the application of strychnine and bicuculline, the frequency of 6 Hz observed in the control recording (Figure 3.2.18 A) was reduced to 2 Hz (Figure 3.2.18 B) while the amplitude increased. These results are similar to those found in *rd10* (compare Figure 3.2.11).

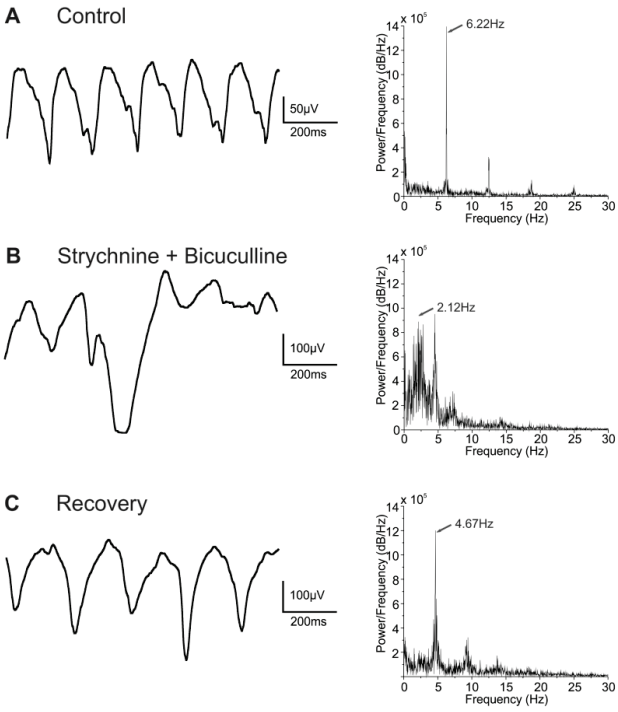

Figure 3.2.18 Effect of inhibition blockers on oscillations in the retina of an MNU treated mouse. A) Filtered control recording displaying LFPs with frequency of ~6 Hz. B) Co-application of strychnine and bicuculline reduced the frequency to ~2 Hz but amplitude increased many fold (notice the change in scale bar). C) The effect was reversible but not completely. Right panel shows the FFTs of the recordings under control, application and washout phase for the depiction of oscillation's frequency.

In summary, *rd10* retinae showed rhythmic electrical activity with frequencies in the range of 4 – 7 Hz. The pharmacological analysis revealed that both excitatory and inhibitory pathways are involved in the generation of rhythmic activity. Moreover, electrical coupling seems to be a prerequisite for the generation of oscillations in *rd10*. Interestingly, oscillations were also observed in retinae of MNU treated mice. Thus, the generation of oscillations seems to be a common feature of retinal degeneration.

4. Discussion

In retinitis pigmentosa (RP) the photoreceptors in the retina degenerate over time but the inner retinal network, in particular the retinal output neurons, the ganglion cells (RGCs) persist. RGCs are a suitable target for electrical stimulation by retinal prostheses. However, in recent years evidence has grown that considerable remodelling occurs in the remaining retina which might interfere with this therapeutic approach (Gargini *et al.*, 2007; Phillips *et al.*, 2010). To establish therapeutic approaches, suitable animal models are needed that must be characterized in detail. This study investigates the anatomical and physiological changes in the retina of a mouse model of RP, the *rd10* mouse. So far, most studies have been performed on another RP model, the *rd1* mouse. The studies on *rd1* retina describe in detail the photoreceptor degeneration, the rewiring that takes place in the inner retina as well as changes in functional properties of retinal neurons (Strettoi *et al.*, 2002; Strettoi *et al.*, 2003). In particular, the generation of rhythmic electrical activity – retinal oscillations - was analysed in *rd1* (Ye & Goo, 2007b; Borowska *et al.*, 2011; Menzler & Zeck, 2011).When comparing *rd10* and *rd1*, two differences are obvious. First, photoreceptor degeneration starts later and progresses with slower pace in *rd10* than in *rd1*, making it a better model for human RP. Second, the oscillations occur with a low frequency in *rd10* (3 – 5 Hz) but with higher frequency in *rd1* (10 – 15 Hz). One plausible explanation for the frequency difference would be that, as the degeneration process differs between the two mouse models the mechanisms that underlie those oscillations also differ. The results of the pharmacological approach in the present study argue against this idea. Despite differences in the frequency the origin of the oscillations seems to be quite similar in both mouse models. Moreover, oscillations - this time with frequencies of 4 – 6 Hz - could also be observed in a third model, in which photoreceptor degeneration was initiated by treatment with the toxic agent MNU.

4.1 Retinal degeneration and remodelling progresses in the retina of *rd10* mouse

Recent studies have revealed the degeneration of the outer retina, changes in the retinal thickness and retinal remodelling occurring in *rd10* mice by using immunohistochemical staining on vertical sections of different postnatal stages (Gargini *et al.*, 2007; Phillips *et al.*, 2010). The immunohistochemical results in this thesis in principle were in concordance with

the recently published data. In this study, various postnatal stages (P6, P14, P20, P25, P32, P45, P60, and 6 months) were studied using a variety of antibodies against different cell types and proteins. As published by others (Gargini *et al.*, 2007; Phillips *et al.*, 2010) an ongoing reduction in the number of photoreceptor cell rows in the ONL was observed during development of the *rd10* retina. Compared to adult wild type mouse retina (Figure 3.1.5 A), rod bipolar cells of *rd10* mice stained with the antibody against PKCα (Figure 3.1.5 B-E) showed no obvious alteration in their somata, axons, and terminal systems. However, due to degeneration of rod photoreceptors, rod bipolar cells showed a clear loss of their dendrites. Additionally, some of the rod bipolar somata were dislocated between ONL and OPL. Antibodies against calbindin stain the horizontal cells located in the outermost row of the INL close to the OPL. While Gargini *et al*. (Gargini *et al.*, 2007) reported only slight changes in horizontal cells in *rd10* retina, more pronounced changes were described by Phillips and co-workers (Phillips *et al.*, 2010). In this study, horizontal cells displayed pronounced sprouting of ectopic processes in later stages of degeneration (Figure 3.1.6 C - E). Hence, this study confirms the report of Phillips *et al*. (Phillips *et al.*, 2010). The weakly stained CabP-positive amacrine cells in the INL and displaced amacrine cells in the GCL were found in wild type as well as in *rd10* retina. Additionally, the three fine layers in the IPL which are formed by the stratification of ON- and OFF-cholinergic and NOS-positive amacrine cells were also present in *rd10* retina (Haverkamp & Wässle, 2000). Thus, the general architecture of the inner retina, especially the IPL, barely seems to be changed at least until P32,

As a consequence of the loss of rod bipolar cell dendrites during retinal degeneration in *rd10*, the mGluR6 staining pattern in the OPL changes (Gargini *et al.*, 2007) and the expression level of mGluR6 dramatically decreases (Figure 3.1.7 C). This is most likely due to the degeneration of bipolar cell dendrites. The receptor mGluR6 is crucial for signal transmission in the ON pathways in the mouse retina. In addition to mGluR6, the G-protein G_o was localized to the dendritic tips of ON-bipolar cells (Vardi, 1998). L-AP4 hyperpolarizes ON-bipolar cells by activating mGluR6 and starting a G_o dependent pathway that leads to the closure of cation channels, most likely TRPM1 (Slaughter & Miller, 1981; Koike *et al.*, 2010a; Koike *et al.*, 2010b; Krizaj *et al.*, 2010; Morgans *et al.*, 2010; Nakamura *et al.*, 2010; Dhingra *et al.*, 2011; Kaur & Nawy, 2012). TRPM1 can be found in ON-bipolar cells after 6 months of degeneration, but the TRPM1 expression level seems to be reduced (Figure 3.1.8 C). The large variability in the pharmacological experiments with L-AP4 (Figure 3.2.10)

might result from differences in the expression level of mGluR6 and TRPM1 in bipolar cells during remodelling of the retina (Figures 3.1.7 and 3.1.8).

4.2 Oscillations in *rd10* retina

In the attempts to restore vision, success crucially depends on the functional integrity of the remaining retinal network including ganglion cells and their ability to reliably transmit visual signals to the brain. In both *rd1* and *rd10*, spontaneous rhythmic electrical activity was observed. Rhythmic activity is evident in both ganglion cell spiking and in oscillations in local field potentials recorded using multi electrode arrays (MEAs). The origin of this rhythmic electrical activity is not entirely clear, but some mechanisms have been proposed for *rd1*. Rhythms display frequencies of 10 – 15 Hz in *rd1*, but of 3 – 5 Hz in *rd10*. However, as *rd10* is increasingly being used to study the process of retinal degeneration as well as a model to develop experimental therapies, it is important to understand the mechanisms underlying the spontaneous rhythmic activity. This study, therefore, investigated whether the mechanisms suggested to elicit rhythmic activity in *rd1* also apply for *rd10*. It was found, that despite the differences observed in the frequencies, the origin of rhythmic electrical activity in *rd1* and *rd10* seems to be quite similar.

In principle there are several possibilities how rhythmic activity could be generated. First, excitatory cells like bipolar cells might display endogenous rhythmic activity. Second, a continuous excitatory drive from bipolar cells could be modulated by inhibition that arises from rhythmic activity of amacrine cells. Indeed, spontaneous activity in amacrine cells has been reported (Feigenspan *et al.*, 1998; Petit-Jacques *et al.*, 2005). Finally, both mechanisms might contribute to rhythmic activity. In both *rd1* and *rd10*, blockage of ionotropic glutamate receptors abolishes oscillations, indicating that glutamatergic neurons – most likely bipolar cells - are a major drive for rhythmic activity (Ye & Goo, 2007b; Borowska *et al.*, 2011; Menzler & Zeck, 2011). In *rd10* during blockade of glycinergic receptors and $GABA_A$ receptors oscillations persisted (Figure 3.2.11). However, the frequency was reduced to around 1 Hz while the amplitude of the LFPs was increased 4 – 5 fold. Additional blockage of $GABA_B$ and $GABA_C$ receptors further reduced the frequency to 0.2 - 1 Hz and increased the LFP amplitude (Figure 3.2.12). These results indicate that rhythmic activity in *rd10* arises even in the absence of inhibitory input and, therefore, most likely originates from bipolar cell

activity. Yet, inhibitory mechanisms modulate both frequency and amplitude of the oscillations. Blockade of ionotropic glutamate receptors abolishes the effects of inhibitory receptor blockers (Figure 3.2.13). This might indicate that inhibitory receptor blockade acts presynaptically to the glutamate receptors, and hence on the bipolar cells. On the other hand, activity of amacrine cells seems to strongly depend on glutamatergic input (Borowska *et al.*, 2011; Trenholm *et al.*, 2012). In this case, inhibitory blockers would be without effect when at the same time excitatory input to amacrine cells is blocked.

For *rd1*, results with inhibitory blockers are less consistent. Menzler and Zeck (Menzler & Zeck, 2011) described an overall reduction in LFP frequency and increase in LFP amplitude with the application of bicuculline or strychnine. Strychnine alone had a stronger effect than bicuculline. However, judging from their supplementary Figure 2, strychnine barely changed the LFP frequency. Ye and Goo (Ye & Goo, 2007b) found that strychnine and picrotoxin, another blocker of $GABA_A$ receptors, either alone or in combination increased the LFP amplitude 2 – 3 fold while the frequency was reduced to values around 4 – 5 Hz (as judged from their Figure 4). This corresponds to a roughly two fold decrease in frequency in *rd1*, while in *rd10* frequency was reduced 3 - 5 fold by strychnine and bicuculline and even stronger if all inhibitory receptors were blocked (Figure 3.2.12).

In recordings obtained from bipolar cells and AII amacrine cells of *rd1* retina, spontaneous oscillations in membrane potential were observed that strongly resembled rhythmic activity recorded using MEAs (Borowska *et al.*, 2011; Trenholm *et al.*, 2012). The authors suggest that rhythmic activity originates from the tight interaction between cone ON-bipolar cells and AII amacrine cells. AII amacrine cells contact cone ON-bipolar cells via electrical synapses in form of gap junctions (Famiglietti & Kolb, 1975; Kolb & Nelson, 1983; Tsukamoto *et al.*, 2001; Deans *et al.*, 2002; Trexler *et al.*, 2005). In fact, MFA that was shown to block gap junctions in the retina (Pan *et al.*, 2007; Veruki & Hartveit, 2009) abolished oscillations in both *rd1* (Borowska *et al.*, 2011; Menzler & Zeck, 2011; Trenholm *et al.*, 2012) and *rd10* [present study; (Toychiev *et al.*, 2013)]. Interestingly, ON-bipolar cells express hyperpolarization-activated and cyclic nucleotide-gated (HCN) channels (Müller *et al.*, 2003; Ivanova & Müller, 2006; Fyk-Kolodziej & Pourcho, 2007; Knop *et al.*, 2008). In several systems, HCN channels function as pacemaker channels (DiFrancesco, 1981; Kaupp & Seifert, 2001) and could, therefore, be the source of spontaneous rhythmic activity in ON-

bipolar cells. However, blocking HCN channel function using either Cs^+ or ZD7288 did not abolish oscillations in the membrane potential of cone ON-bipolar cells in *rd1* retina (Trenholm *et al.*, 2012). HCN channel blockers reduced the frequency from 10 Hz to around 6 Hz, but increased the power at the peak oscillatory frequency by more than 700%. In this study in *rd10* retina such an increase in power was not observed. In *rd10*, Cs^+ and ZD7288 mostly reduced the second peak of the power spectrum but only slightly diminished the frequency of the first peak.

In summary, despite the differences in the process of degeneration and the different frequencies of spontaneous rhythmic activity in *rd1* and *rd10*, there seem to be only small differences in the pharmacological modulation of rhythmic activity in both models. This indicates that the cellular origin of the spontaneous activity may be quite similar in *rd1* and *rd10*. Could the difference in frequencies between *rd1* and *rd10* be attributed to different genetic backgrounds? In *rd10* the frequency observed in LFP oscillation is modulated by a variety of ion channels, amongst them HCN channels, glycine receptors, and GABA receptors (this study). Differences in the expression level of any of these channels between mice of different genetic backgrounds might, therefore, affect the frequency of the oscillations. Animals used in this study carried the *rd10* mutation in a C57BL/6 background. Trenholm and colleagues recorded oscillations in the membrane potential of AII amacrine cells and cone ON-bipolar cells in retinal slices from animals carrying the *rd1* mutation in the same background. They found frequencies of around 15 Hz [see e.g. their Figure 1, (Trenholm *et al.*, 2012)]. These values are very different from those obtained in the present study for *rd10*, but consistent with data obtained by the same authors from animals carrying the *rd1* mutation in a different genetic background and with previous reports on *rd1* retina using MEA recordings (Ye & Goo, 2007b; Margolis *et al.*, 2008; Stasheff, 2008; Borowska *et al.*, 2011; Goo *et al.*, 2011a).

This study (Figure 3.2.6 and Figure 3.2.7) as well as studies of others (Menzler & Zeck, 2011) provided evidence that rhythmic electrical activity might spread across the retina in form of a wave. This is reminiscent of waves of retinal activity observed during the early postnatal period before eye opening (Feller *et al.*, 1997; Wong, 1999) and of the propagation of electrical excitation in the heart. It is not entirely clear why spontaneous activity originating at one spot in the retina should dominate oscillations over a larger retinal area, but once generated the pacemaker wave could easily spread across the retina through the gap junctional

network between the AII amacrine cells (Kolb & Famiglietti, 1974). Further studies will have to identify the mechanism underlying the generation of such waves and will have to address the question why robust spontaneous activity disappears entirely for longer time and comes back (Figure 3.2.6 and Figure 3.2.7).

4.3 Why does spontaneous rhythmical activity originate in the retina of *rd1* and *rd10* mice?

In principle, there are several ways how spontaneous rhythmic activity could arise in *rd1* or *rd10* retina. First, it might result from substantial remodelling and rewiring processes described in the remaining retinal tissue upon photoreceptor degeneration. During remodelling, new connections between retinal neurons might be formed that generate pacemaker activity and might transform the retina into a self-signalling neuronal network (Strettoi & Pignatelli, 2000; Marc & Jones, 2003; Strettoi *et al.*, 2003; Jones & Marc, 2005; Marc *et al.*, 2007; Phillips *et al.*, 2010). However, this model fails to explain why oscillations can be observed in *rd10* mice at postnatal week 2, when photoreceptors are still present and no substantial remodelling has occurred (Jae *et al.*, 2013). Second, the functional properties of retinal neurons, in particular bipolar cells, might change at early stages of degeneration when photoreceptors are still present. These changes include the aberrant expression of ionotropic glutamate receptors and the loss of expression or reduced activation of metabotropic glutamate receptors on ON-bipolar cells as well as the increase of GABA mediated currents (Strettoi & Pignatelli, 2000; Varela *et al.*, 2003; Marc *et al.*, 2007; Chua *et al.*, 2009; Puthussery *et al.*, 2009). Finally, oscillations might develop independently of remodelling or functional changes simply as a response of the retinal network to the lack of input from photoreceptors. Trenholm *et al*. (Trenholm *et al.*, 2012) reported that in wild type retina, blockage of photoreceptor input by application of the glutamate receptor blockers NBQX and L-AP4 induced oscillations in both cone ON-bipolar cells and AII amacrine cells similar to those observed in *rd1* retina. This would suggest that the lack of photoreceptor input is sufficient to trigger oscillations in the retina.

In this study, preliminary experiments were performed on an alternative model for retinal degeneration. Treatment with the pharmacological agent MNU leads to blindness caused by selective photoreceptor apoptosis via oxidative stress (Nambu *et al.*, 1997; Yoshizawa *et al.*, 2000; Tsubura *et al.*, 2010). Animals received MNU via intraperitoneal injection and MEA

recordings were performed 7 - 10 days after injection. Oscillations with frequencies of 4 – 6 Hz were recorded in the baseline of control recordings of retinae from MNU treated animals (Figure 3.2.17, Figure 3.2.18). Anatomical studies conducted by Rösch et al. (Rösch *et al.*, 2014a) showed that two weeks after injection all photoreceptors had disappeared.

4.4 How does rhythmic activity in *rd10* retina compare to that observed in other parts of the CNS?

While rhythmic activity in the *rd10* retina seems to be a consequence of a pathological process, oscillations can be observed under physiological conditions in other parts of the CNS. Oscillations were found in the cortex, thalamus (Steriade & Deschenes, 1984; Steriade *et al.*, 1993), hippocampus (Buzsaki & Draguhn, 2004) as well as in the olfactory bulb (Hayar *et al.*, 2004; Schaefer *et al.*, 2006; Liu & Shipley, 2008; Fukunaga *et al.*, 2012). Oscillations can be generated within the neuronal network, e.g. by excitation followed by feedback inhibition. On the other hand, rhythmic activity can arise intrinsically in single neurons generated by the interplay of the ion channels expressed by these neurons. Neurons with rhythmic firing activity are known as "pacemaker neurons" (Llinas, 1988). Many pacemaker neurons express members of one or two classes of ion channels: the sodium channels underlying the "persistent" tetrodotoxin-sensitive (TTX-sensitive) sodium currents (I_{NaP}) and hyperpolarization-activated and cyclic nucleotide-gated (HCN) channels. I_{NaP} plays an important role in the boosting of excitatory synaptic inputs, acceleration of firing rates, and development of oscillatory neuronal activities (Taylor & Bezanilla, 1983; Crill, 1996). I_{NaP} becomes activated at relatively negative membrane potentials and depolarizes the cell, which finally can initiate an action potential. In the retina, I_{NaP} is found in dopaminergic amacrine cells that display a low spontaneous firing rate (Feigenspan *et al.*, 1998). The properties of HCN channels are considered unique: they become activated during hyperpolarization, thus the currents were termed as I_h (h for hyperpolarization-activated), I_f (f for funny) or I_q (q for queer). In vertebrates, the HCN family comprises four members (HCN1 - 4). HCN channels conduct Na^+ and K^+ (Edman *et al.*, 1987; Gauss *et al.*, 1998; Santoro *et al.*, 1998) and are modulated by cyclic nucleotides (Ludwig *et al.*, 1998). In the retina, all four isoforms are expressed (Müller *et al.*, 2003; Ivanova & Müller, 2006; Fyk-Kolodziej & Pourcho, 2007; Knop *et al.*, 2008). However, the present study suggests that in *rd10* retina HCN channels play a modulatory rather than a crucial role in the generation of spontaneous rhythmic

activity. Blocking HCN channels did not abolish spontaneous rhythmic activity in *rd10* retina (Figure 3.2.15 and Figure 3.2.16).

4.5 Therapeutic approaches for RP

Currently, there is no treatment for RP. However, the persistent inner retina provides a target for therapies. One possibility is driving retinal activity via electrical stimulation by neural prostheses or optical stimulation using ectopically expressed light sensitive proteins.

4.5.1 Prosthetic approach

The existing prosthetic devices stimulate retinal cells either from a subretinal or from an epiretinal position. Stimulation currents need to be adjusted for each stimulation electrode in a time consuming way in order to achieve a light sensation in the patient. The BiMEA prosthesis (see chapter 1.6) is based on electrode shafts that penetrate the retina from the vitreal side. Each shaft carries electrodes that enable stimulation of the retina at different depths as well as recording electrodes that enable to monitor the retinal output from the site of stimulation. Using a feedback system, such a device could adjust the stimulation current for each electrode autonomously.

One problem all prosthetic approaches have to struggle with is resolution. The diameter of a cone in the human fovea is 2.5 µm, i.e. roughly 1/100 degree of the visual field. The size of subretinal electrodes lies in the range of 50 µm (Gekeler *et al.*, 2007; Wilke *et al.*, 2011; Zrenner *et al.*, 2011). Penetrating shafts as used in the BiMEA system would be even further apart and hence, the resolution achievable with such a system would be lower. On the other hand, the size of the camera image that is fed into the encoder can be adjusted by the system and very large arrays of electrodes could be used to stimulate the retina. Such a system might yield a resolution sufficient for basic object discrimination and recognition tasks.

Electrical stimulation would not discriminate between ON- and OFF-cells. Hence, from each stimulation site the brain might receive the information that light intensity increased and decreased at the same time. Most probably, the plasticity of the brain could cope with this dilemma after a training phase. However, using an optogenetic approach might avoid this problem in the first place.

4.5.2 Optogenetic approach

Optogenetics utilizes the ectopic expression of light addressable molecules to change the membrane potential of the targeted cell by an increase in light intensity. The most widely used actuator is channelrhodopsin-2 from Chlamydomonas reinhardtii (ChR2), a light-gated cation channel that depolarizes cells upon light activation (Nagel *et al.*, 2003; Boyden *et al.*, 2005). Halorhodopsin (NpHR) is a light triggered chloride pump that hyperpolarizes cells upon light activation (Zhao *et al.*, 2008; Ullrich *et al.*, 2013).

The genes coding for actuators can be introduced into retinal cells via electroporation – which only works in experimental animals – or by the use of viruses as gene shuttles. Actuators can be expressed in many different retinal cell types by using promoters that drive expression irrespective of the cell type. Expression of optogenetic actuators was shown to restore photosensitivity in animal models of RP at the level of the retina and cortex as well as behaviourally. Several studies expressed ChR2 using viral transfection with unspecific promoters (Bi *et al.*, 2006; Lin *et al.*, 2008; Tomita *et al.*, 2009; Thyagarajan *et al.*, 2010; Tomita *et al.*, 2010). They showed that all ganglion cells were depolarized by light, regardless of whether they were ON- or OFF-ganglion cells.

Using cell type specific promoters, expression can be restricted specifically to cell types of interest. Lagali *et al.* (Lagali *et al.*, 2008) targeted ChR2 to ON-bipolar cells in *rd1* mice and could elicit stable light responses in ganglion cells. Behavioural studies on *rd1* mice expressing ChR2 in ON-bipolar cells revealed visual responses.

Busskamp et al. used adeno-associated viruses (AAVs) and a cone specific promoter to express halorhodopsin specifically in cones in two RP mouse models (Busskamp *et al.*, 2010). Viruses were delivered to the retina when the cones became light-insensitive. Light activation of halorhodopsin triggers hyperpolarizing responses similar to light responses in normal cones. At the level of retinal ganglion cells, ON and OFF ganglion cells as well as direction selective cells showed typical responses upon light stimulation. Similarly, light-evoked activity was measured in the cortex and visually evoked behaviour was documented.

Optogenetic approaches have targeted several different cell types within the retina: photoreceptor cells (Busskamp *et al.*, 2010), bipolar cells (Lagali *et al.*, 2008; Doroudchi *et al.*, 2011), and ganglion cells (Bi *et al.*, 2006; Lin *et al.*, 2008; Ivanova & Pan, 2009; Zhang *et al.*, 2009; Ivanova *et al.*, 2010).

The combined expression of ChR2 and halorhodopsin might improve light triggered retinal signalling. ChR2 could be expressed in cells of the ON pathway while halorhodopsin could be expressed in cells of the OFF pathway. In both cases the natural response polarity of the pathway would be maintained. Viral delivery of ChR2 to ON-bipolar cells has recently been described (Doroudchi *et al.*, 2011). However, currently no promoters are known that would enable the specific targeting of OFF-bipolar cells. ChR2 could be expressed in AII amacrine cells. AII cells activate cone ON-bipolar cells and inhibit cone OFF-bipolar cells and thus, in principle, activation of ON and OFF cells could be achieved with a single kind of actuator.

At present the light sensitivity of optogenetically engineered retinal cells is too low to be activated by ambient light levels. Sensitivity might be increased by increasing the number of actuator molecules in the cell membrane, e.g. by using strong promoters and high virus titers, and by increasing the current produced by an actuator molecule upon absorption of a single photon by site-directed mutagenesis. It is to be expected that in the future, light sensitivity and specificity of expression will both be improved.

4.6 Outlook

This study shows that, despite the differences in the onset and speed of degeneration and the different frequencies observed in rhythmic electrical activity in *rd1* and *rd10* retina, the origin of the oscillations seems to be quite similar in both mouse models. Moreover, oscillations could also be observed in a third model, in which photoreceptor degeneration was not the consequence of a genetic disease but was initiated by treatment with the toxic agent MNU. From these data one can conclude that oscillatory activity in the inner retinal network is a general feature observed after photoreceptor degeneration. According to the current model (Goo *et al.*, 2011a; Jae *et al.*, 2013; Toychiev *et al.*, 2013), oscillations originate by the interplay between cone ON-bipolar cells and AII amacrine cells via electrical coupling.

Several questions need to be addressed in the future.

First and most importantly, it must be tested whether the oscillatory activity in the degenerated retina interferes with the electrical stimulation by the prosthesis. It is conceivably that cells that are trapped in an unphysiological bursting mode are less susceptible to electrical stimulation. If so, ways must be found to suppress oscillatory activity in order to increase the susceptibility to electrical stimulation. The present study showed that oscillations can be

abolished by blockers of glutamatergic transmission and by blocking gap junctions. Whether under these conditions, ganglion cells can still be electrically stimulated by electrodes needs to be investigated in future experiments.

Secondly, the question why the frequency of retinal oscillations differs between different degeneration models still remains unanswered. The present study revealed only small differences between the pharmacological modulation of rhythmic activity in *rd1* and *rd10*. This indicates that the cellular origin of the spontaneous activity seems to be quite similar in the two models. In *rd10* the frequency observed in LFP oscillation is modulated by a variety of ion channels, amongst them HCN channels, glycine receptors, and GABA receptors. Differences in the expression level of any of these channels might, therefore, affect the frequency of the oscillations.

Thirdly, the impact of gap junctions on retinal oscillations should be addressed. AII amacrine cells are coupled via gap junctions to cone ON-bipolar cells. Hence, these gap junctions most probably are of vital importance in the generation of oscillations. However, AII amacrine cells are also coupled to each other via gap junctions. These gap junctions could allow for extensive lateral coupling of oscillatory activity within the retinal network as well as for the propagation of oscillatory waves as shown in Figure 3.2.6. The gap junctions between AII/AII and AII/bipolar cell differ as they contain different connexins (O'Brien *et al.*, 1996; Condorelli *et al.*, 1998; Dermietzel *et al.*, 2000). Pharmacologically, it should be possible to dissect the impact of the two types of gap junctions on retinal oscillations. Dopamine reduces AII/AII coupling (Mills & Massey, 1995) through the activation of D1-type dopamine receptors (Hampson *et al.*, 1992), the formation of cAMP and activation of protein kinase A (Hampson *et al.*, 1992; Liu & Cooper, 1996). In contrast, the permeability of the gap junctions between AIIs and ON-bipolar cells appears to be regulated by nitric oxide (Mills & Massey, 1995). Nitric oxide activates guanylate cyclases, thereby increasing the intracellular cGMP concentration. The gap junction permeability seems to be regulated by phosphorylation mediated by protein kinase G.

Clearly, while over the last years we have gained considerable insight into the process of retinal degeneration and several important issues still need clarification in further studies.

5. References

Barhoum, R., Martinez-Navarrete, G., Corrochano, S., Germain, F., Fernandez-Sanchez, L., de la Rosa, E.J., de la Villa, P. & Cuenca, N. (2008) Functional and structural modifications during retinal degeneration in the rd10 mouse. *Neuroscience*, **155**, 698-713.

Berger, F., Borchard, U., Gelhaar, R., Hafner, D. & Weis, T. (1994) Effects of the bradycardic agent ZD 7288 on membrane voltage and pacemaker current in sheep cardiac Purkinje fibres. *Naunyn-Schmiedeberg's archives of pharmacology*, **350**, 677-684.

Berson, E.L. (1993) Retinitis pigmentosa. The Friedenwald Lecture. *Investigative ophthalmology & visual science*, **34**, 1659-1676.

Bi, A., Cui, J., Ma, Y.P., Olshevskaya, E., Pu, M., Dizhoor, A.M. & Pan, Z.H. (2006) Ectopic expression of a microbial-type rhodopsin restores visual responses in mice with photoreceptor degeneration. *Neuron*, **50**, 23-33.

Biswas, S., Haselier, C., Mataruga, A., Thumann, G., Walter, P. & Müller, F. (2014) Pharmacological Analysis of Intrinsic Neuronal Oscillations in rd10 Retina. *PloS one*, **9**, e99075.

Blanks, J.C. & Johnson, L.V. (1984) Specific binding of peanut lectin to a class of retinal photoreceptor cells. A species comparison. *Investigative ophthalmology & visual science*, **25**, 546-557.

Bloomfield, S.A. & Dacheux, R.F. (2001) Rod vision: pathways and processing in the mammalian retina. *Progress in retinal and eye research*, **20**, 351-384.

Bloomfield, S.A. & Miller, R.F. (1986) A functional organization of ON and OFF pathways in the rabbit retina. *The Journal of neuroscience : the official journal of the Society for Neuroscience*, **6**, 1-13.

Bok, D. (2005) Ciliary neurotrophic factor therapy for inherited retinal diseases: pros and cons. *Retina*, **25**, S27-S28.

Borowska, J., Trenholm, S. & Awatramani, G.B. (2011) An intrinsic neural oscillator in the degenerating mouse retina. *The Journal of neuroscience : the official journal of the Society for Neuroscience*, **31**, 5000-5012.

BoSmith, R.E., Briggs, I. & Sturgess, N.C. (1993) Inhibitory actions of ZENECA ZD7288 on whole-cell hyperpolarization activated inward current (If) in guinea-pig dissociated sinoatrial node cells. *British Journal of Pharmacology*, **110**, 343-349.

Bowes, C., Li, T., Danciger, M., Baxter, L.C., Applebury, M.L. & Farber, D.B. (1990) Retinal degeneration in the rd mouse is caused by a defect in the beta subunit of rod cGMP-phosphodiesterase. *Nature*, **347**, 677-680.

Boycott, B.B. & Wässle, H. (1974) The morphological types of ganglion cells of the domestic cat's retina. *The Journal of physiology*, **240**, 397-419.

Boycott, B.B. & Wässle, H. (1991) Morphological Classification of Bipolar Cells of the Primate Retina. *The European journal of neuroscience*, **3**, 1069-1088.

Boyden, E.S., Zhang, F., Bamberg, E., Nagel, G. & Deisseroth, K. (2005) Millisecond-timescale, genetically targeted optical control of neural activity. *Nature neuroscience*, **8**, 1263-1268.

Briggman, K.L., Helmstaedter, M. & Denk, W. (2011) Wiring specificity in the direction-selectivity circuit of the retina. *Nature*, **471**, 183-188.

Bringmann, A., Iandiev, I., Pannicke, T., Wurm, A., Hollborn, M., Wiedemann, P., Osborne, N.N. & Reichenbach, A. (2009) Cellular signalling and factors involved in Müller cell gliosis: neuroprotective and detrimental effects. *Progress in retinal and eye research*, **28**, 423-451.

Brown, H. & Difrancesco, D. (1980) Voltage-clamp investigations of membrane currents underlying pace-maker activity in rabbit sino-atrial node. *The Journal of physiology*, **308**, 331-351.

Brown, H., Difrancesco, D. & Noble, S. (1979) Cardiac pacemaker oscillation and its modulation by autonomic transmitters. *The Journal of Experimental Biology*, **81**, 175-204.

Brown, J.E. & Major, D. (1966) Cat retinal ganglion cell dendritic fields. *Experimental neurology*, **15**, 70-78.

Bruckner, R. (1951) [Slit-lamp microscopy and ophthalmoscopy in rat and mouse]. *Documenta Ophthalmologica.*, **5-6**, 452-554.

Bunker, C.H., Berson, E.L., Bromley, W.C., Hayes, R.P. & Roderick, T.H. (1984) Prevalence of retinitis pigmentosa in Maine. *American journal of ophthalmology*, **97**, 357-365.

Busskamp, V., Duebel, J., Balya, D., Fradot, M., Viney, T.J., Siegert, S., Groner, A.C., Cabuy, E., Forster, V., Seeliger, M., Biel, M., Humphries, P., Paques, M., Mohand-Said, S., Trono, D., Deisseroth, K., Sahel, J.A., Picaud, S. & Roska, B. (2010) Genetic reactivation of cone photoreceptors restores visual responses in retinitis pigmentosa. *Science*, **329**, 413-417.

Buzsaki, G. & Draguhn, A. (2004) Neuronal oscillations in cortical networks. *Science*, **304**, 1926-1929.

Canola, K., Angenieux, B., Tekaya, M., Quiambao, A., Naash, M.I., Munier, F.L., Schorderet, D.F. & Arsenijevic, Y. (2007) Retinal stem cells transplanted into models of late stages of retinitis pigmentosa preferentially adopt a glial or a retinal ganglion cell fate. *Investigative ophthalmology & visual science*, **48**, 446-454.

Carter-Dawson, L.D., LaVail, M.M. & Sidman, R.L. (1978) Differential effect of the rd mutation on rods and cones in the mouse retina. *Investigative ophthalmology & visual science*, **17**, 489-498.

Chader, G.J., Weiland, J. & Humayun, M.S. (2009) Artificial vision: needs, functioning, and testing of a retinal electronic prosthesis. *Progress* in *Brain Research*, **175**, 317-332.

Chang, B., Hawes, N.L., Hurd, R.E., Davisson, M.T., Nusinowitz, S. & Heckenlively, J.R. (2002) Retinal degeneration mutants in the mouse. *Vision Research*, **42**, 517-525.

Chen, Y.Y., Liu, S.L., Hu, D.P., Xing, Y.Q. & Shen, Y. (2014) N -methyl- N -nitrosourea-induced retinal degeneration in mice. *Experimental eye research*, **121**, 102-113.

Chow, A.Y., Bittner, A.K. & Pardue, M.T. (2010) The artificial silicon retina in retinitis pigmentosa patients (an American Ophthalmological Association thesis). *Transactions of the American Ophthalmological Society*, **108**, 120-154.

Chow, A.Y., Chow, V.Y., Packo, K.H., Pollack, J.S., Peyman, G.A. & Schuchard, R. (2004) The artificial silicon retina microchip for the treatment of vision loss from retinitis pigmentosa. *Archives of ophthalmology*, **122**, 460-469.

Chua, J., Fletcher, E.L. & Kalloniatis, M. (2009) Functional remodelling of glutamate receptors by inner retinal neurons occurs from an early stage of retinal degeneration. *Journal of Comparative Neurology*, **514**, 473-491.

Cleland, B.G., Levick, W.R. & Wässle, H. (1975) Physiological identification of a morphological class of cat retinal ganglion cells. *The Journal of physiology*, **248**, 151-171.

Condorelli, D.F., Parenti, R., Spinella, F., Trovato Salinaro, A., Belluardo, N., Cardile, V. & Cicirata, F. (1998) Cloning of a new gap junction gene (Cx36) highly expressed in mammalian brain neurons. *The European journal of neuroscience*, **10**, 1202-1208.

Crill, W.E. (1996) Persistent sodium current in mammalian central neurons. *Annual review of physiology*, **58**, 349-362.

Dacheux, R.F. & Raviola, E. (1986) The rod pathway in the rabbit retina: a depolarizing bipolar and amacrine cell. *The Journal of neuroscience : the official journal of the Society for Neuroscience*, **6**, 331-345.

Deans, M.R., Volgyi, B., Goodenough, D.A., Bloomfield, S.A. & Paul, D.L. (2002) Connexin36 is essential for transmission of rod-mediated visual signals in the mammalian retina. *Neuron*, **36**, 703-712.

Dermietzel, R., Kremer, M., Paputsoglu, G., Stang, A., Skerrett, I.M., Gomes, D., Srinivas, M., Janssen-Bienhold, U., Weiler, R., Nicholson, B.J., Bruzzone, R. & Spray, D.C. (2000) Molecular and functional diversity of neural connexins in the retina. *The Journal of neuroscience : the official journal of the Society for Neuroscience*, **20**, 8331-8343.

Dhingra, A., Fina, M.E., Neinstein, A., Ramsey, D.J., Xu, Y., Fishman, G.A., Alexander, K.R., Qian, H., Peachey, N.S., Gregg, R.G. & Vardi, N. (2011) Autoantibodies in melanoma-associated retinopathy target TRPM1 cation channels of retinal ON bipolar cells. *The Journal of neuroscience : the official journal of the Society for Neuroscience*, **31**, 3962-3967.

DiFrancesco, D. (1981) A study of the ionic nature of the pace-maker current in calf Purkinje fibres. *The Journal of physiology*, **314**, 377-393.

Doroudchi, M.M., Greenberg, K.P., Liu, J., Silka, K.A., Boyden, E.S., Lockridge, J.A., Arman, A.C., Janani, R., Boye, S.E., Boye, S.L., Gordon, G.M., Matteo, B.C., Sampath, A.P., Hauswirth, W.W. & Horsager, A. (2011) Virally delivered channelrhodopsin-2 safely and effectively restores visual function in multiple mouse models of blindness. *Molecular therapy : the journal of the American Society of Gene Therapy*, **19**, 1220-1229.

Edman, A., Gestrelius, S. & Grampp, W. (1987) Current activation by membrane hyperpolarization in the slowly adapting lobster stretch receptor neurone. *The Journal of physiology*, **384**, 671-690.

Eisenfeld, A.J., Bunt-Milam, A.H. & Sarthy, P.V. (1984) Müller cell expression of glial fibrillary acidic protein after genetic and experimental photoreceptor degeneration in the rat retina. *Investigative ophthalmology & visual science*, **25**, 1321-1328.

Enz, R. & Bormann, J. (1995) Expression of glycine receptor subunits and gephyrin in single bipolar cells of the rat retina. *Visual neuroscience*, **12**, 501-507.

Euler, T. & Wässle, H. (1995) Immunocytochemical identification of cone bipolar cells in the rat retina. *The Journal of comparative neurology*, **361**, 461-478.

Famiglietti, E.V. (1992) Polyaxonal amacrine cells of rabbit retina: morphology and stratification of PA1 cells. *Journal of Comparative Neurology*, **316**, 391-405.

Famiglietti, E.V., Jr. & Kolb, H. (1975) A bistratified amacrine cell and synaptic cirucitry in the inner plexiform layer of the retina. *Brain research*, **84**, 293-300.

Farajian, R., Pan, F., Akopian, A., Volgyi, B. & Bloomfield, S.A. (2011) Masked excitatory crosstalk between the ON and OFF visual pathways in the mammalian retina. *The Journal of physiology*, **589**, 4473-4489.

Feigenspan, A., Gustincich, S., Bean, B.P. & Raviola, E. (1998) Spontaneous activity of solitary dopaminergic cells of the retina. *The Journal of neuroscience : the official journal of the Society for Neuroscience*, **18**, 6776-6789.

Feller, M.B., Butts, D.A., Aaron, H.L., Rokhsar, D.S. & Shatz, C.J. (1997) Dynamic processes shape spatiotemporal properties of retinal waves. *Neuron*, **19**, 293-306.

Friedman, D.S., O'Colmain, B.J., Munoz, B., Tomany, S.C., McCarty, C., de Jong, P.T., Nemesure, B., Mitchell, P., Kempen, J. & Eye Diseases Prevalence Research, G. (2004) Prevalence of age-related macular degeneration in the United States. *Archives of ophthalmology*, **122**, 564-572.

Fukunaga, I., Berning, M., Kollo, M., Schmaltz, A. & Schaefer, A.T. (2012) Two distinct channels of olfactory bulb output. *Neuron*, **75**, 320-329.

Fyk-Kolodziej, B. & Pourcho, R.G. (2007) Differential distribution of hyperpolarization-activated and cyclic nucleotide-gated channels in cone bipolar cells of the rat retina. *Journal of Comparative Neurology*, **501**, 891-903.

Gaillard, F. & Sauve, Y. (2007) Cell-based therapy for retina degeneration: the promise of a cure. *Vision Research*, **47**, 2815-2824.

Garcia-Fernandez, J.M., Jimenez, A.J. & Foster, R.G. (1995) The persistence of cone photoreceptors within the dorsal retina of aged retinally degenerate mice (rd/rd): implications for circadian organization. *Neuroscience letters*, **187**, 33-36.

Gargini, C., Terzibasi, E., Mazzoni, F. & Strettoi, E. (2007) Retinal organization in the retinal degeneration 10 (rd10) mutant mouse: a morphological and ERG study. *Journal of Comparative Neurology*, **500**, 222-238.

Gauss, R., Seifert, R. & Kaupp, U.B. (1998) Molecular identification of a hyperpolarization-activated channel in sea urchin sperm. *Nature*, **393**, 583-587.

Gehrs, K.M., Anderson, D.H., Johnson, L.V. & Hageman, G.S. (2006) Age-related macular degeneration--emerging pathogenetic and therapeutic concepts. *Annals of Medicine*, **38**, 450-471.

Gekeler, F., Szurman, P., Grisanti, S., Weiler, U., Claus, R., Greiner, T.O., Volker, M., Kohler, K., Zrenner, E. & Bartz-Schmidt, K.U. (2007) Compound subretinal prostheses with extra-ocular parts designed for human trials: successful long-term implantation in pigs. *Graefe's archive for clinical and experimental ophthalmology = Albrecht von Graefes Archiv fur klinische und experimentelle Ophthalmologie*, **245**, 230-241.

Ghosh, K.K., Bujan, S., Haverkamp, S., Feigenspan, A. & Wässle, H. (2004) Types of bipolar cells in the mouse retina. *Journal of Comparative Neurology*, **469**, 70-82.

Goo, Y.S., Ahn, K.N., Song, Y.J., Ahn, S.H., Han, S.K., Ryu, S.B. & Kim, K.H. (2011a) Spontaneous Oscillatory Rhythm in Retinal Activities of Two Retinal Degeneration (rd1 and rd10) Mice. *The Korean Journal of Physiology & Pharmacology*, **15**, 415-422.

Goo, Y.S., Ye, J.H., Lee, S., Nam, Y., Ryu, S.B. & Kim, K.H. (2011b) Retinal ganglion cell responses to voltage and current stimulation in wild-type and rd1 mouse retinas. *Journal of Neural Engineering*, **8**, 035003.

Grun, G. (1975) Structural basis of the functional development of the retina in the cichlid Tilapia leucosticta (teleostei). *Journal of embryology and experimental morphology*, **33**, 243-257.

Hampson, E.C., Vaney, D.I. & Weiler, R. (1992) Dopaminergic modulation of gap junction permeability between amacrine cells in mammalian retina. *The Journal of neuroscience : the official journal of the Society for Neuroscience*, **12**, 4911-4922.

Harris, N.C. & Constanti, A. (1995) Mechanism of block by ZD 7288 of the hyperpolarization-activated inward rectifying current in guinea pig substantia nigra neurons in vitro. *Journal of neurophysiology*, **74**, 2366-2378.

Hartong, D.T., Berson, E.L. & Dryja, T.P. (2006) Retinitis pigmentosa. *Lancet*, **368**, 1795-1809.

Haverkamp, S., Kolb, H. & Cuenca, N. (2000) Morphological and neurochemical diversity of neuronal nitric oxide synthase-positive amacrine cells in the turtle retina. *Cell and tissue research*, **302**, 11-19.

Haverkamp, S. & Wässle, H. (2000) Immunocytochemical analysis of the mouse retina. *Journal of Comparative Neurology*, **424**, 1-23.

Haverkamp, S., Wässle, H., Duebel, J., Kuner, T., Augustine, G.J., Feng, G. & Euler, T. (2005) The primordial, blue-cone color system of the mouse retina. *The Journal of neuroscience : the official journal of the Society for Neuroscience*, **25**, 5438-5445.

Hayar, A., Karnup, S., Shipley, M.T. & Ennis, M. (2004) Olfactory bulb glomeruli: external tufted cells intrinsically burst at theta frequency and are entrained by patterned olfactory input. *The Journal of neuroscience : the official journal of the Society for Neuroscience*, **24**, 1190-1199.

Herrold, K.M. (1967) Pigmentary degeneration of the retina induced by N-methyl-N-nitrosourea. An experimental study in syrian hamsters. *Archives of Ophthalmology*, **78**, 650-653.

Honrubia, F.M. & Elliott, J.H. (1970) Dendritic fields of the retinal ganglion cells in the cat. *Archives of Ophthalmology*, **84**, 221-226.

Huang, Y., Enzmann, V. & Ildstad, S.T. (2011) Stem cell-based therapeutic applications in retinal degenerative diseases. *Stem Cell Reviews and Reports*, **7**, 434-445.

Ivanova, E., Hwang, G.S., Pan, Z.H. & Troilo, D. (2010) Evaluation of AAV-mediated expression of Chop2-GFP in the marmoset retina. *Investigative ophthalmology & visual science*, **51**, 5288-5296.

Ivanova, E. & Müller, F. (2006) Retinal bipolar cell types differ in their inventory of ion channels. *Visual neuroscience*, **23**, 143-154.

Ivanova, E. & Pan, Z.H. (2009) Evaluation of the adeno-associated virus mediated long-term expression of channelrhodopsin-2 in the mouse retina. *Molecular vision*, **15**, 1680-1689.

Jae, S.A., Ahn, K.N., Kim, J.Y., Seo, J.H., Kim, H.K. & Goo, Y.S. (2013) Electrophysiological and Histologic Evaluation of the Time Course of Retinal Degeneration in the rd10 Mouse Model of Retinitis Pigmentosa. *The Korean Journal of Physiology & Pharmacology*, **17**, 229-235.

Jensen, R.J. & Rizzo, J.F., 3rd (2008) Activation of retinal ganglion cells in wild-type and rd1 mice through electrical stimulation of the retinal neural network. *Vision Research*, **48**, 1562-1568.

Jeon, C.J., Strettoi, E. & Masland, R.H. (1998) The major cell populations of the mouse retina. *The Journal of neuroscience : the official journal of the Society for Neuroscience*, **18**, 8936-8946.

Jeong, E., Paik, S.S., Jung, S.W., Chun, M.H. & Kim, I.B. (2011) Morphological and functional evaluation of an animal model for the retinal degeneration induced by N-methyl-N-nitrosourea. *Anatomy & Cell Biology*, **44**, 314-323.

Jimenez, A.J., Garcia-Fernandez, J.M., Gonzalez, B. & Foster, R.G. (1996) The spatio-temporal pattern of photoreceptor degeneration in the aged rd/rd mouse retina. *Cell and tissue research*, **284**, 193-202.

Jones, B.W. & Marc, R.E. (2005) Retinal remodelling during retinal degeneration. *Experimental eye research*, **81**, 123-137.

Kanyshkova, T., Pawlowski, M., Meuth, P., Dube, C., Bender, R.A., Brewster, A.L., Baumann, A., Baram, T.Z., Pape, H.C. & Budde, T. (2009) Postnatal expression pattern of HCN channel isoforms in thalamic neurons: relationship to maturation of thalamocortical oscillations. *The Journal of neuroscience : the official journal of the Society for Neuroscience*, **29**, 8847-8857.

Kaupp, U.B. & Seifert, R. (2001) Molecular diversity of pacemaker ion channels. *Annual review of physiology*, **63**, 235-257.

Kaur, T. & Nawy, S. (2012) Characterization of Trpm1 desensitization in ON bipolar cells and its role in downstream signalling. *The Journal of physiology*, **590**, 179-192.

Keeler, C.E. (1924) The Inheritance of a Retinal Abnormality in White Mice. *Proceedings of the National Academy of Sciences of the United States of America*, **10**, 329-333.

Knop, G.C., Seeliger, M.W., Thiel, F., Mataruga, A., Kaupp, U.B., Friedburg, C., Tanimoto, N. & Müller, F. (2008) Light responses in the mouse retina are prolonged upon targeted deletion of the HCN1 channel gene. *The European journal of neuroscience*, **28**, 2221-2230.

Koike, C., Numata, T., Ueda, H., Mori, Y. & Furukawa, T. (2010a) TRPM1: a vertebrate TRP channel responsible for retinal ON bipolar function. *Cell Calcium*, **48**, 95-101.

Koike, C., Obara, T., Uriu, Y., Numata, T., Sanuki, R., Miyata, K., Koyasu, T., Ueno, S., Funabiki, K., Tani, A., Ueda, H., Kondo, M., Mori, Y., Tachibana, M. & Furukawa, T. (2010b) TRPM1 is a component of the retinal ON bipolar cell transduction channel in the mGluR6 cascade. *Proceedings of the National Academy of Sciences of the United States of America*, **107**, 332-337.

Koizumi, A., Jakobs, T.C. & Masland, R.H. (2004) Inward rectifying currents stabilize the membrane potential in dendrites of mouse amacrine cells: patch-clamp recordings and single-cell RT-PCR. *Molecular vision*, **10**, 328-340.

Kolb, H. & Famiglietti, E.V. (1974) Rod and cone pathways in the inner plexiform layer of cat retina. *Science*, **186**, 47-49.

Kolb, H. & Gouras, P. (1974) Electron microscopic observations of human retinitis pigmentosa, dominantly inherited. *Investigative Ophthalmology & Visual Science*, **13**, 487-498.

Kolb, H. & Nelson, R. (1983) Rod pathways in the retina of the cat. *Vision Research*, **23**, 301-312.

Krizaj, D., Huang, W., Furukawa, T., Punzo, C. & Xing, W. (2010) Plasticity of TRPM1 expression and localization in the wild type and degenerating mouse retina. *Vision Research*, **50**, 2460-2465.

Lagali, P.S., Balya, D., Awatramani, G.B., Munch, T.A., Kim, D.S., Busskamp, V., Cepko, C.L. & Roska, B. (2008) Light-activated channels targeted to ON bipolar cells restore visual function in retinal degeneration. *Nature neuroscience*, **11**, 667-675.

LaVail, M.M., Matthes, M.T., Yasumura, D. & Steinberg, R.H. (1997) Variability in rate of cone degeneration in the retinal degeneration (rd/rd) mouse. *Experimental eye research*, **65**, 45-50.

Liang, L., Katagiri, Y., Franco, L.M., Yamauchi, Y., Enzmann, V., Kaplan, H.J. & Sandell, J.H. (2008) Long-term cellular and regional specificity of the photoreceptor toxin, iodoacetic acid (IAA), in the rabbit retina. *Visual neuroscience*, **25**, 167-177.

Lin, B., Koizumi, A., Tanaka, N., Panda, S. & Masland, R.H. (2008) Restoration of visual function in retinal degeneration mice by ectopic expression of melanopsin. *Proceedings of the National Academy of Sciences of the United States of America*, **105**, 16009-16014.

Lin, B., Masland, R.H. & Strettoi, E. (2009) Remodelling of cone photoreceptor cells after rod degeneration in rd mice. *Experimental eye research*, **88**, 589-599.

Liu, N. & Cooper, N.G. (1996) The Ca2+/calmodulin-dependent protein kinase II-associated protein complex isolated from chicken retina. *Journal of molecular neuroscience : MN*, **7**, 1-12.

Liu, S. & Shipley, M.T. (2008) Multiple conductances cooperatively regulate spontaneous bursting in mouse olfactory bulb external tufted cells. *The Journal of neuroscience : the official journal of the Society for Neuroscience*, **28**, 1625-1639.

Llinas, R.R. (1988) The intrinsic electrophysiological properties of mammalian neurons: insights into central nervous system function. *Science*, **242**, 1654-1664.

Ludwig, A., Zong, X., Jeglitsch, M., Hofmann, F. & Biel, M. (1998) A family of hyperpolarization-activated mammalian cation channels. *Nature*, **393**, 587-591.

Maccaferri, G., Mangoni, M., Lazzari, A. & DiFrancesco, D. (1993) Properties of the hyperpolarization-activated current in rat hippocampal CA1 pyramidal cells. *Journal of neurophysiology*, **69**, 2129-2136.

Marc, R.E. & Jones, B.W. (2003) Retinal remodelling in inherited photoreceptor degenerations. *Molecular Neurobiology*, **28**, 139-147.

Marc, R.E., Jones, B.W., Anderson, J.R., Kinard, K., Marshak, D.W., Wilson, J.H., Wensel, T. & Lucas, R.J. (2007) Neural reprogramming in retinal degeneration. *Investigative ophthalmology & visual science*, **48**, 3364-3371.

Marc, R.E., Jones, B.W., Watt, C.B. & Strettoi, E. (2003) Neural remodelling in retinal degeneration. *Progress in retinal and eye research*, **22**, 607-655.

Margolis, D.J., Newkirk, G., Euler, T. & Detwiler, P.B. (2008) Functional stability of retinal ganglion cells after degeneration-induced changes in synaptic input. *The Journal of neuroscience : the official journal of the Society for Neuroscience*, **28**, 6526-6536.

Masland, R.H. (2001) The fundamental plan of the retina. *Nature neuroscience*, **4**, 877-886.

Masu, M., Iwakabe, H., Tagawa, Y., Miyoshi, T., Yamashita, M., Fukuda, Y., Sasaki, H., Hiroi, K., Nakamura, Y., Shigemoto, R. & et al. (1995) Specific deficit of the ON response in visual transmission by targeted disruption of the mGluR6 gene. *Cell*, **80**, 757-765.

Mataruga, A., Kremmer, E. & Müller, F. (2007) Type 3a and type 3b OFF cone bipolar cells provide for the alternative rod pathway in the mouse retina. *Journal of Comparative Neurology*, **502**, 1123-1137.

Menzler, J. & Zeck, G. (2011) Network oscillations in rod-degenerated mouse retinas. *The Journal of neuroscience : the official journal of the Society for Neuroscience*, **31**, 2280-2291.

Miller, R.F. & Dowling, J.E. (1970) Intracellular responses of the Müller (glial) cells of mudpuppy retina: their relation to b-wave of the electroretinogram. *Journal of neurophysiology*, **33**, 323-341.

Mills, S.L. & Massey, S.C. (1995) Differential properties of two gap junctional pathways made by AII amacrine cells. *Nature*, **377**, 734-737.

Morgans, C.W., Bayley, P.R., Oesch, N.W., Ren, G., Akileswaran, L. & Taylor, W.R. (2005) Photoreceptor calcium channels: insight from night blindness. *Visual neuroscience*, **22**, 561-568.

Morgans, C.W., Brown, R.L. & Duvoisin, R.M. (2010) TRPM1: the endpoint of the mGluR6 signal transduction cascade in retinal ON-bipolar cells. *Bioessays*, **32**, 609-614.

Morgans, C.W., Zhang, J., Jeffrey, B.G., Nelson, S.M., Burke, N.S., Duvoisin, R.M. & Brown, R.L. (2009) TRPM1 is required for the depolarizing light response in retinal ON-bipolar cells. *Proceedings of the National Academy of Sciences of the United States of America*, **106**, 19174-19178.

Müller, F., Boos, R. & Wässle, H. (1992) Actions of GABAergic ligands on brisk ganglion cells in the cat retina. *Visual neuroscience*, **9**, 415-425.

Müller, F., Scholten, A., Ivanova, E., Haverkamp, S., Kremmer, E. & Kaupp, U.B. (2003) HCN channels are expressed differentially in retinal bipolar cells and concentrated at synaptic terminals. *The European journal of neuroscience*, **17**, 2084-2096.

Müller, F., Wässle, H. & Voigt, T. (1988) Pharmacological modulation of the rod pathway in the cat retina. *Journal of neurophysiology*, **59**, 1657-1672.

Nagar, S., Krishnamoorthy, V., Cherukuri, P., Jain, V. & Dhingra, N.K. (2009) Early remodelling in an inducible animal model of retinal degeneration. *Neuroscience*, **160**, 517-529.

Nagel, G., Szellas, T., Huhn, W., Kateriya, S., Adeishvili, N., Berthold, P., Ollig, D., Hegemann, P. & Bamberg, E. (2003) Channelrhodopsin-2, a directly light-gated cation-selective membrane channel. *Proceedings of the National Academy of Sciences of the United States of America*, **100**, 13940-13945.

Naka, K. & Garraway, N.R. (1975) Morphological and functional identifications of catfish retinal neurons. I. Classical morphology. *Journal of neurophysiology*, **38**, 53-71.

Nakajima, M., Nambu, H., Shikata, N., Senzaki, H., Miki, H. & Tsubura, A. (1996) Pigmentary degeneration induced by N-methyl-N-nitrosourea and the fate of pigment epithelial cells in the rat retina. *Pathology International*, **46**, 874-882.

Nakajima, Y., Iwakabe, H., Akazawa, C., Nawa, H., Shigemoto, R., Mizuno, N. & Nakanishi, S. (1993) Molecular characterization of a novel retinal metabotropic glutamate receptor mGluR6 with a high agonist selectivity for L-2-amino-4-phosphonobutyrate. *Journal of Biological Chemistry*, **268**, 11868-11873.

Nakamura, M., Sanuki, R., Yasuma, T.R., Onishi, A., Nishiguchi, K.M., Koike, C., Kadowaki, M., Kondo, M., Miyake, Y. & Furukawa, T. (2010) TRPM1 mutations are associated with the complete form of congenital stationary night blindness. *Molecular vision*, **16**, 425-437.

Nambu, H., Yuge, K., Nakajima, M., Shikata, N., Takahashi, K., Miki, H., Uyama, M. & Tsubura, A. (1997) Morphologic characteristics of N-methyl-N-nitrosourea-induced retinal degeneration in C57BL mice. *Pathology International*, **47**, 377-383.

Nan, Y., Zhang, Q., Ren, C., Huang, X., Gao, J., Li, X. & Pu, M. (2013) Functional evaluation of iodoacetic acid induced photoreceptor degeneration in the cat. *Science China Life Science*, **56**, 524-530.

Nelson, R. (1973) A comparison of electrical properties of neurons in Necturus retina. *Journal of neurophysiology*, **36**, 519-535.

Nelson, R., von Litzow, A., Kolb, H. & Gouras, P. (1975) Horizontal cells in cat retina with independent dendritic systems. *Science*, **189**, 137-139.

Noell, W.K., Walker, V.S., Kang, B.S. & Berman, S. (1966) Retinal damage by light in rats. *Investigative Ophthalmology & Visual Science*, **5**, 450-473.

Nomura, A., Shigemoto, R., Nakamura, Y., Okamoto, N., Mizuno, N. & Nakanishi, S. (1994) Developmentally regulated postsynaptic localization of a metabotropic glutamate receptor in rat rod bipolar cells. *Cell*, **77**, 361-369.

O'Brien, J., al-Ubaidi, M.R. & Ripps, H. (1996) Connexin 35: a gap-junctional protein expressed preferentially in the skate retina. *Molecular biology of the cell*, **7**, 233-243.

O'Hearn, T.M., Sadda, S.R., Weiland, J.D., Maia, M., Margalit, E. & Humayun, M.S. (2006) Electrical stimulation in normal and retinal degeneration (*rd1*) isolated mouse retina. *Vision Research*, **46**, 3198-3204.

Ogino, H., Ito, M., Matsumoto, K., Yagyu, S., Tsuda, H., Hirono, I., Wild, C.P. & Montesano, R. (1993) Retinal degeneration induced by N-methyl-N-nitrosourea and detection of 7-methyldeoxyguanosine in the rat retina. *Toxicologic Pathology*, **21**, 21-25.

Olveczky, B.P., Baccus, S.A. & Meister, M. (2003) Segregation of object and background motion in the retina. *Nature*, **423**, 401-408.

Pan, F., Mills, S.L. & Massey, S.C. (2007) Screening of gap junction antagonists on dye coupling in the rabbit retina. *Visual neuroscience*, **24**, 609-618.

Peichl, L. & Gonzalez-Soriano, J. (1994) Morphological types of horizontal cell in rodent retinae: a comparison of rat, mouse, gerbil, and guinea pig. *Visual neuroscience*, **11**, 501-517.

Petit-Jacques, J., Volgyi, B., Rudy, B. & Bloomfield, S. (2005) Spontaneous oscillatory activity of starburst amacrine cells in the mouse retina. *Journal of neurophysiology*, **94**, 1770-1780.

Phillips, M.J., Otteson, D.C. & Sherry, D.M. (2010) Progression of neuronal and synaptic remodelling in the rd10 mouse model of retinitis pigmentosa. *Journal of Comparative Neurology*, **518**, 2071-2089.

Piyathaisere, D.V., Margalit, E., Chen, S.J., Shyu, J.S., D'Anna, S.A., Weiland, J.D., Grebe, R.R., Grebe, L., Fujii, G., Kim, S.Y., Greenberg, R.J., De Juan, E., Jr. & Humayun, M.S. (2003) Heat effects on the retina. *Ophthalmic surgery, lasers & imaging : the official journal of the International Society for Imaging in the Eye*, **34**, 114-120.

Pourcho, R.G. (1996) Neurotransmitters in the retina. *Current Eye Research*, **15**, 797-803.

Puthussery, T., Gayet-Primo, J., Pandey, S., Duvoisin, R.M. & Taylor, W.R. (2009) Differential loss and preservation of glutamate receptor function in bipolar cells in the rd10 mouse model of retinitis pigmentosa. *The European journal of neuroscience*, **29**, 1533-1542.

Rapp, L.M. & Williams, T.P. (1980) The role of ocular pigmentation in protecting against retinal light damage. *Vision Research*, **20**, 1127-1131.

Rasmussen, K.E. (1974) Fixation in aldehydes. A study on the influence of the fixative, buffer, and osmolarity upon the fixation of the rat retina. *Journal of ultrastructure research*, **46**, 87-102.

Rivolta, C., Sharon, D., DeAngelis, M.M. & Dryja, T.P. (2002) Retinitis pigmentosa and allied diseases: numerous diseases, genes, and inheritance patterns. *Humam Molecular Genetics*, **11**, 1219-1227.

Rösch, S., Johnen, S., Mataruga, A., Müller, F., Pfarrer, C. & Walter, P. (2014a) Selective photoreceptor degeneration by intravitreal injection of N-methyl-N-nitrosourea. *Investigative ophthalmology & visual science*, **55**, 1711-1723.

Rösch, S., Johnen, S., Mazinani, B., Müller, F., Pfarrer, C. & Walter, P. (2014b) The effects of iodoacetic acid on the mouse retina. *Graefe's archive for clinical and experimental ophthalmology*.

Santoro, B., Liu, D.T., Yao, H., Bartsch, D., Kandel, E.R., Siegelbaum, S.A. & Tibbs, G.R. (1998) Identification of a gene encoding a hyperpolarization-activated pacemaker channel of brain. *Cell*, **93**, 717-729.

Sarthy, V. (2007) Focus on molecules: glial fibrillary acidic protein (GFAP). *Experimental eye research*, **84**, 381-382.

Satoh, T.O. & Yamada, M. (2000) A bradycardiac agent ZD7288 blocks the hyperpolarization-activated current (I(h)) in retinal rod photoreceptors. *Neuropharmacology*, **39**, 1284-1291.

Schaefer, A.T., Angelo, K., Spors, H. & Margrie, T.W. (2006) Neuronal oscillations enhance stimulus discrimination by ensuring action potential precision. *PLoS biology*, **4**, e163.

Schiller, P.H. (2010) Parallel information processing channels created in the retina. *Proceedings of the National Academy of Sciences of the United States of America*, **107**, 17087-17094.

Schmitz, F., Konigstorfer, A. & Sudhof, T.C. (2000) RIBEYE, a component of synaptic ribbons: a protein's journey through evolution provides insight into synaptic ribbon function. *Neuron*, **28**, 857-872.

Schubert, T. & Euler, T. (2010) Retinal processing: global players like it local. *Current Biology*, **20**, R486-488.

Scott, P.A., Kaplan, H.J. & Sandell, J.H. (2011) Anatomical evidence of photoreceptor degeneration induced by iodoacetic acid in the porcine eye. *Experimental eye research*, **93**, 513-527.

Shen, Y., Rampino, M.A., Carroll, R.C. & Nawy, S. (2012) G-protein-mediated inhibition of the Trp channel TRPM1 requires the Gbetagamma dimer. *Proceedings of the National Academy of Sciences of the United States of America*, **109**, 8752-8757.

Slaughter, M.M. & Miller, R.F. (1981) 2-amino-4-phosphonobutyric acid: a new pharmacological tool for retina research. *Science*, **211**, 182-185.

Smith, A.J., Bainbridge, J.W. & Ali, R.R. (2009) Prospects for retinal gene replacement therapy. *Trends in Genetics*, **25**, 156-165.

Stasheff, S.F. (2008) Emergence of sustained spontaneous hyperactivity and temporary preservation of OFF responses in ganglion cells of the retinal degeneration (rd1) mouse. *Journal of neurophysiology*, **99**, 1408-1421.

Steriade, M., Contreras, D., Curro Dossi, R. & Nunez, A. (1993) The slow (< 1 Hz) oscillation in reticular thalamic and thalamocortical neurons: scenario of sleep rhythm generation in interacting thalamic and neocortical networks. *The Journal of neuroscience : the official journal of the Society for Neuroscience*, **13**, 3284-3299.

Steriade, M. & Deschenes, M. (1984) The thalamus as a neuronal oscillator. *Brain research*, **320**, 1-63.

Strauss, O. (2005) The retinal pigment epithelium in visual function. *Physiological Review*, **85**, 845-881.

Strettoi, E. & Pignatelli, V. (2000) Modifications of retinal neurons in a mouse model of retinitis pigmentosa. *Proceedings of the National Academy of Sciences of the United States of America*, **97**, 11020-11025.

Strettoi, E., Pignatelli, V., Rossi, C., Porciatti, V. & Falsini, B. (2003) Remodelling of second-order neurons in the retina of rd/rd mutant mice. *Vision Research*, **43**, 867-877.

Strettoi, E., Porciatti, V., Falsini, B., Pignatelli, V. & Rossi, C. (2002) Morphological and functional abnormalities in the inner retina of the rd/rd mouse. *The Journal of neuroscience : the official journal of the Society for Neuroscience*, **22**, 5492-5504.

Sung, C.H. & Chuang, J.Z. (2010) The cell biology of vision. *The Journal of cell biology*, **190**, 953-963.

Suzuki, H. & Pinto, L.H. (1986) Response properties of horizontal cells in the isolated retina of wild-type and pearl mutant mice. *The Journal of neuroscience : the official journal of the Society for Neuroscience*, **6**, 1122-1128.

Suzuki, S. & Kaneko, A. (1990) Identification of bipolar cell subtypes by protein kinase C-like immunoreactivity in the goldfish retina. *Visual neuroscience*, **5**, 223-230.

Szel, A., van Veen, T. & Rohlich, P. (1994) Retinal cone differentiation. *Nature*, **370**, 336.

Taomoto, M., Nambu, H., Senzaki, H., Shikata, N., Oishi, Y., Fujii, T., Miki, H., Uyama, M. & Tsubura, A. (1998) Retinal degeneration induced by N-methyl-N-nitrosourea in Syrian golden hamsters. *Graefe's archive for clinical and experimental ophthalmology*, **236**, 688-695.

Taylor, R.E. & Bezanilla, F. (1983) Sodium and gating current time shifts resulting from changes in initial conditions. *The Journal of general physiology*, **81**, 773-784.

Taylor, S., Chen, J., Luo, J. & Hitchcock, P. (2012) Light-induced photoreceptor degeneration in the retina of the zebrafish. *Methods in Molecular Biology*, **884**, 247-254.

Thyagarajan, S., van Wyk, M., Lehmann, K., Lowel, S., Feng, G. & Wässle, H. (2010) Visual function in mice with photoreceptor degeneration and transgenic expression of channelrhodopsin 2 in ganglion cells. *The Journal of neuroscience : the official journal of the Society for Neuroscience*, **30**, 8745-8758.

tom Dieck, S., Altrock, W.D., Kessels, M.M., Qualmann, B., Regus, H., Brauner, D., Fejtova, A., Bracko, O., Gundelfinger, E.D. & Brandstatter, J.H. (2005) Molecular dissection of the photoreceptor ribbon synapse: physical interaction of Bassoon and RIBEYE is essential for the assembly of the ribbon complex. *The Journal of cell biology*, **168**, 825-836.

Tomita, H., Sugano, E., Fukazawa, Y., Isago, H., Sugiyama, Y., Hiroi, T., Ishizuka, T., Mushiake, H., Kato, M., Hirabayashi, M., Shigemoto, R., Yawo, H. & Tamai, M. (2009) Visual properties of transgenic rats harboring the channelrhodopsin-2 gene regulated by the thy-1.2 promoter. *PloS one*, **4**, e7679.

Tomita, H., Sugano, E., Isago, H., Hiroi, T., Wang, Z., Ohta, E. & Tamai, M. (2010) Channelrhodopsin-2 gene transduced into retinal ganglion cells restores functional vision in genetically blind rats. *Experimental eye research*, **90**, 429-436.

Toychiev, A.H., Ivanova, E., Yee, C.W. & Sagdullaev, B.T. (2013) Block of gap junctions eliminates aberrant activity and restores light responses during retinal degeneration. *The Journal of neuroscience : the official journal of the Society for Neuroscience*, **33**, 13972-13977.

Trenholm, S., Borowska, J., Zhang, J., Hoggarth, A., Johnson, K., Barnes, S., Lewis, T.J. & Awatramani, G.B. (2012) Intrinsic oscillatory activity arising within the electrically coupled AII amacrine-ON cone bipolar cell network is driven by voltage-gated Na+ channels. *The Journal of physiology*, **590**, 2501-2517.

Trexler, E.B., Li, W. & Massey, S.C. (2005) Simultaneous contribution of two rod pathways to AII amacrine and cone bipolar cell light responses. *Journal of neurophysiology*, **93**, 1476-1485.

Tsubura, A., Yoshizawa, K., Kuwata, M. & Uehara, N. (2010) Animal models for retinitis pigmentosa induced by MNU; disease progression, mechanisms and therapeutic trials. *Histology and Histopathology*, **25**, 933-944.

Tsukamoto, Y., Morigiwa, K., Ueda, M. & Sterling, P. (2001) Microcircuits for night vision in mouse retina. *The Journal of neuroscience : the official journal of the Society for Neuroscience*, **21**, 8616-8623.

Uga, S. & Katsume, K. (1969) [Structure and function of the Müller cells in the human retina. I. Reactions of the Müller cells in the degenerating retina]. *Nippon Ganka Gakkai zasshi*, **73**, 1632-1642.

Ullrich, S., Gueta, R. & Nagel, G. (2013) Degradation of channelopsin-2 in the absence of retinal and degradation resistance in certain mutants. *Biological chemistry*, **394**, 271-280.

Van Hook, M.J. & Berson, D.M. (2010) Hyperpolarization-activated current (I(h)) in ganglion-cell photoreceptors. *PloS one*, **5**, e15344.

Vaney, D.I., Sivyer, B. & Taylor, W.R. (2012) Direction selectivity in the retina: symmetry and asymmetry in structure and function. *Nature Review. Neuroscience*, **13**, 194-208.

Vardi, N. (1998) Alpha subunit of Go localizes in the dendritic tips of ON bipolar cells. *Journal of Comparative Neurology*, **395**, 43-52.

Varela, C., Igartua, I., De la Rosa, E.J. & De la Villa, P. (2003) Functional modifications in rod bipolar cells in a mouse model of retinitis pigmentosa. *Vision Research*, **43**, 879-885.

Veruki, M.L. & Hartveit, E. (2009) Meclofenamic acid blocks electrical synapses of retinal AII amacrine and on-cone bipolar cells. *Journal of neurophysiology*, **101**, 2339-2347.

Veruki, M.L., Oltedal, L. & Hartveit, E. (2010) Electrical coupling and passive membrane properties of AII amacrine cells. *Journal of neurophysiology*, **103**, 1456-1466.

Volgyi, B., Xin, D., Amarillo, Y. & Bloomfield, S.A. (2001) Morphology and physiology of the polyaxonal amacrine cells in the rabbit retina. *Journal of Comparative Neurology*, **440**, 109-125.

Wang, W., Noel, J., Kaplan, H.J. & Dean, D.C. (2011) Circulating reactive oxidant causes apoptosis of retinal pigment epithelium and cone photoreceptors in the mouse central retina. *Ophthalmol and Eye Diseases*, **3**, 45-54.

Wässle, H. (2004) Parallel processing in the mammalian retina. *Nature Review. Neuroscience*, **5**, 747-757.

Wässle, H. & Boycott, B.B. (1991) Functional architecture of the mammalian retina. *Physiological Reviews*, **71**, 447-480.

Wässle, H., Grunert, U., Martin, P.R. & Boycott, B.B. (1994) Immunocytochemical characterization and spatial distribution of midget bipolar cells in the macaque monkey retina. *Vision research*, **34**, 561-579.

Weiland, J.D., Liu, W. & Humayun, M.S. (2005) Retinal prosthesis. *Annual Review of Biomedical Engineering*, **7**, 361-401.

Werblin, F.S. & Dowling, J.E. (1969) Organization of the retina of the mudpuppy, Necturus maculosus. II. Intracellular recording. *Journal of neurophysiology*, **32**, 339-355.

West, R.W. & Dowling, J.E. (1972) Synapses onto different morphological types of retinal ganglion cells. *Science*, **178**, 510-512.

Wilke, R., Gabel, V.P., Sachs, H., Bartz Schmidt, K.U., Gekeler, F., Besch, D., Szurman, P., Stett, A., Wilhelm, B., Peters, T., Harscher, A., Greppmaier, U., Kibbel, S., Benav, H., Bruckmann, A., Stingl, K., Kusnyerik, A. & Zrenner, E. (2011) Spatial resolution and perception of patterns mediated by a subretinal 16-electrode array in patients blinded by hereditary retinal dystrophies. *Investigative ophthalmology & visual science*, **52**, 5995-6003.

Wong, R.O. (1999) Retinal waves and visual system development. *Annual Review of Neuroscience*, **22**, 29-47.

Wyatt, H.J. & Day, N.W. (1976) Specific effects of neurotransmitter antagonists on ganglion cells in rabbit retina. *Science*, **191**, 204-205.

Yamauchi, Y., Kimura, K., Agawa, T., Tsukahara, R., Mishima, M., Yamakawa, N. & Goto, H. (2011) Correlation between high-resolution optical coherence tomography (OCT) images and histopathology in an N-methyl-N-nitrosourea-induced retinal degeneration rat model. *British Journal of Ophthalmology*, **95**, 1161-1165.

Yau, K.W. & Hardie, R.C. (2009) Phototransduction motifs and variations. *Cell*, **139**, 246-264.

Ye, J.H. & Goo, Y.S. (2007a) Comparison of voltage parameters for the stimulation of normal and degenerate retina. *Conference Proceedings. IEEE Engineering in Medicine and Biology Society*, **2007**, 5783-5786.

Ye, J.H. & Goo, Y.S. (2007b) The slow wave component of retinal activity in rd/rd mice recorded with a multi-electrode array. *Physiological Measurement*, **28**, 1079-1088.

Yoshizawa, K., Yang, J., Senzaki, H., Uemura, Y., Kiyozuka, Y., Shikata, N., Oishi, Y., Miki, H. & Tsubura, A. (2000) Caspase-3 inhibitor rescues N -methyl- N -nitrosourea-

induced retinal degeneration in Sprague-Dawley rats. *Experimental eye research*, **71**, 629-635.

Zhang, Y., Ivanova, E., Bi, A. & Pan, Z.H. (2009) Ectopic expression of multiple microbial rhodopsins restores ON and OFF light responses in retinas with photoreceptor degeneration. *The Journal of neuroscience : the official journal of the Society for Neuroscience*, **29**, 9186-9196.

Zhao, S., Cunha, C., Zhang, F., Liu, Q., Gloss, B., Deisseroth, K., Augustine, G.J. & Feng, G. (2008) Improved expression of halorhodopsin for light-induced silencing of neuronal activity. *Brain cell biology*, **36**, 141-154.

Zhou, Z.J. & Lee, S. (2008) Synaptic physiology of direction selectivity in the retina. *The Journal of physiology*, **586**, 4371-4376.

Zrenner, E. (2002) Will retinal implants restore vision? *Science*, **295**, 1022-1025.

Zrenner, E., Bartz-Schmidt, K.U., Benav, H., Besch, D., Bruckmann, A., Gabel, V.P., Gekeler, F., Greppmaier, U., Harscher, A., Kibbel, S., Koch, J., Kusnyerik, A., Peters, T., Stingl, K., Sachs, H., Stett, A., Szurman, P., Wilhelm, B. & Wilke, R. (2011) Subretinal electronic chips allow blind patients to read letters and combine them to words. *Proceedings of the Royal Society - biological sciences*, **278**, 1489-1497.

Acknowledgements

For every beginning there is an end. The journey of a thousand miles begins with one step. Today as I take the step of culminating my doctor thesis, it is my privilege to express my deep sense of gratitude and reverence to Prof. Frank Müller, Institute of Complex System-4, Jülich, who through his expertise has helped me right from his constant encouragement, immense patience, productive criticisms and inspiring supervision during the course of this learn.

I owe my special gratitude to Prof. Marc Spehr, Abteilung Chemosensorik Institut für Biologie II, RWTH, Aachen, for being my second supervisor and for taking out his valuable time from his busy schedule and to evaluate this thesis. I appreciate and thank him for all the support.

I would like to thank Prof. Christoph Fahlke, Director, ICS-4 and all the ICS-4 members for the constant support. I have found a new family and home away from home with you all.

I would like to give my deepest thanks to Dr. Anja Mataruga, for her valuable time and suggestions in making this dissertation and without her help it would have been a tough job. Special thanks to Dr. Johnny Hendriks for helping with data analysis and software related queries.

I express my heartfelt thanks to Christoph Aretzweiler for giving all technical support, especially for making immunohistochemistry staining and for being present to solve all problems in the laboratory.

I would like to thank Daniel Portz also for giving expertise support on solving instrument related problems and also in providing small-small gadgets which makes experiments easy and handling.

I am highly grateful to DFG (German Research Foundation) for funding this project and all the BiMEA consortium members for their constant and active support and suggestions for the project.

I would like to thank International Helmholtz Research School of Biophysics and Soft Matter (IHRS BioSoft) for their financial support for the soft skill courses during the tenure of PhD. Special thanks to Thorsten Auth and Anita Eckert, they made official procedures very easy.

Finally a huge recognition goes out to my pillars of strength: my husband, family and friends, thank you all for always giving your unconditional love and support and endless patience.

Jai Guru Dev !!!

Curriculum vitae

Personal Information : Sonia Biswas

Wiesenstraße 6G, Apartment No. 175

52428, Jülich

Nordrhein-Westfalen, Deutschland

Tel.: +49 176 32583601

E-mail: s.biswas@fz-juelich.de

biswas.sonia@gmail.com

Birth : October 28, 1982 – Haridwar, INDIA

Education and academic degree :

2011 - Till date	Ph.D Thesis, Institute of Complex System-4, Forschungszentrum Jülich GmbH, Jülich, Germany.
2007 - 2009	M.Phil. Biophysics, National Institute of Mental Health and Neuroscience, Bangalore, Karnataka, INDIA.
2003 - 2005	M.Sc. Biophysics, Govind Ballab Pant University of Agriculture and Technology, Pantnagar, Uttarakhand, INDIA.
2000 - 2003	B.Sc. Botany, Zoology, Chemistry, Chinmaya Degree College, Haridwar, Uttarakhand, INDIA.
2000	10+2, Science (Biology), All India Senior School Certificate Examination, Haridwar, Uttarakhand, INDIA.

Languages : English, Hindi, Bengali

Publication : **Biswas S**, Haselier C, Mataruga A, Thumann G, Walter P, Müller F., "Pharmacological analysis of intrinsic neuronal oscillations in *rd10* retina", PLoS One. 2014. PMID: 24918437.

Talks : 8th November 2013, Artificial Vision Symposium 2013, Aachen, Germany.
Sonia Biswas, F. Müller, "Characterization of the Retinitis Pigmentosa (RP) mouse model, RD-10: A morphological and electrophysiological study"

Congress Participation / poster contributions :

22nd Neuro-DoWo (Neurobiology Doctoral Student Workshop), July 28-29, 2011, Bonn, Germany.

Sonia Biswas, Benjamin Usai and Frank Müller. Optical and electrophysiological recordings of retinal ganglion cells of transgenic mice expressing the genetically encoded calcium sensor TN-L15.

10th Göttingen Meeting of German Neuroscience Society, March 13-16, 2013, Göttingen, Germany.

Sonia Biswas and Frank Müller. Characterization of the Retinitis Pigmentosa (RP) mouse model, *rd-10*: A morphological and electrophysiological study.

8th PRO RETINA Research-Colloquium Potsdam - Retinal Degeneration, March 22-23, 2013, Potsdam, Germany.

Sonia Biswas and Frank Müller. Characterization of the Retinitis Pigmentosa (RP) mouse model, *rd-10*: A morphological and electrophysiological study.

European Retina Meeting, October 02-05, 2013, Alicante, Spain.

Sonia Biswas and Frank Müller. Characterization of the Retinitis Pigmentosa (RP) mouse model, *rd-10*: A morphological and electrophysiological study.

Band / Volume 83
Microscopic description of the inverse Faraday effect at subpicosecond time scales
D. Popova (2014), 183 pp
ISBN: 978-3-89336-962-1

Band / Volume 84
Neutron Scattering
Lectures of the JCNS Laboratory Course held at Forschungszentrum Jülich and at the Heinz Maier-Leibnitz Zentrum Garching
edited by Th. Brückel, G. Heger, D. Richter, G. Roth and R. Zorn (2014), ca. 360 pp
ISBN: 978-3-89336-965-2

Band / Volume 85
Neutron Scattering
Experiment Manuals of the JCNS Laboratory Course held at Forschungszentrum Jülich and at the Heinz Maier-Leibnitz Zentrum Garching
edited by Th. Brückel, G. Heger, D. Richter, G. Roth and R. Zorn (2014), ca. 195 pp
ISBN: 978-3-89336-966-9

Band / Volume 86
Development and Characterization of a Microfluidic Magnetic Oscillation Reactor for Enzymes
D. Jussen (2014), xxi, 131 pp
ISBN: 978-3-89336-974-4

Band / Volume 87
Submolecular imaging with single particle atomic force sensors
G. Kichin (2014), 140 pp
ISBN: 978-3-89336-976-8

Band / Volume 88
Multiscale Multimodel Simulation of Micromagnetic Singularities
C. Andreas (2014), xix, 188 pp
ISBN: 978-3-89336-983-6

Band / Volume 89
***Ab initio* description of transverse transport due to impurity scattering in transition-metals**
B. C. Zimmermann (2014), 164 pp
ISBN: 978-3-89336-985-0

Band / Volume 90
Ladungstransport durch Graphenschichten und GaAs-Nanodrähte untersucht mit einem Multispitzen-Rastertunnelmikroskop
S. Korte (2014), 96 pp
ISBN: 978-3-89336-990-4

Band / Volume 91
6th Georgian-German School and Workshop in Basic Science
A. Kacharava (Ed.) (2014), CD
ISBN: 978-3-89336-991-1

Band / Volume 92
Ab initio investigations of π-conjugated-molecule-metal interfaces for molecular electronics and spintronics
M. Callsen (2014), viii, 155 pp
ISBN: 978-3-89336-992-8

Band / Volume 93
Ladungstransportmessungen an Si(111) Oberflächen mit einem Multispitzen-Rastertunnelmikroskop
M. Blab (2014), iv, 132, X pp
ISBN: 978-3-89336-997-3

Band / Volume 94
Functional Soft Matter
Lecture Notes of the 46th IFF Spring School 2015
23 February – 06 March, 2015 Jülich, Germany
ed. by J. Dhont, G. Gompper, G. Meier, D. Richter, G. Vliegenthart, R. Zorn
(2015), ca. 600 pp
ISBN: 978-3-89336-999-7

Band / Volume 95
2-Steps in 1-pot: enzyme cascades for the synthesis of chiral vicinal amino alcohols
T. Sehl (2014), XIV, 167 pp
ISBN: 978-3-95806-001-2

Band / Volume 96
Immunohistochemical and electrophysiological characterization of the mouse model for Retinitis Pigmentosa, *rd10*
S. Biswas (2014), XII, 119 pp
ISBN: 978-3-95806-011-1

Weitere ***Schriften des Verlags im Forschungszentrum Jülich*** unter
http://wwwzb1.fz-juelich.de/verlagextern1/index.asp

Schlüsseltechnologien / Key Technologies
Band / Volume 96
ISBN 978-3-95806-011-1

JÜLICH
FORSCHUNGSZENTRUM